

# Politecnico di Torino

Nanotechnologies for ICTs

*Master's Thesis Project*

## CHARACTERIZATION OF ORGANIC ELECTROCHEMICAL TRANSISTORS PRINTED WITH 3D-STEREOLITHOGRAPHY

FABIO DE BORTOLI



*Candidate:*  
Fabio De Bortoli  
240270

*Supervisor:*  
Dr. Matteo COCUZZA

July 2019

## ABSTRACT

---

The Master Thesis work presented here has been developed in order to study and characterise the performances of organic electrochemical transistors (OECT), fabricated by stereolithographic printing. OECTs are devices whose functional part is constituted by a semiconducting organic material. The general structure and the working principle are similar to traditional transistors, with some differences in the kind of charge which is transported in the channel. The physics of the device and a physical-mathematical model are thoroughly described in this work. An overview of the most common organic materials is presented. Nowadays the most commonly exploited material for this kind of devices is PEDOT, a conductive polymer which can be used as a filler inserted in an insulating polymeric matrix. In this work, in order to fabricate the functional part of the transistor, a polymeric mixture composed by PEGDA (an insulating resin which confers the structure and the mechanical properties to the final product) and PEDOT (which is conductive and confers the electrical properties to the device) is exploited. A review of the main printing techniques is presented, with a particular focus on stereolithography, a 3D printing technique. Stereolithography is widely exploited in micro and nanotechnology, but the novelty of this work consists in employing this technique to print OECTs. A stereolithographic process consists in reticulating a resin through the exposure to a laser source, which follows a particular path set by the user. The polymeric mixture is loaded into the stereolithographic printer, and through a particular software, many parameters can be customized, such as the layout and the design of the device, the laser power or the laser speed. Two different channel widths have been printed on the same substrate and tested. After the printing process, the final product undergoes a thermal treatment, after which is ready to be tested and analysed. In this work, a characterization of the devices has been performed, with the goal of analysing the performances from a qualitative and quantitative point of view and finding the best electrical parameters and conditions with which this kind of devices can be operated. In order to perform electrical measurements, an electrolyte with a known concentration is needed, and in this work a saline solution of NaCl has been chosen. A trans-characteristic curve (drain-source current as a function of gate-source voltage) and an output characteristic curve (drain-source current as a function of drain-source voltage) can be generated exploiting a sourcemeter. Also the transient behaviour of the devices has been analysed. The transistors showed good performances in terms of amount of current flowing in the channel and be-

tween the terminal, of threshold voltage and transconductance. Moreover they showed quite fast response times. OECTs showed to be advantageous since they allow to use a small amount of material during fabrication (reducing the costs), and in terms of mechanical and electrical properties; in the future such a device could be exploited as biosensor, due to its performances and to the fact that it requires a small amount of analyte in order to be operated.

## CONTENTS

---

1	INTRODUCTION	1
2	THEORY	8
2.1	Organic-based transistors working principle . . . . .	8
2.2	OECT - Device Physics . . . . .	15
2.2.1	Electronic Circuit . . . . .	17
2.2.2	Ionic Circuit . . . . .	19
2.2.3	Steady-State Model . . . . .	20
2.2.4	Transient State Model . . . . .	24
2.2.5	Transconductance Model . . . . .	26
2.3	OECT Materials . . . . .	29
2.4	OECT Printing Techniques . . . . .	31
2.4.1	Ink-Jet Printing . . . . .	31
2.4.2	Stereolithography . . . . .	32
3	MATERIALS	37
3.1	PEGDA-575 . . . . .	38
3.2	Photo-initiators and Irgacure 819 . . . . .	40
3.3	Conductive Polymers and PEDOT:PSS . . . . .	45
3.4	SpotHT . . . . .	52
3.5	Surfactants and DMSO . . . . .	53
4	METHODS AND EXPERIMENTAL SECTION	55
4.1	Obtaining PEDOT from Clevios PH 1000 (PEDOT:PSS)	56
4.2	Resin composition . . . . .	61
4.3	Stereolithographic process . . . . .	62
4.4	Thermal treatment . . . . .	69
4.5	Metallization of the contacts . . . . .	70
4.6	Electrical characterizations . . . . .	70
5	RESULTS AND DISCUSSION	73
5.1	Morphological characterization . . . . .	73
5.2	Comparison between the two precipitation methods . .	77
5.3	Thermal treatment effectiveness . . . . .	83
5.4	Electrical characterization of Organic Electrochemical Transistors . . . . .	85
5.4.1	Resistance measurement . . . . .	85
5.4.2	Trans-characteristic measurement . . . . .	86
5.4.3	Output characteristic measurements . . . . .	95
5.4.4	Rise-time and fall-time analysis . . . . .	97
6	CONCLUSION	100
	BIBLIOGRAPHY	101

## LIST OF FIGURES

---

Figure 1.1	A scheme of a general OECT, [1] . . . . .	1
Figure 1.2	A scheme of a general MOSFET, [1] . . . . .	3
Figure 1.3	A scheme of a general ISFET, [1] . . . . .	3
Figure 1.4	A classic OFET in aqueous medium, [1] . . . . .	5
Figure 1.5	A classic ISOFET, [1] . . . . .	5
Figure 1.6	A classic EGOFET, [1] . . . . .	6
Figure 2.1	Charge distribution on the two sides of the dielectric in a FET system, [22] . . . . .	9
Figure 2.2	Double layer formation in an EGOFET, [22] . . . . .	10
Figure 2.3	OECT scheme and working principle, [22] . . . . .	11
Figure 2.4	Depletion operational mode of an OECT, [22] . . . . .	12
Figure 2.5	Accumulation operational mode of an OECT, [22] . . . . .	13
Figure 2.6	Charge distribution in the entire volume of an OECT channel, [22] . . . . .	14
Figure 2.7	Channel and gate capacitances behaviour, [22] . . . . .	17
Figure 2.8	Electronic circuit model of an OECT, [22] . . . . .	18
Figure 2.9	Ionic circuit model of an OECT, [22] . . . . .	19
Figure 2.10	Geometrical representation of the channel, [23] . . . . .	21
Figure 2.11	Output characteristic behaviour of an OECT, [23] . . . . .	22
Figure 2.12	Drain-source current variations, for different gate voltages, [23] . . . . .	23
Figure 2.13	Gate current transient response, [23] . . . . .	25
Figure 2.14	Current-time response, [23] . . . . .	26
Figure 2.15	Transient behaviour of an OECT, [23] . . . . .	27
Figure 2.16	Chemical structure of PEDOT:PSS, [22] . . . . .	29
Figure 2.17	The two operational modes of ink-jet printing, [73] . . . . .	31
Figure 2.18	Stereolithography main steps: 3D design realization, 2D-slicing, printing; [77] . . . . .	33
Figure 2.19	Scheme of the internal structure of a bottom-to-top stereolithography apparatus, with laser, moveable plate and resin reservoir; [77] . . . . .	34
Figure 2.20	Structure of a top-to-bottom stereolithographic system; [77] . . . . .	35
Figure 3.1	Chemical structure of poly(ethylene glycol), [84] . . . . .	38
Figure 3.2	Chemical structure of poly(ethylene glycol)diacrylate, [84] . . . . .	38
Figure 3.3	Molecular structure of Irgacure, [84] . . . . .	42
Figure 3.4	Radical formation starting from Irgacure, [84] . . . . .	43
Figure 3.5	Cross-linking mechanism, [84] . . . . .	43

Figure 3.6	Absorption spectrum of Irgacure 819, [84] . . .	44
Figure 3.7	Sigmoidal model of the percolation curve, [84]	46
Figure 3.8	Polaron generation mechanism, [84] . . . . .	48
Figure 3.9	EDOT polymerization reaction, [84] . . . . .	49
Figure 3.10	PEDOT doping mechanism, [84] . . . . .	50
Figure 3.11	PEDOT:PSS formation, [84] . . . . .	51
Figure 3.12	Chemical structure of DMSO, [84] . . . . .	54
Figure 4.1	Benzoid and quinoid structures of PEDOT, [84]	56
Figure 4.2	Clevios precipitation in sulphuric acid 0.5 M .	57
Figure 4.3	Centrifuge employed to separate precipitate and supernatant . . . . .	58
Figure 4.4	Phase separation at the end of the centrifugation	59
Figure 4.5	Precipitated PEDOT at the end of the process .	60
Figure 4.6	Stereolithographic apparatus employed in this work . . . . .	63
Figure 4.7	Samples with different PEGDA-PEDOT proportions . . . . .	65
Figure 4.8	Compact model of the OECT design, developed with the software Rhinoceros . . . . .	66
Figure 4.9	Exploded model of the OECT design, developed with the software Rhinoceros . . . . .	67
Figure 4.10	Technical view of the OECT, useful to observe the main geometrical parameters of the section	67
Figure 4.11	Oven and vacuum pump employed to perform the thermal treatment . . . . .	69
Figure 4.12	OECT under analysis and setup . . . . .	71
Figure 4.13	Sourcemeater and instrumentation employed for the analysis . . . . .	72
Figure 5.1	A FESEM image of Clevios PH 1000, where the presence of crystals and flakes can be noticed .	73
Figure 5.2	Homogeneous dispersion of flakes in Clevios PH 1000 . . . . .	74
Figure 5.3	A TEM image of precipitated PEDOT . . . . .	75
Figure 5.4	PEDOT crystals . . . . .	75
Figure 5.5	Aggregation of PEDOT flakes . . . . .	76
Figure 5.6	Percolation curve obtained using the old precipitation method (in sulphuric acid); data are in semi-logarithmic scale (on the y-axis) . . .	77
Figure 5.7	Percolation curve obtained using the new precipitation method (in ethanol); data are in semi-logarithmic scale (on the y-axis) . . . . .	78

Figure 5.8	Summary of the best conductivity values of both precipitation method; in the label of the x-axis, at first the solvent used is declared, then the time of UltraTurrax between parentheses, and then the percentage of PEDOT in the polymeric mixture . . . . .	81
Figure 5.9	An example of printed OECT . . . . .	82
Figure 5.10	Optical microscope view of the 700 $\mu$ m wide channel . . . . .	82
Figure 5.11	Optical microscope view of the 300 $\mu$ m wide channel . . . . .	83
Figure 5.12	Resistance values of samples with and without thermal treatment . . . . .	84
Figure 5.13	IV curves of the OECT; sweep along drain voltage, gate voltage floating . . . . .	85
Figure 5.14	Trans-characteristic of OECT printed with the first precipitation method (in sulphuric acid) . . . . .	86
Figure 5.15	Trans-characteristic of OECT printed with the second precipitation method (in ethanol) . . . . .	87
Figure 5.16	First precipitation (in sulphuric acid), $V_{ds} = -100$ mV . . . . .	88
Figure 5.17	Second precipitation (in ethanol), $V_{ds} = -100$ mV . . . . .	88
Figure 5.18	First precipitation (in sulphuric acid), $V_{ds} = -500$ mV . . . . .	89
Figure 5.19	Second precipitation (in ethanol), $V_{ds} = -500$ mV . . . . .	89
Figure 5.20	Comparison of $I_{on}/I_{off}$ ratios between first and second precipitation methods, and between the two channel widths . . . . .	90
Figure 5.21	Comparison of transconductance values between first and second precipitation methods, and between the two channel widths . . . . .	91
Figure 5.22	Comparison of threshold voltages between first and second precipitation methods, and between the two channel widths . . . . .	91
Figure 5.23	Trans-characteristic curves at different drain voltages, for 700 $\mu$ m wide channel . . . . .	92
Figure 5.24	Transconductance values at different drain voltages, for 700 $\mu$ m wide channel . . . . .	92
Figure 5.25	Threshold voltages at different drain voltages, for 700 $\mu$ m wide channel . . . . .	93
Figure 5.26	Trans-characteristic curves at different drain voltages, for 300 $\mu$ m wide channel . . . . .	93
Figure 5.27	Transconductance values at different drain voltages, for 300 $\mu$ m wide channel . . . . .	94
Figure 5.28	Threshold voltages at different drain voltages, for 300 $\mu$ m wide channel . . . . .	94

Figure 5.29	Output characteristics at different gate voltages, for 700 $\mu\text{m}$ wide channel . . . . .	95
Figure 5.30	Conductance values at different gate voltages, for 700 $\mu\text{m}$ wide channel . . . . .	96
Figure 5.31	Output characteristics at different gate voltages, for 300 $\mu\text{m}$ wide channel . . . . .	96
Figure 5.32	Conductance values at different gate voltages, for 300 $\mu\text{m}$ wide channel . . . . .	97
Figure 5.33	Input square wave and corresponding current measured, for 700 $\mu\text{m}$ wide channel . . . . .	98
Figure 5.34	Rise-time analysis, for 700 $\mu\text{m}$ wide channel, considering the 90% and 10% of the current flowing in the channel . . . . .	98
Figure 5.35	Fall-time analysis, for 700 $\mu\text{m}$ wide channel, considering the 90% and 10% of the current flowing in the channel . . . . .	99

## LIST OF TABLES

---

Table 5.1	Densities and boiling point of ethanol and sulphuric acid, the two solvents used in the precipitation procedures . . . . .	79
-----------	--	----

## INTRODUCTION

---

Organic electrochemical transistors (OECTs) are devices whose basic structure is similar to the one that characterises conventional devices like FETs but, as the name suggests, exploit organic molecules as functional material in order to have a transduction mechanism (in contrast) with traditional MOSFET devices based on silicon technology, and whose working principle differs in some aspects from FETs. A scheme of a basic OECT device is shown in Fig.1.1. The aim of this work is to try to fabricate OECT exploiting 3D printing technology and to characterise the final product in order to find the best operating conditions, with the future prospective of exploiting these devices for biosensing applications, since nowadays OECT are mainly employed as biosensors.

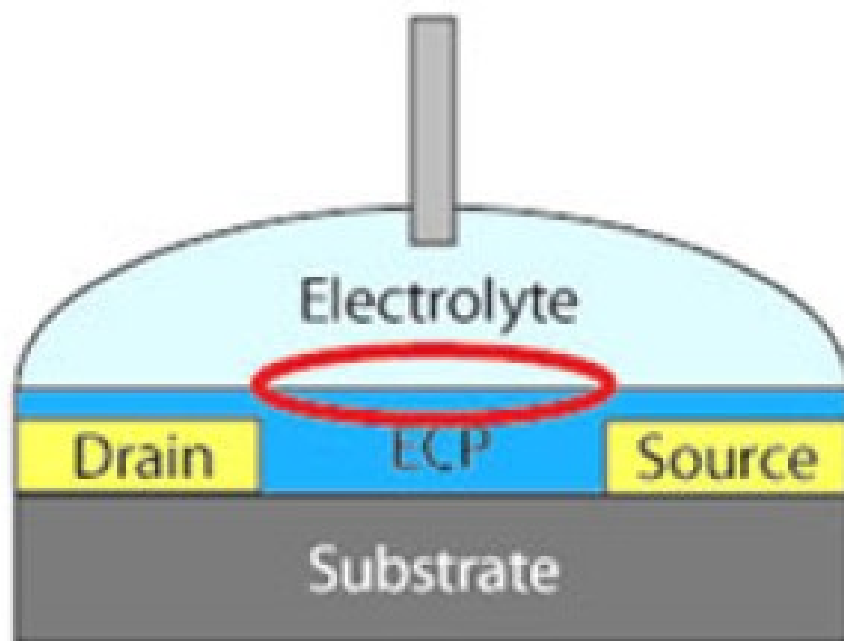


Figure 1.1: A scheme of a general OECT, [1]

But what is it exactly a biosensor? The official definition of biosensor is, according to the International Union of Pure and Applied Chemistry (IUPAC), a device which exploits biochemical reactions (usually mediated by enzymes) in order to detect various chemical compounds, normally employing electrical, optical, or thermal signals [1]. The first prototype of biosensor was developed by Clark

and Lyons in 1962, who managed to detect glucose concentrations in blood [2]. This is a very important milestone for the biosensing field, and since that moment, a lot of research and consistent efforts have been involved in order to expand the field and to improve this kind of devices. Especially by the end of the '90s, with the development and advancement of micro and nanotechnology, biosensing area grew very fast and the aim became creating portable devices able to detect the main analytes found in the human body (such as blood gases, haemoglobin, glucose, ions, salts, calcium, urea). Medicine and biology led to focusing the application of these devices for sensitive assays that could be characterised by fast response, simple fabrication, and low cost, and especially used for point-of-care diagnostic and emergency tests. In the last few years the trend has moved to the detection of DNA (for virus targeting) and antigens (which can be probed by well determined antibodies), especially exploiting labelled molecules, such as enzymes or fluorescent probes, in order to optically monitor the process.

Many classes of transistors exist which can be employed as biosensors, and in order to understand how OECT works, it is useful to briefly underline the main characteristics and working principles of the other kinds of transistors. The most popular class of transistor is the one of field-effect transistors (FETs). As a particular case, the metal-oxide-semiconductor FET (acronym: MOSFET) is the most famous architecture exploited in both analogical and digital circuits. Traditional MOSFET devices (depicted in Fig.1.2) are based on the so-called field-effect: the modulation of the voltage applied through a metal gate electrode changes the number of mobile electrons (if n type transistor are considered) or holes (if instead p type transistor are taken into account), and consequently modulates the current; a thin insulating layer (called gate dielectric) physically separates the gate electrode from the semiconductor body of the transistor [1]. In this class of devices, the threshold voltage (the minimum voltage required to switch on the transistor), depends only on the metal and the semiconductor properties and parameters.

Another variant of the FETs is the ion-sensitive field effect transistor (ISFET, showed in Fig.1.3), where a reference electrode replaces the gate, in this way another physical quantity which affects the threshold voltage is the potential at the electrolyte-insulator interface. This kind of devices is very suitable for the detection of ions and charged molecules, such as DNA, since a variation of the analyte concentration will lead to a change in the interface potential and consequently, as a final result, a change in the conductance.

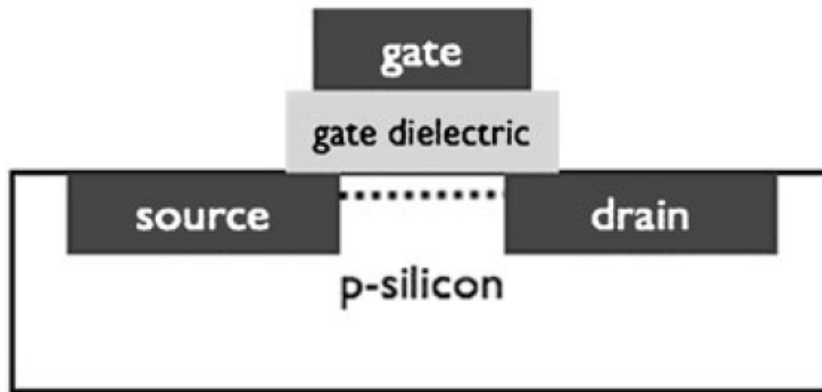


Figure 1.2: A scheme of a general MOSFET, [1]

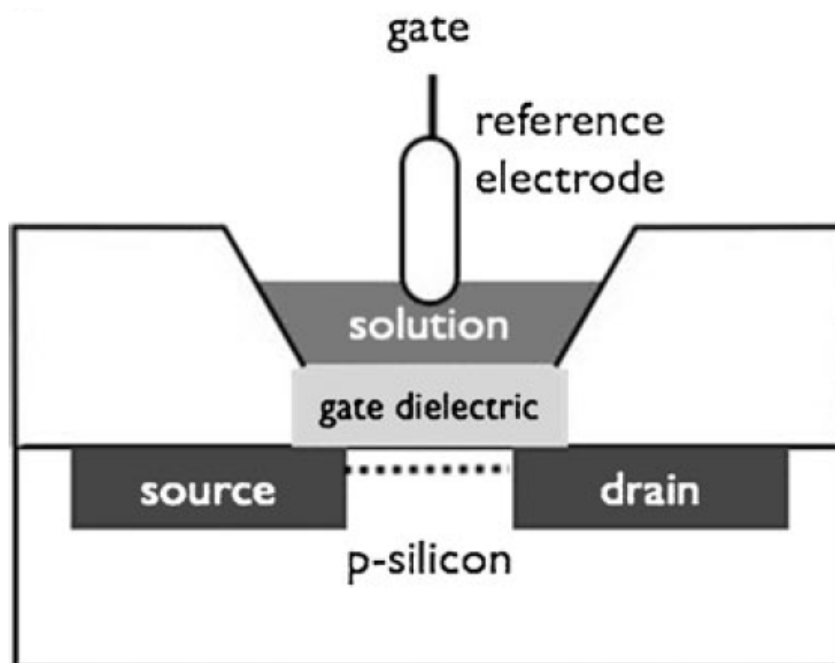


Figure 1.3: A scheme of a general ISFET, [1]

Although, the main limits of the conventional transistors based on silicon technology are the high cost of silicon (with respect to most of the organic materials) combined with the drawbacks deriving from the scaling process. These limits led to the emergence of the class of organic devices. The first example is represented by the organic thin-film transistors (OTFTs) whose main advantage is that they can be fabricated at low cost exploiting easy printing techniques on flexible substrates [3],[4]. Moreover, a great advantage of organic-based devices is the possibility of tuning their performances by customising the properties of the specific organic material used, since in each case a particular compound must be linked or attached to the surface and therefore specific physical and chemical properties are required. Cur-

rently, performance and stability of organic devices, regarding logic integrated circuits, are not at the same level of the inorganic ones yet, but they are very appropriate for optoelectronic display [5], photovoltaics [6], and sensors [7],[8],[9],[10], and in general for all those applications which can stand lower charge carrier mobility.

Organic electronic materials gained increasingly more appeal and concern, particularly due to their low-cost and consequently low-cost production over large areas, which led to the development and manufacture of the so-called OFETs (= Organic Field-Effect Transistor) [11]. This kind of devices exploits conjugated, semiconducting small organic molecules and polymers and their main important advantages with respect to MOSFETs are easy fabrication processes on different substrates and tunable electronic properties due to the versatility of organic molecules. In the last thirty years, a lot of progress has been achieved and materials with mobilities above the one of amorphous silicon have been studied and achieved [12],[13].

In OFET devices (depicted in Fig.1.4), an insulator layer physically separates the gate from the semiconductor channel, as in MOSFETs. When the gate is negatively (positively) polarized in a p-channel (n-channel) device, free holes (electrons) in the semiconductor are drawn toward the semiconductor-insulator interface to compensate an equivalent negative (positive) charge at the gate-insulator interface. This leads to the formation of a conducting channel at the semiconductor-insulator interface. When a negative (positive) voltage is applied between source and drain, holes (electrons) are injected from the source and current flows inside the channel. The gate voltage required to switch the transistor from its "off" state to its "on" state, or equivalently the voltage required to establish a conducting transistor channel, is called the threshold voltage, which constitutes a key physical quantity of the OFETs. The OFET characteristics are greatly affected by the properties of the dielectric-insulator interface. This makes OFETs a perfect transducer for sensor applications.

A particular case of OFET-based biosensors is the so-called ion-sensitive organic FET (ISOFET) [14], whose structure is showed in Fig.1.5, where the gate electrode is substituted by a reference electrode; the electrolyte is in contact with the insulator, the reference electrode is dipped into the electrolyte and the drain current is driven by the potential of the electrolyte-insulator interface. By making the insulator sensitive to a given analyte, it is possible to detect a wide range of biomolecules.

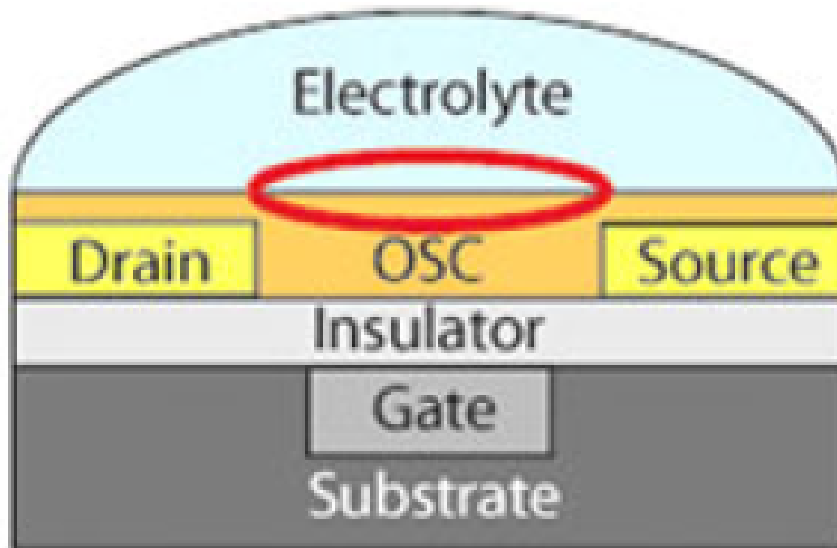


Figure 1.4: A classic OFET in aqueous medium, [1]

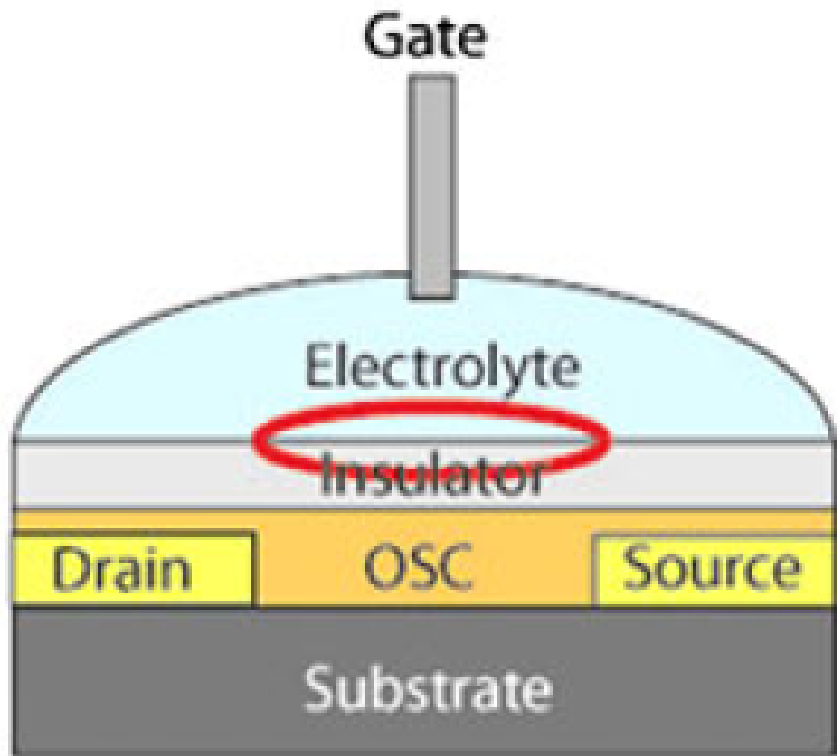


Figure 1.5: A classic ISOFET, [1]

Another important class is constituted by the so-called EGOFETs (Electrolyte-Gated Organic Field Effect Transistor), whose scheme is depicted in Fig.1.6, which have attracted much attention in the last few years due to their low voltage operation compared to OFETs gated through conventional solid dielectrics. In a p-channel EGOFET

device, when the gate is positively biased, the anions of the electrolyte drift away from the electrolyte-semiconductor interface, while the cations are attracted toward the electrolyte-gate interface, resulting in the formation of an electrical double layer (EDL) at both interfaces.

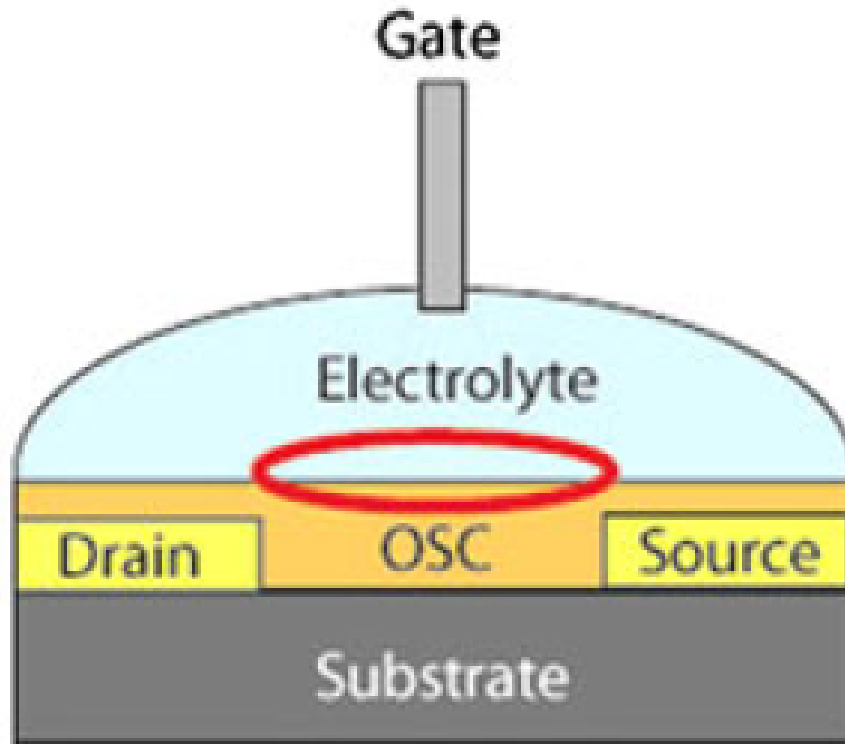


Figure 1.6: A classic EGOFET, [1]

The first OECT was developed during the '80s by Wrighton et al. [15]. An organic electrochemical transistor consists basically of three-terminals, two of them (called source and drain) connected not by silicon but by an organic conducting material; the third terminal, called gate, interacts with the channel through an electrolyte (usually liquid). The working principle of OECTs is physically translated on the doping and de-doping of the polymer, through which the conductivity of the channel is modified.

Electropolymerization of the conducting polymer (performed on microelectrodes) was the first technique exploited in order to fabricate these transistors. Conductive polymers typically used were polypyrrole [15], polyaniline [16],[17] and polythiophene [18],[19]. But in the last few years, new advancements and improvements in microtechnology and printed electronics led to a renovated interest in OECTs. Nowadays, an increasing number of devices is produced us-

ing printed polymers (through screen printing, inkjet printing, full-3D printing), and the most common polymer used as functional material is poly(3,4-ethylenedioxythiophene) doped with poly(styrene sulfonate) (PEDOT:PSS) [20].

OECTs which exploit PEDOT:PSS as functional material are usually on devices, which means that the presence of PSS makes PEDOT conducting when no bias is applied on the gate. When a gate voltage is applied, the cations in the electrolyte diffuse into the polymer bulk in order to compensate the negatively charged sulfonate groups present on the PSS backbone. Subsequently, the hole density is decreased, a phenomenon which results in a decrease of the conductivity of the polymer; as a consequence, a lower current flows in the channel. Due to the fact that they convert an ionic current into an electronic current, OECTs are very suitable to monitor biological phenomena. Moreover, one of the big advantages of OECTs is they work at very low voltages, usually below 1V, and this is a great advantage since it makes them perfectly suited to be used as biosensors even in aqueous media, an environment where low voltages are required to avoid undesired redox reactions.

Biosensors based on OECTs can be considered as the next generation of the so-called microelectrochemical enzyme transistor [21]. This kind of devices is characterised by an architecture very similar to the one developed by Wrighton [15],[16],[17],[18],[19]. However, the switching mechanism between the two redox states of the polymer does not originate from gate polarization, but in contrast it is a consequence of an enzymatic reaction (where the phenomenon of electron transfer is involved).

## THEORY

---

### 2.1 ORGANIC-BASED TRANSISTORS WORKING PRINCIPLE

In a field-effect transistor, the main functional part is a thin surface region, while, as it will be explained better later, in an OECT device the entire volume of the channel is involved [22]. In a FET, a thin insulating layer (denominated as gate dielectric) physically separates the organic semiconductor channel and the metal gate. When a voltage is applied between the gate and the channel the so-called field-effect doping mechanism is generated, which consists in the accumulation of mobile electronic charge near the interface with the dielectric, which is balanced by a charge sheet located at the interface between gate electrode and dielectric. These two charge sheets correspond to the two parallel plates of a capacitor, where the capacitance is inversely proportional to the distance between the two plates (thin dielectric layers lead to very high amounts of induced charge and consequently to very high drain currents). The gate-dielectric-channel structure of a FET is sketched in Fig.2.1.

In an EGOFET, a double-layer capacitor is formed at the electrolyte-channel interface (schematically depicted in Fig.2.2). The charge sheet in the channel is compensated by an ionic charge sheet in the electrolyte, forming the first layer, and then other ions are rearranged inside the electrolyte in the proximity of the first charge layer in order to form the second one. This configuration can be considered as a limit case of FET, because the thickness of the dielectric is reduced to dimensions of the same order of magnitude of the ionic radius, resulting in very high capacitances.

Instead, the main characteristic of the organic electrochemical transistors consists in having an organic conductive film which is in direct contact with the electrolyte, where the gate electrode is dipped, as showed in Fig.2.3.

The system source-channel-drain is qualitatively the same as in traditional MOSFET devices, where the two metal electrodes establish a direct contact with the organic conductive film and define the path through which electrons (or holes) flow. The working principle of an OECT consists in the fact that ions are injected into the organic

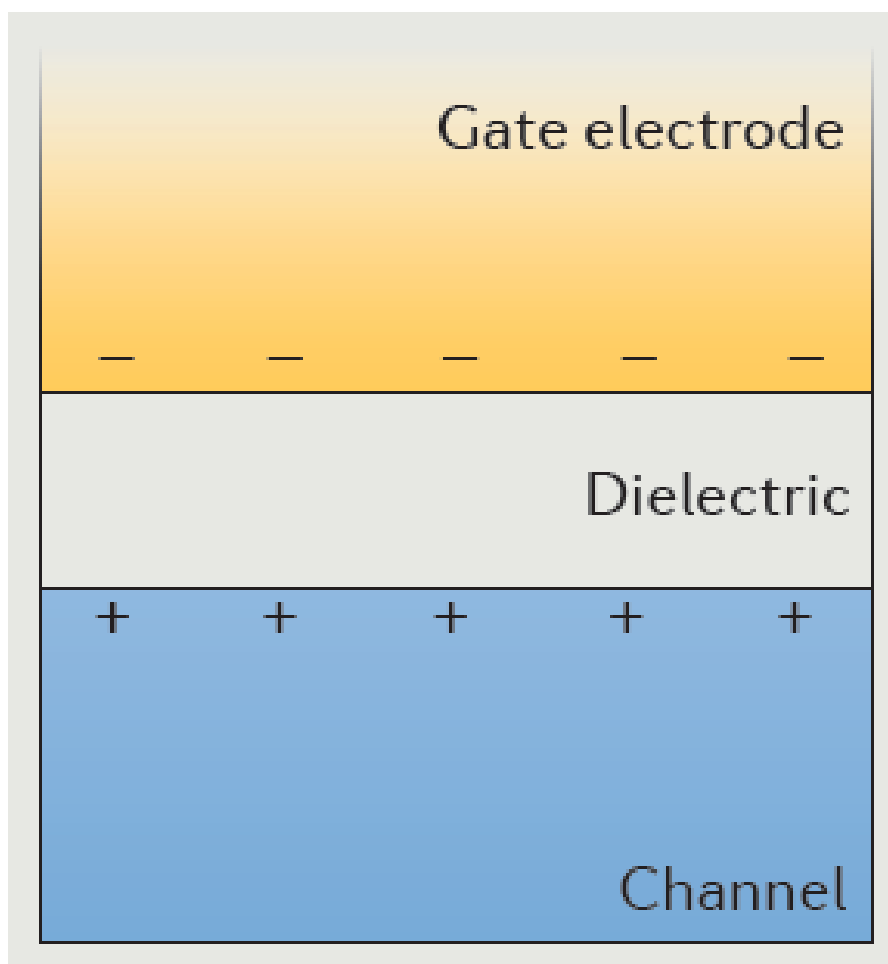


Figure 2.1: Charge distribution on the two sides of the dielectric in a FET system, [22]

conductive film from the electrolyte solution, changing its doping level and hence its conductivity, since the two physical quantities are strictly related [23]. As in a classical MOSFET, the device operation is controlled by the two distinct voltages applied to the gate (which controls ions injection into the channel and consequently the doping state, also called redox state, of the organic film) and to the drain (which leads to a drain-source current, directly proportional to the quantity of mobile carriers in the conductive channel); both of the voltages are referred to the source electrode. OECTs, in the same way as MOSFETs and OFETs, can be exploited as a switch, where the output (the drain current) is controlled by the gate voltage (which is the input), or as an amplifier where, as the name suggests, the power of the input signal is amplified at the output [24].

OECTs devices are typically manufactured and produced exploiting the conductive polymer poly(3,4 ethylenedioxythiophene), called PEDOT, doped with poly(styrene sulfonate), (PSS); the entire system

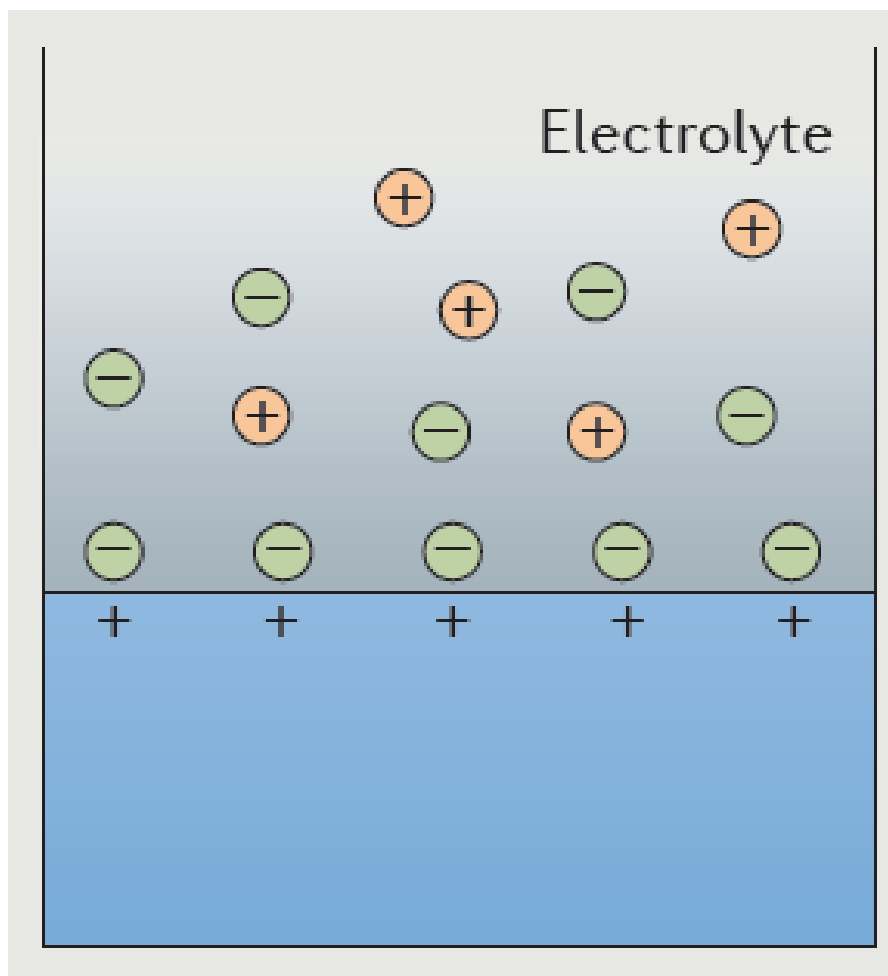


Figure 2.2: Double layer formation in an EGOFET, [22]

is referred to with the acronym PEDOT:PSS. The PEDOT is semiconducting and, employing electrochemistry notation, is oxidized (which corresponds to a p-type doping), therefore the mobile carriers are the holes which can jump from one molecular chain to another through hopping mechanism, resulting in a hole current when an enough high drain voltage is applied. These holes are compensated by the sulfonate anions of PSS, which can be contemplated as ionized acceptors from a solid-state physics point of view [25]. The typical operational mode of this class of OECTs, based on PEDOT:PSS, is the so-called depletion mode (schematically depicted in Fig.2.4): when zero gate bias is applied, a hole current flows in the channel (and the transistor is considered in the ON state), while instead when a positive gate voltage is applied, the cations from the electrolyte are injected into the semiconducting channel so that the anions are neutralized (this mechanism is called compensation doping and corresponds to make p type silicon by implanting donor atoms). Consequently, the number of holes in the channel is reduced and the film is de-doped since at the source there is not an enough supply of holes that are extracted

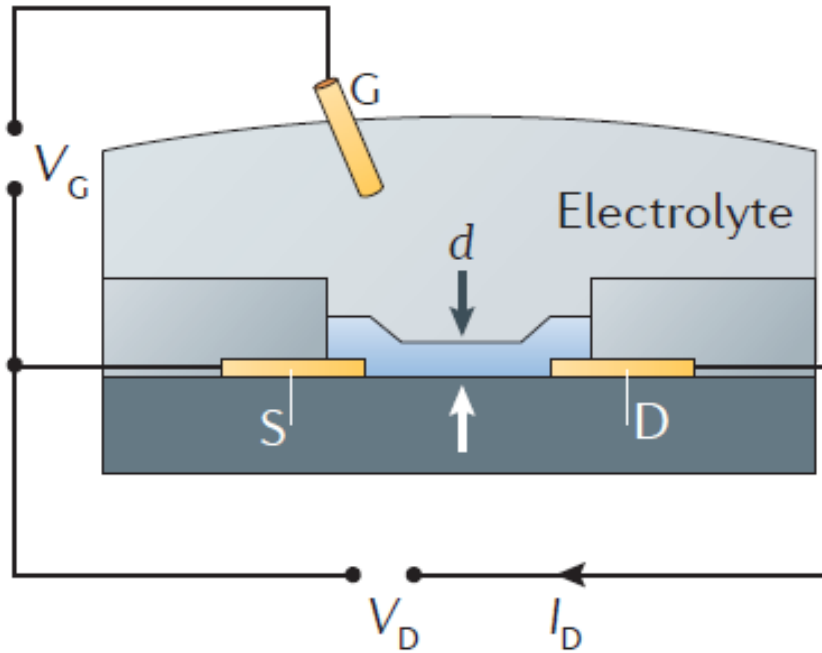


Figure 2.3: OECT scheme and working principle, [22]

at the drain. This ultimately leads to a drop in the drain current, and when this happens the device reaches the so-called OFF state [23]. Summarising, it can be said that, when operating in depletion mode, the OECT is normally in the ON state.

In contrast with the previous case, the OECT can alternatively work in the accumulation mode (depicted in Fig.2.5), where it is normally in the OFF state since there is a very small number of mobile holes in the channel. When a negative gate voltage is applied, anions are injected into the channel leading to an accumulation of holes, and the device is said to be in the ON state [26].

As stated before, in an OECT, since the functional part is not simply a thin layer, the charge configuration is not described by a parallel plate capacitance but by a volumetric capacitance (which can be many orders of magnitude larger) due to the fact that ions penetrate the semiconductor, as showed in Fig.2.6. If compared with a FET of similar size, in an OECT a higher electronic charge in the channel and consequently a larger drain current is induced at the same gate voltage.

Therefore, OECTs can be exploited as very efficient and powerful switches or amplifiers, since large modulations in the drain current

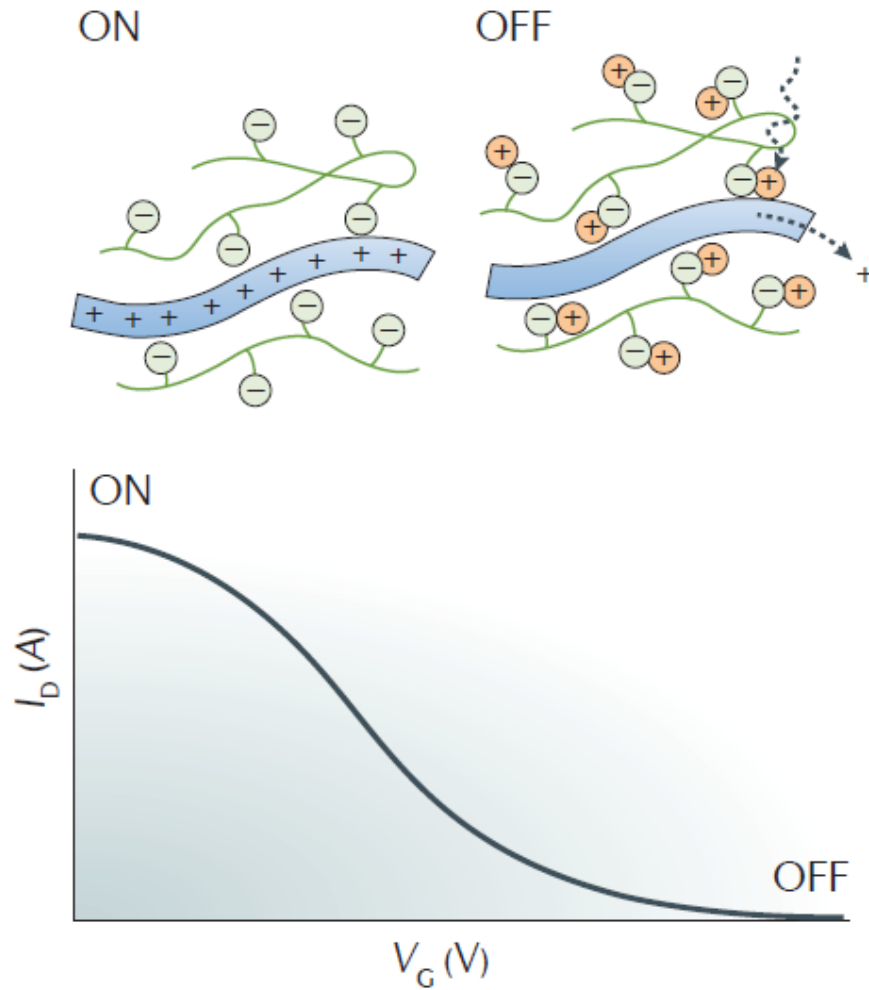


Figure 2.4: Depletion operational mode of an OEFT, [22]

can be appreciated even for low gate voltages [24],[27]. Exploiting electrolytes instead of dielectric capacitors (as in MOSFET) allows for large flexibility in device design and architecture, and an easy integration with a quite large variety of substrates. The easy tunability of organic molecules enables a very efficient optimization of ion and electron transport in the channel and effective biofunctionalization. Because of these features, OEFTs are being explored for a large variety of applications, such as neural interfaces [28],[29], chemical and biological sensors [30],[31], printed circuits [32],[33] and neuromorphic devices [34],[35].

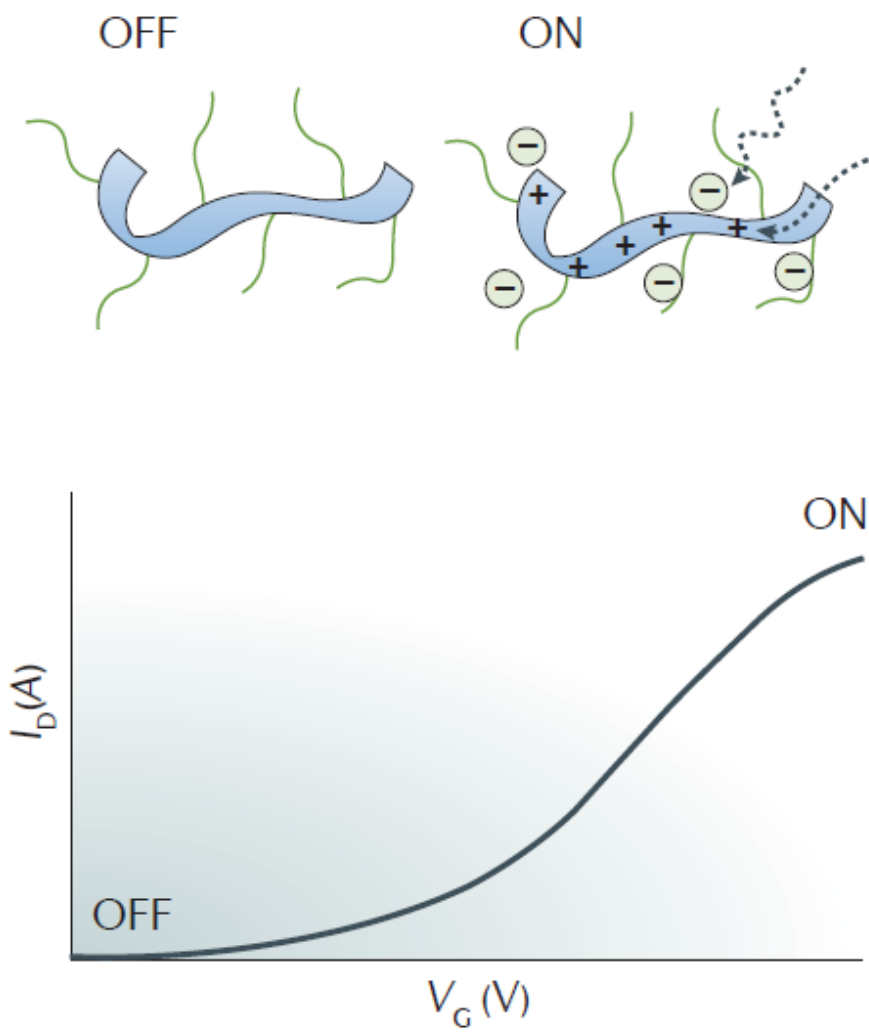


Figure 2.5: Accumulation operational mode of an OEET, [22]

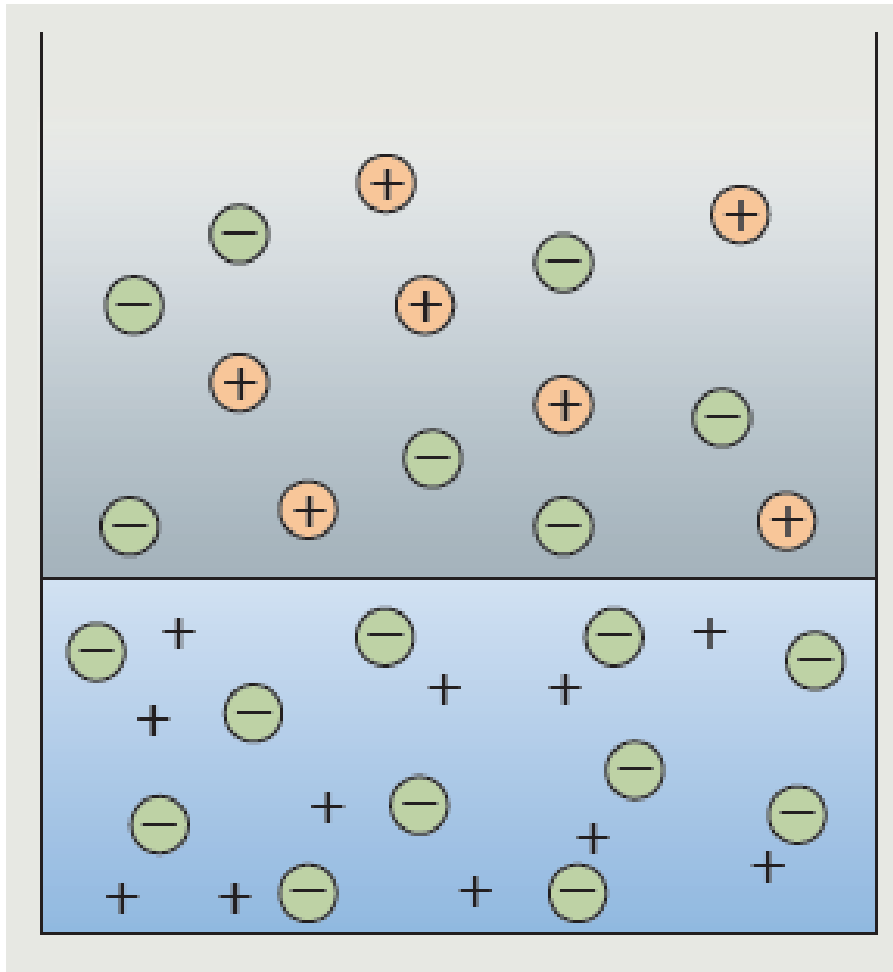


Figure 2.6: Charge distribution in the entire volume of an OECT channel, [22]

## 2.2 OEET - DEVICE PHYSICS

OEETs transduce small gate voltage signals into large changes in drain current values. To describe this transduction mechanism usually a transfer curve is exploited as a model, which plots the drain current as a function of the gate voltage. The two previous pictures show, very roughly and qualitatively, the transfer curve for depletion and accumulation modes respectively. The slope of the transfer curve represents the transduction efficiency and switching speed of the device; the higher is the slope (the steeper the transfer curve), the larger the change in drain current for a given gate voltage signal; this means that if the curve slope is very high, two very narrow gate voltage values can be distinguished (since their corresponding current values will be different) and that the device will be switched very fast with respect to an OEET characterised by a lower slope. The switching efficiency of the OEET is straightforwardly computed exploiting transconductance (which corresponds to the first derivative of the curve), and it is given by:

$$g_m = \frac{\partial I_{DS}}{\partial V_{GS}} \quad (2.1)$$

Due to the fact that OEETs response depends on the volume exposed to the electrolyte (therefore involving much more material in the process), these devices show very high transconductance values, (on the order of mS for micrometric devices) [24].

The behaviour of OEETs in steady-state, operated in depletion mode, has been described by two different approaches in literature. The first model, developed by Prigodin et al. [23],[36], considers the point of view of solid-state physics: according to this model the switching mechanism derives from a decrease of the hole mobility inside the organic semiconductor, induced by cations which enter the organic film from the electrolyte when a positive voltage is applied on the gate. A second approach, proposed by Robinson et al. [37], exploits electrochemistry and electrostatics concepts; here the switching mechanism derives from the de-doping of the organic channel which leads to a decrease of the hole density. An empirical relationship was assumed for the conductivity of the organic film and an assumed dopant density was used as a boundary condition. These assumptions allowed for numerical solutions of the steady-state current-voltage characteristics. These models, although very useful in highlighting important aspects of OEET physics, do not deal with the transient characteristics of OEETs.

As a convention, the source contact is grounded (or equivalently the voltage applied is equal to zero), while a voltage is applied to the drain contact with to the ground. When a positive gate voltage (always related to the ground) is applied, the electrolyte injects cations into the organic channel. As a consequence, the organic film is depopulated and therefore also the source-drain decreases.

Moreover OEET transconductance can be calculated very precisely exploiting Bernard's model [23]. In this model it is assumed that, in order to measure steady-state and transient response, the ions coming from the electrolyte diffuse into the channel and change its electronic conductivity in the entire volume. In order to simplify, the device can be divided into two circuits: an ionic circuit, which describes the behaviour of ions flowing in the gate-electrolyte-channel system, and an electronic circuit, which describes the flow of electrons (or holes) in the source-channel-drain structure according to Ohm's law.

OEETs and EGOETs represent two limits for ion penetration: the first ones represent the limit for free penetration into the volume of the channel (in many works it has been demonstrated how capacitance is proportional to film thickness [26],[29],[38]), while the second corresponds to the limit for accumulation at the channel surface. Other kinds of devices show a mixed behaviour which is in the middle between these two limits [39],[40], from which it can be deduced the existence of a threshold for ion injection. While the physics of injection and transport in organic semiconductors for mobile carriers have been thoroughly analysed in the last thirty years, the mechanisms of ion injection and transport in organic semiconductors still remain quite mysterious.

In electrolyte-gated OEET, other parameters occur in the device physics. The nature and geometry of the gate electrode control the fraction of gate voltage which is dropped across the channel [41],[42]. If a polarizable gate electrode, (made of Pt or Au for example), is employed, in the ionic circuit two separate capacitors will be present: one of them corresponds to the electrical double layer which is built at the gate-electrolyte interface, the second one corresponds to the channel volumetric capacitance. Since these two capacitors are in series, the applied gate voltage drops across the smaller capacitor; in order to have an efficient gating, the gate electrode capacitance must be at least ten times higher than the channel capacitance, otherwise a large fraction of the applied gate voltage will drop at the gate-electrolyte interface, as showed in Fig.2.7.

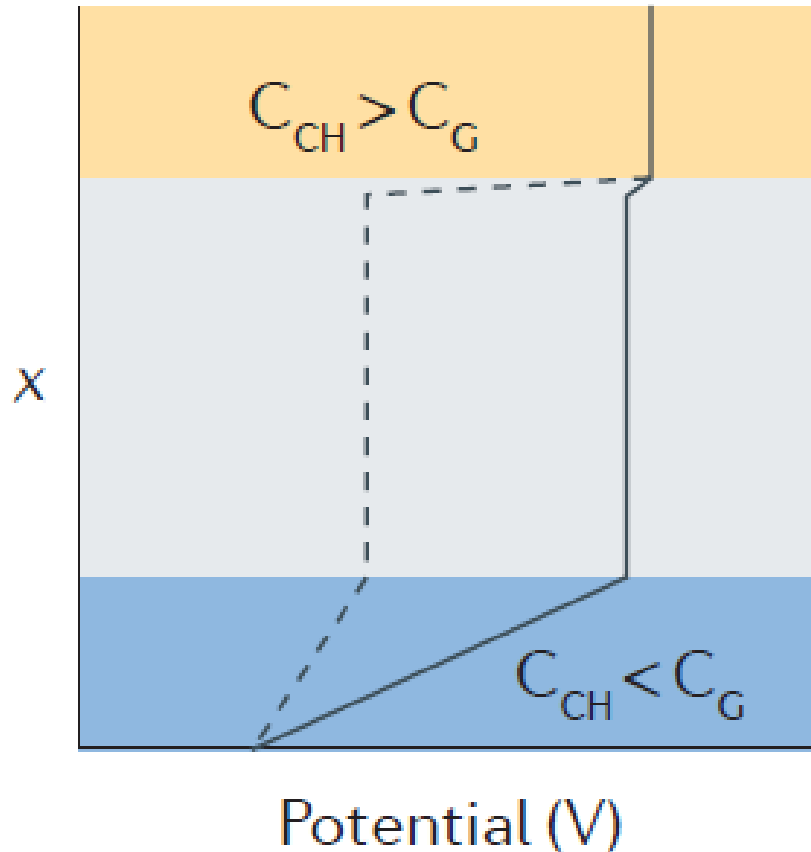


Figure 2.7: Channel and gate capacitances behaviour, [22]

Such a large gate capacitance can be obtained exploiting a thick PEDOT:PSS gate electrode or, as an alternative, a non-polarizable gate electrode, (for example as Ag/AgCl), can be used, with a negligible the voltage drop at the gate-electrolyte interface [43].

The last point to be highlighted is that the nature of the electrolyte (which can be liquid, solid, or a gel) and the ion concentration influence the response time of the transistor because the electrolyte conductivity determines the resistance of the ionic circuit [44].

### 2.2.1 Electronic Circuit

The electronic circuit (Fig.2.8) is modelled through a resistor, where the charge drifts under the influence of the local potential (the same way as in MOSFET devices); therefore hole density and mobility are two very important parameters.

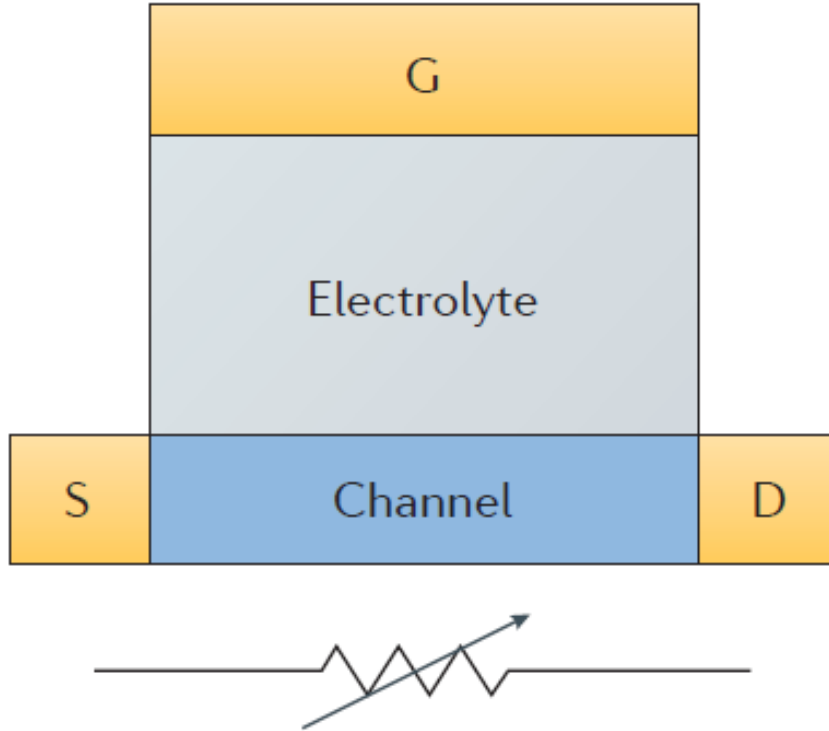


Figure 2.8: Electronic circuit model of an OEET, [22]

The electronic circuit can be modelled exploiting Ohm's law, and the current  $J$  varies along the channel length linearly with the gradient of the potential (or equivalently the electric field):

$$J(x) = q\mu p(x) \frac{dV(x)}{dx} \quad (2.2)$$

Where  $q$  stands for the elementary electron charge,  $\mu$  is the hole mobility (which is considered constant),  $p(x)$  represents the hole density and  $dV(x)/dx$  denotes the electric field. Field-dependent and carrier concentration-dependent mobilities can be implemented into the model in order to predict more accurately the device behaviour, but constant mobility constitutes a quite efficient approximation. When a positive voltage is applied through the gate, carrier concentration inside the semiconductor is described by the de-doping mechanism: cations from the electrolyte are injected into the semiconductor film, and each injected cation compensates one acceptor inside the organic film (this phenomenon corresponds to the compensation doping of silicon). This phenomenon consists in a two-step process which maintains charge balance inside the organic semiconductor film at steady-state: for each cation which enters the organic film, a hole is extracted at the source but it is not replaced by injection at the drain. The conductivity of the undoped organic semiconductor is considered negligible. In this framework, the effective dopant density in a certain

volume  $v$  (denoted by lowercase  $v$  in order to distinguish it from the voltage, denoted by uppercase  $V$ ) of semiconductor material is expressed as:

$$p = p_0 \left( 1 - \frac{Q}{qp_0v} \right) \quad (2.3)$$

Where  $p_0$  corresponds to the hole density in the organic semiconductor before the application of the gate voltage and  $Q$  denotes the total charge due to the cations injected in the organic film from the electrolyte. To simplify the model, it is considered that the organic film is not affected by the injection of negative ions in the channel. Moreover, to ease the numerical calculations, all the charge densities involved are considered to be uniform across the entire thickness of the organic semiconductor film, but this approximation limits the applicability and the validity of this model only to thin films.

### 2.2.2 Ionic Circuit

By contrast, the ionic circuit (Fig.2.9) is described by a resistor (denoted by  $R_S$ , which represents the ions flowing in the electrolyte), in series with a capacitor (denoted by  $C_{ch}$ , which corresponds to the storage of ions inside the channel). It is assumed that only a capacitive process occurs, where ions injected in the channel do not exchange charge with the organic film but electrostatically compensate the presence of opposite charges [45]. This corresponds to stating that no electrochemical reactions occur between the electrolyte and the conductive channel.

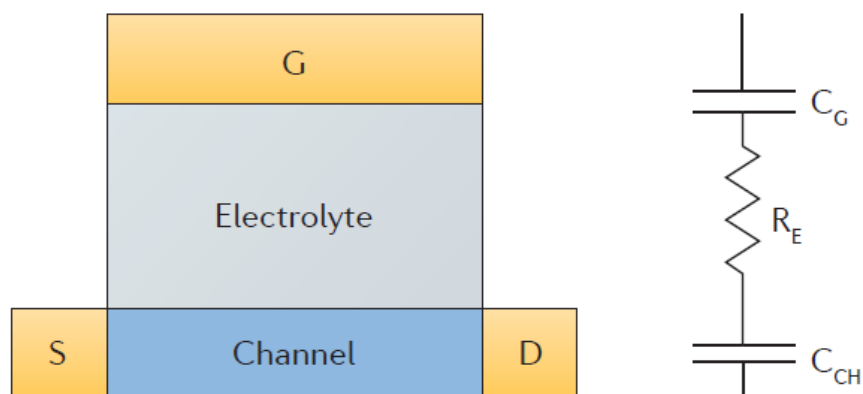


Figure 2.9: Ionic circuit model of an OEET, [22]

At steady state, the capacitor is charged and the gate current goes to zero.

The resistor represents the conductivity and, at the same time, measures the ionic strength of the electrolyte, while the capacitor takes into account the polarization at the two interfaces, between film and electrolyte and between gate and electrolyte. Since the capacitance per unit area of the PEDOT:PSS is very high (on the order of a supercapacitor capacitance), [43] it will be higher than the gate capacitance. In this model it is supposed that no reaction occurs at the gate electrode, [46],[47],[48],[32] and it is also assumed that the device operates in the so-called non-Faradaic regime (an operational background where the current induced by the redox processes is null or negligible), but this could be a problem in devices where Faradaic processes are not negligible, such as devices which operates at voltages high enough to generate electrolysis of aqueous electrolytes [49]. When a voltage is applied to the gate, the behaviour of this element is similar to the one of a charging capacitor:

$$Q(t) = Q_{SS}(1 - e^{-t/\tau_i}) \quad (2.4)$$

Where  $Q_{SS} = C_{ch}\Delta V$  is the total charge flowing through the circuit (with  $\Delta V$  representing the voltage applied across the electrolyte), while the ionic transit time is defined as  $\tau_i = C_{ch}R_S$ ; capacitance per unit area is denoted by  $c_{ch}$ . For simplicity, the concentration and potential dependence of the ionic double layer capacitance are neglected and therefore  $c_{ch}$  is considered as a constant value.

### 2.2.3 Steady-State Model

The geometry of the device channel employed to develop the model is very simple and represented in Fig.2.10.  $W$ ,  $T$ , and  $L$  represent the width, the thickness, and the length of the channel.

Considering a slice with a differential length  $dx$  along the length of the channel, the charge in the organic film at steady-state can be computed very easily exploiting the following equation:

$$Q(x) = c_{ch}W(V_{gs} - V(x))dx \quad (2.5)$$

Where  $V_{gs}$  is the voltage applied to the gate, and  $V(x)$  is the spatial voltage profile inside the organic channel. This expression states

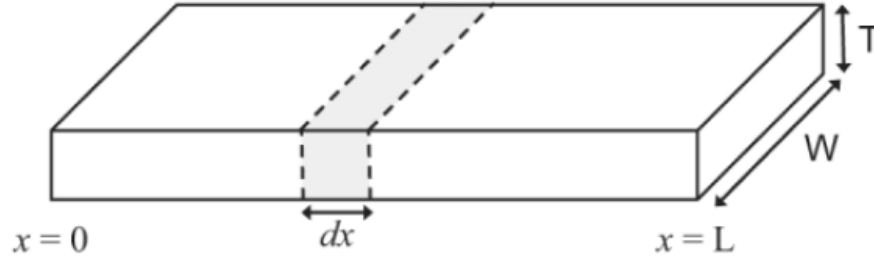


Figure 2.10: Geometrical representation of the channel, [23]

that the charge from the ionic circuit is coupled to the voltage in the electronic circuit at a position  $x$  along the organic film.

Combining this last equation with Ohm's law stated before it is possible to obtain the equation required to compute the OECT current at steady state:

$$J(x) = q\mu p_0 \left[ 1 - \frac{V_{gs} - V(x)}{V_p} \right] \frac{dV(x)}{dx} \quad (2.6)$$

Where  $V_p$  is the pinch-off voltage (defined as  $qp_0T/c_{ch}$ ); at steady-state, it is required to have the source-drain current density spatially constant due to continuity condition, therefore the previous equation can be solved explicitly for different operational regimes. Taking into account that  $V_{gs} \geq 0$ , the output characteristic (drain-source current vs drain-source voltage) will be represented by the kind of curve showed in Fig.2.11.

In the first quadrant (equivalent to  $V_{ds} > 0$ ) two regimes are present: at first, when  $V_{ds} < V_{gs}$  de-doping will occur everywhere in the channel; locating the source and the drain at  $x = 0$  and  $x = L$  respectively, the previous equation can be manipulated in order to obtain the current expression:

$$I = G \left[ 1 - \frac{V_{gs} - V_{ds}/2}{V_p} \right] V_{ds} \quad (2.7)$$

Where  $G$  (calculated as  $G = q\mu p_0 WT/L$ ) represents the conductance of the organic channel. The second regime arises when  $V_{ds}$  overcomes  $V_{gs}$ , and consequently the de-doping mechanism will occur only in that part of the device where  $V(x) < V_{gs}$ ; the current in this latter regime can be expressed through:

$$I = G \left[ 1 - \frac{V_{gs}^2}{2V_p} \right] \quad (2.8)$$

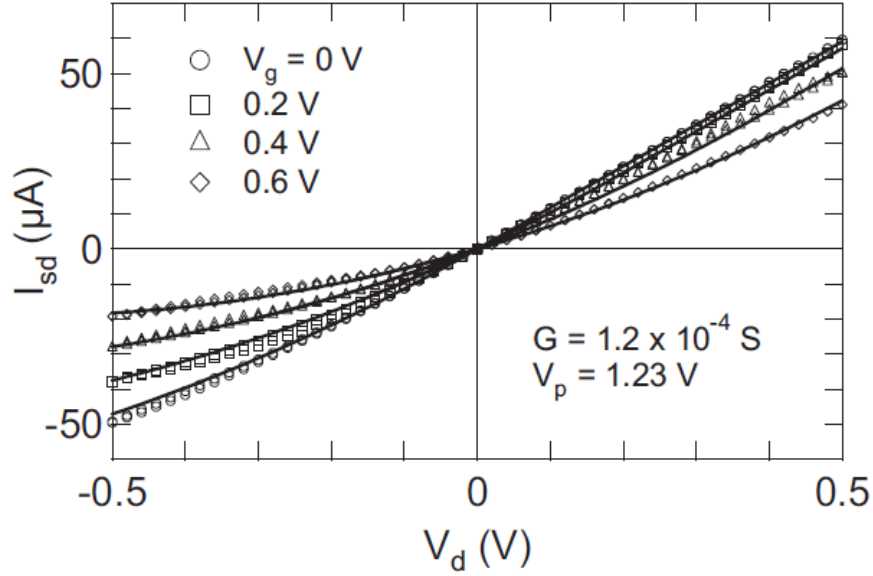


Figure 2.11: Output characteristic behaviour of an OEET, [23]

In this last regime the current varies linearly with the drain voltage; when  $V_{ds} = V_{gs}$  the linear behaviour begins.

In the third quadrant (which corresponds to  $V_{ds} < 0$ ), the organic semiconductor channel can be completely de-doped when the local density of injected cations corresponds to the intrinsic dopant density of the organic film; from a mathematical point of view, this is true when  $(V_{gs} - V_{ds} \geq V_p)$ , therefore the drain voltage value at the onset of saturation can be written as  $V_{ds,sat} = V_{gs} - V_p$ . In this situation the semiconductor will be depleted in the region near the drain contact, but the holes injected will be drifted toward the drain anyway. If  $V_{ds} > V_{ds,sat}$ , the edge of the depleted region will move toward the source. For long channel devices, the coordinate of the depleted region edge near the source contact will not considerably change with  $V_{ds}$ , consequently the source-drain current will saturate; by contrast, in short channel devices, the extent of the depletion region will be shifted appreciably while  $V_{ds}$  is increased (in absolute value), therefore saturation will not occur and the current will continue to increase[50]. In the limit of long channels, for  $V_{ds} \leq V_{ds,sat}$ , current will depend only on the saturation drain voltage at saturation for a particular gate voltage:

$$I = -\frac{GV_{ds,sat}^2}{2V_p} \quad (2.9)$$

This model is based on the assumption that steady-state is reached after the application of a gate voltage, but this is not the case if

voltage sweep measurements are performed since some deviations from the model could arise at high gate voltages [51],[50],[32],[37]. Another non-ideality factor can occur in some applications where the organic semiconductor employed is sufficiently conductive that it can be also exploited for leads, interconnects, or contacts to the organic film [46],[51],[47],[48],[32],[36],[37], where a significant voltage can drop across regions of the device which are not in direct contact with the gate; this is equivalent to the addition of a series resistance in the electronic circuit. Deviations from ideal behaviour include a larger negative voltage when saturation occurs and a reduced gating for positive drain voltage. Furthermore, it is possible to suppress gating at large positive drain voltages if the applied gate voltage is less than the voltage within the active (gated) region. In addition to transistors or logic elements, OECTs have been used for many sensing applications [7]. For these devices it is important to understand the relative, device response upon gating, and the relevant parameter is  $\Delta I_{ds}/I_{ds}$ , where  $\Delta I_{ds}$  is the change in current upon application of a gate voltage (Fig.2.12).

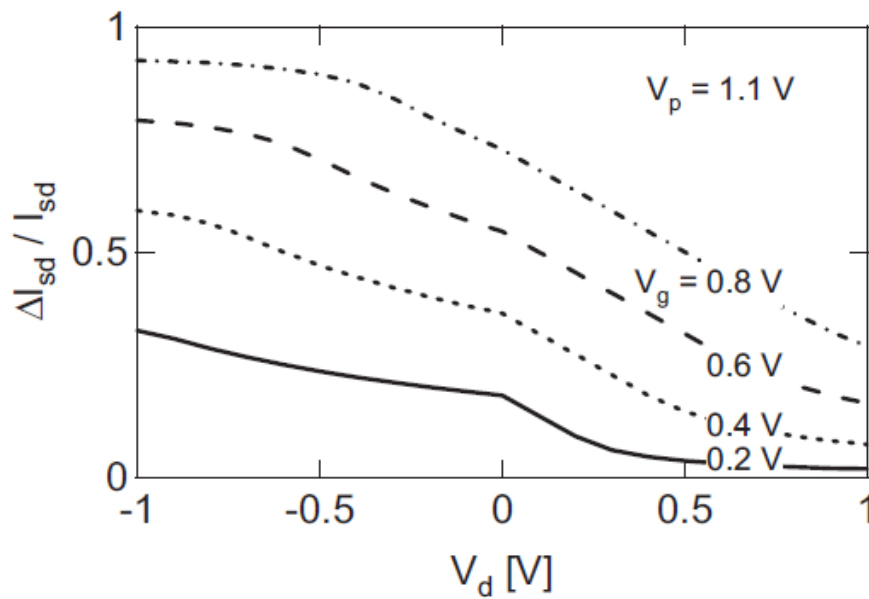


Figure 2.12: Drain-source current variations, for different gate voltages, [23]

The related device response increases with increasing gate voltage, especially at negative drain voltages.

### 2.2.4 Transient State Model

The transient behaviour of OEETs can be described taking into account two particular effects: the injection of a cation from the electrolyte into the organic semiconducting channel, and the removal of a hole at the source electrode. To simplify the calculations, the voltage and hole density spatial dependence are ignored and an average ionic current and hole density are employed.

Exploiting the expression of the effective dopant density, the transient response for current can be expressed as:

$$I(t) \approx G \left(1 - \frac{Q(t)}{qp_0v}\right) V_{ds} - f \frac{dQ(t)}{dt} \quad (2.10)$$

Where  $f$  is a proportionality constant which takes into account for the spatial inhomogeneity of the de-doping mechanism; moreover, the parameter  $f$  depends on the gate-source and drain-source voltages. Two experimental conditions have to be considered in the analysis of the ionic circuit response: constant gate current and constant gate voltage. If a constant current is forced to flow through the electrolyte, the kinetics of the ionic circuit can be changed, shifting the focus to the electronic behaviour of the OEET. With this assumption, the transient behaviour simplifies to:

$$I(t, I_g) = I_o - I_g \left(f + \frac{t}{\tau_e}\right) \quad (2.11)$$

Where  $I_g$  is the constant gate current,  $I_o$  is the output (source-drain) current before the application of a gate current and  $\tau_e = L^2/\mu V_{ds}$  represents the electronic transit time. This equation can be exploited in order to study the transient model without taking into account the ionic circuit, and furthermore this provides an easy way to extract an effective hole mobility in the organic semiconductor film. Typical constant gate current transient response characteristics are shown in Fig.2.13.

If the slope of the source-drain transient curve is plotted as a function of the gate current, it is possible to extract the electronic transit time of the device, and consequently the hole mobility [52]. After gate current is shut off, a slow recovery of the source-drain current occurs due to diffusion of cations from the organic channel back into the electrolyte. The electrolyte model (defined with an ionic circuit) described before is very useful to analyse the transient behaviour under constant gate voltage. In order to simplify the calculations, the transient behaviour is only described for the case where de-doping occurs everywhere within the organic film without saturation effects. An average voltage drop between the semiconducting channel and

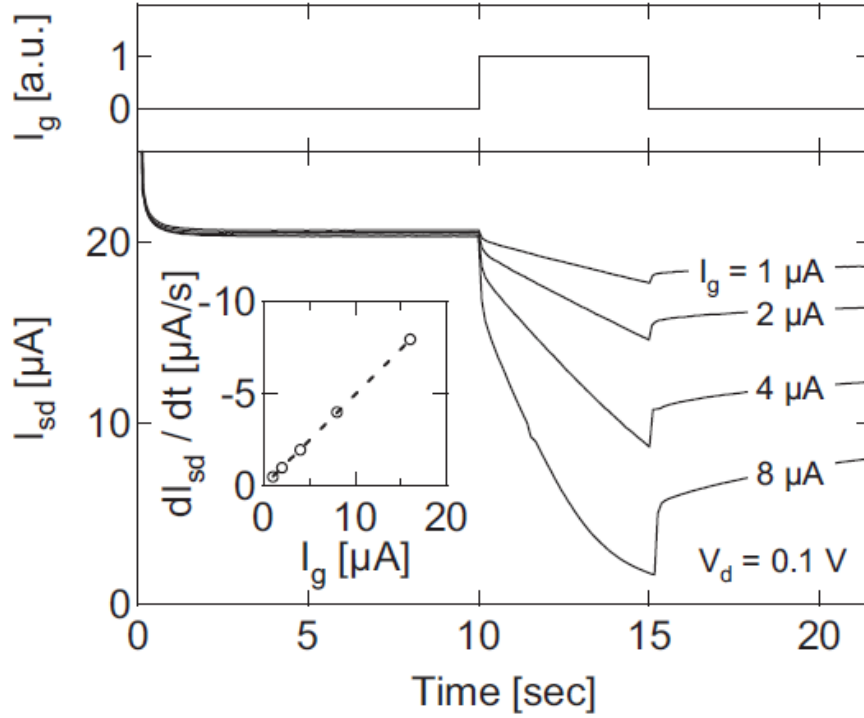


Figure 2.13: Gate current transient response, [23]

the gate electrode ( $\Delta V = V_{gs} - 1/2V_{ds}$ ) must be chosen in order to be sure that transient behaviour is consistent with steady-state characteristics. Exploiting these assumptions, the transient current can be expressed as:

$$I(t, I_g) = I_{SS}(V_{gs}) + \Delta I_{SS} \left(1 - f \frac{\tau_e}{\tau_i}\right) e^{-t/\tau_i} \quad (2.12)$$

Where  $I_{SS}(V_{gs})$  is the steady-state drain-source current at a certain gate voltage  $V_{gs}$  and  $\Delta I_{SS}$  is equal to  $I_{SS}(V_{gs} = 0) - I_{SS}(V_{gs})$ . This leads to a particular transient behaviour, as shown in Fig.2.14.

As shown in the graph, the approach to steady-state after the application of a gate voltage can be represented by a monotonic decay ( $\tau_i > f\tau_e$ ) or by the so-called spike-and-recovery ( $\tau_i < f\tau_e$ ). A monotonic decay is quite explanatory of the fact that the electronic response of the organic film (how quickly holes can be extracted from the channel) is fast enough that can be ignored when the overall transient response is analysed; this is usually the case of short-channel devices and for large drain voltages. A spike-and-recovery indicates that hole transport in the organic film occurs at a relatively slow rate and the transient current is dominated by hole extraction from the channel. Observing the previous equation, it can be stated that the transient

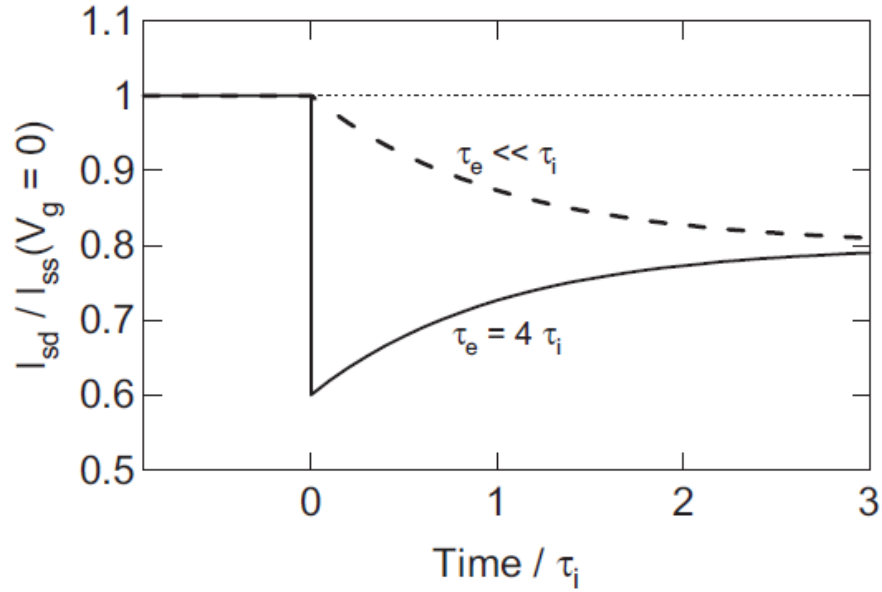


Figure 2.14: Current-time response, [23]

response of an OECT can be characterized by two time-related parameters ( $\tau_i$  and  $\tau_e$ ). The first one, the characteristic time constant for ionic transport in the electrolyte, is computed from the resistance of the electrolyte solution and from the ionic double layer capacitance. Through Gouy-Chapman theory for double layer capacitance it is obtained that  $\tau_i \sim l/C^{1/2}$  (where  $l$  represents the distance between the organic channel and the gate electrode, while  $C$  represents the ionic concentration)[43]. Decreasing the gate electrode distance from the channel or increasing electrolyte concentrations will lead to improved device response times. Since the ratio  $\tau_e/\tau_i$  appears in the equation of the current, it is useful how to calculate it, and it is obtained that  $\tau_e/\tau_i = lL^2/\mu V_{ds}$ . From this relationship, it is straightforward to state that the behaviour of the transient response can be modulated by varying the electrode location, the channel length or the drain voltage. By varying the applied source-drain voltage, the behaviour of the transient can be modified, as shown in Fig.2.15.

### 2.2.5 Transconductance Model

From a quantitative point of view, the transconductance at saturation for depletion-mode devices, can be described by Bernards model using:

$$g_m = \frac{W}{L} d\mu C_{ch} (V_{th} - V_{gs}) \quad (2.13)$$

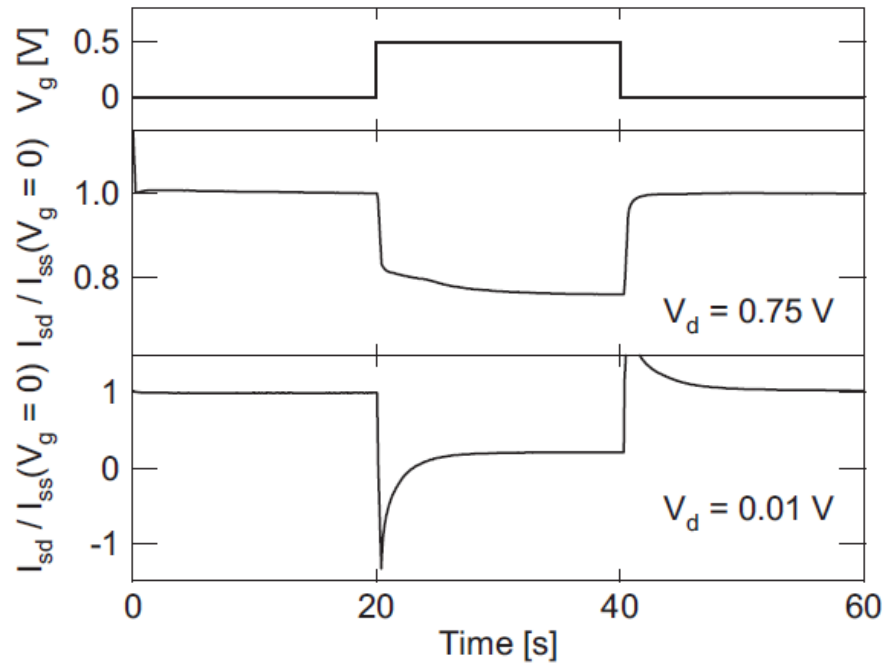


Figure 2.15: Transient behaviour of an OECT, [23]

Where  $W$ ,  $L$ , and  $d$  are the channel width, length and thickness of the transistor, respectively,  $\mu$  is the charge-carrier mobility,  $C_{ch}$  is the capacitance per unit volume of the channel, and  $V_{th}$  is the threshold voltage [29].

If the device is operated in accumulation mode instead of depletion mode, all the voltage terms are reversed in sign. This equation for FETs is very similar, but with two main differences: the product  $dC_{ch}$  is substituted by the capacitance (per unit area) of the MOS capacitor, and the channel thickness is not a parameter of the equation; by contrast in an OECT, the channel thickness is technologically controlled in order to tune the performance of the device.

The volumetric nature of electronic transduction and the high transconductance give OECTs a better amplification performance with respect to different transistor technologies [24], but with the drawback of slow operation time. The response time, according to the Bernardis model, can be limited either by the electronic or the ionic circuit [23]; in the majority of devices, the response time (obtained by taking the product of the resistance of the electrolyte with the capacitance of the channel) is determined by the ionic circuit. It is quite intuitive that the channel capacitance depends on the thickness of the channel itself, consequently as much  $d$  increases as much the OECT becomes slow. Response times around a few tens of  $\mu s$  can be achieved in OECT devices with liquid electrolytes [24]. Therefore, this is suitable for biosensing field (which involves quasi-static transistors), and in order to record electrophysiological signals [53]. If solid electrolytes or gels are used, the OECT will show slower response times, making

them very appropriate for printed electronics applications, where fast transistors are not required [4].

From voltage measurements performed along the OECT channel it can be deduced that the conductivity along the channel varies non-linearly with charge density [37]. This charge density-dependent conductivity, if inserted into the Bernards model, improves the quality of the output curve of OECT devices with PEDOT:PSS channel [54].

## 2.3 OEECT MATERIALS

The channel of OEECTs is typically realized using a conducting polymer, the most common being PEDOT and polypyrrole (PPy), which can be synthesized by solution, vapour-phase or electrochemical polymerization, and successively p-type doped exploiting small anions or polyanions. The molecule of PEDOT:PSS is showed in Fig.2.16:

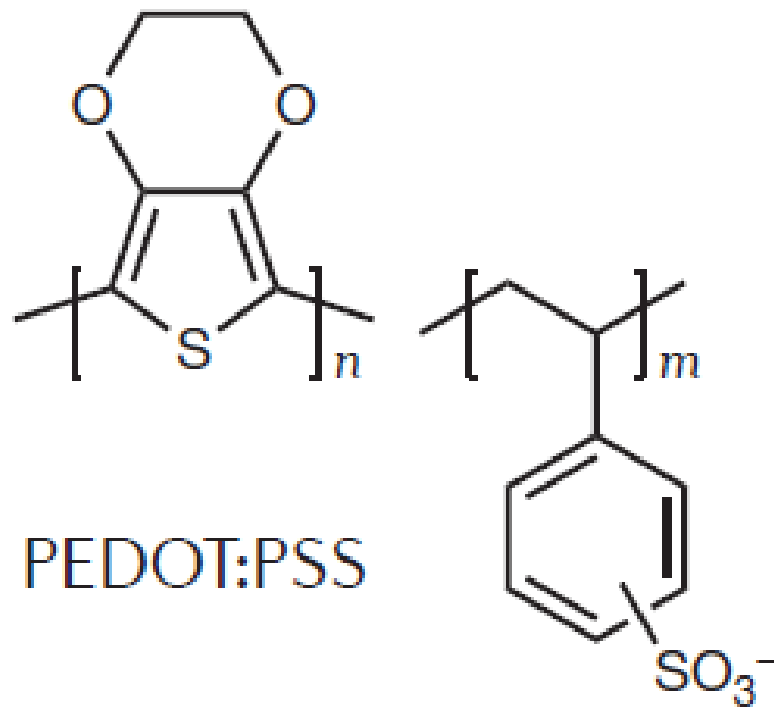


Figure 2.16: Chemical structure of PEDOT:PSS, [22]

PEDOT:PSS, has been extensively investigated and analysed for a wide list of applications in the last 15 years; its popularity comes mainly from the fact that it is commercially available in the form of aqueous solution, allowing an easy deposition of thin films [25]. To obtain this mixture, the EDOT, the monomer of PEDOT, is polymerized in the presence of PSS. Films of PEDOT:PSS obtained from these process show high carrier conductivity. Therefore, the structure and electronic conductivity of these films made of PEDOT:PSS have been extensively studied [55],[56]. Different solvents, surfactants and processes have been tried in order to maximize hole conductivity, which in these days has overcome the value of 1000 S/cm [57]. From some experiments, it can be showed that small ions inside an electrolyte and injected into PEDOT:PSS film are characterised by drift mobilities with values very similar to those in bulk water [58],[59],[60]. Another

characteristic of PEDOT:PSS films is that they exhibit very good electrochemical stability in aqueous electrolytes [61] and can be rendered insoluble in water through by adding crosslinkers molecules: two examples of crosslinkers are (3 glycidyoxypropyl)trimethoxysilane [62],[63] and divinylsulfone [64]. Nowadays, this material very suitable and appropriate for many of the OECT applications, due to its very good properties.

Another example of conducting polymer used as a functional material in OECT is PEDOT conjugated with tosylate group. In the last few years, many efforts have been employed in the research of new materials, in order to find some alternatives to PEDOT:PSS.

## 2.4 OEET PRINTING TECHNIQUES

## 2.4.1 Ink-Jet Printing

Nowadays the most employed printing techniques for OEETs is the so-called ink-jet printing, which consists in the transfer of a particular pattern (made of conductive ink), which defines the functional part of the device, on the surface of a substrate [73],[65],[66]. Generally, printing techniques can be divided into two main categories: contact and non-contact techniques, which can be also denominated impact and non-impact techniques, respectively [67]. In the first class of printing techniques, the ink is dispersed on the surface of a patterned structure which is in contact with the substrate, while in the second category the ink is distributed on the surface of the substrate exploiting nozzles on an ink reservoir which is opened or closed over a specific point according to the fact that the point is part of the pattern or not respectively, and the pattern is defined by moving either the head containing the nozzle or the substrate.

Ink-jet printing is a typical example of non-contact printing technique, and it has been thoroughly studied and applied in many research fields [68],[69], and moreover it has been successfully employed for the fabrication of a many kinds of electronic devices. In the inkjet-printing process, the conductive inks (which must be transferred on the substrate) are ejected from a nozzle in the form of single droplets, whose diameter is more or less the same as the diameter of the ejecting nozzle [70]; each droplet on the surface represents a pixel of the pattern and a solid layer is formed after solvent evaporation is performed. Inkjet-printers are characterised by two operational modes (schematically shown in Fig.2.17): continuous or drop-on-demand mode (DOD) [71],[72].

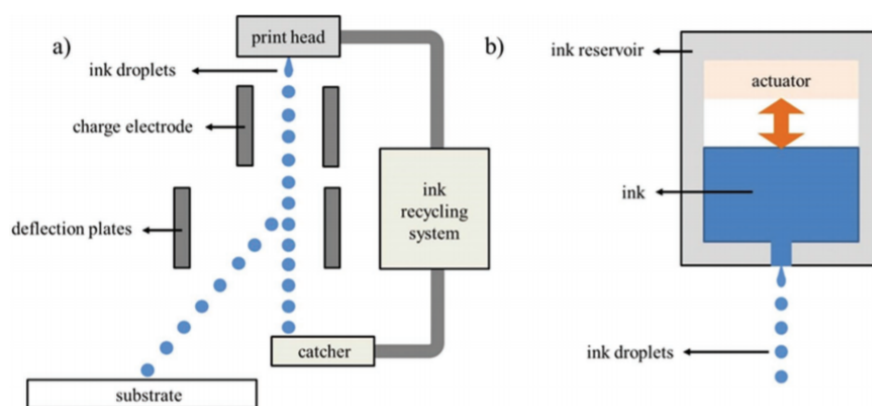


Figure 2.17: The two operational modes of ink-jet printing, [73]

In the first mode, the droplets are ejected continuously by the nozzle, then they get through a deflection system and they are deflected by an electrostatic field onto the surface of the substrate or, if they are not needed, sent away from the substrate. By contrast, in DOD systems, droplets are ejected only when they are needed to hit the substrate. In printed electronics, usually the continuous mode is not used, since the exposure of the droplets to particular environmental conditions could contaminate the ink.

Inkjet-printing is characterized by some advantages with respect to other printing techniques: first, being a digital technique, it does not require a printing master (the device or circuit design can be modified through the software); it requires smaller amounts of inks (leading to less waste amounts) with respect to screen printing or gravure printing [70],[74]; it can be easily adapted to any size of production scale [75]. Despite these advantages, inkjet-printing shows some drawbacks: it is characterised by some constraints in the physical properties of the ink used (such as dynamic viscosity and surface tension), which consequently limits the number of materials which can be deposited [68]; lateral resolution is not so high due to the typical diameter of the generated droplets (around tens of  $\mu\text{m}$ ) [76]; it is characterised by a very low throughput speed, several orders of magnitude lower than the ones showed by printing techniques [68].

Other techniques which are exploited to print OEET devices are the screen printing, which consists in the transfer of a conductive ink on a substrate except for the areas of the substrate covered with a shutter or a stencil, and gravure printing, which consists in engraving the final design on the substrate using two complementary rotatory cylinders (filled with the conductive ink). Despite the fact that these techniques are easy to implement for many kind of devices, they are becoming even less popular with respect to the ink-jet printing due to the fact that the resolution and the performance of the devices manufactured with these two techniques are much worse.

#### 2.4.2 *Stereolithography*

The novelty of this work consists in employing, as a 3D-printing technique for OEET, the so-called stereolithography, which is a solid free-form technique (SFF). Introduced in 1986, stereolithography remains one of the most powerful and versatile of all SFF techniques, since it is characterised by one of the highest fabrication accuracies and increasingly more materials can be printed with it [77]. From the point

of view of accuracy and resolution, stereolithography is the best one among all the SFF techniques, since while in most fabrication techniques the smallest details are around 50-200  $\mu\text{m}$  in size, many stereolithographic printers can generate features with an accuracy of 20  $\mu\text{m}$ . Stereolithography setups have been developed which exploit the two-photon initiation mechanism for polymerization reaction, leading to the fabrication of micron-sized structures with sub-micron resolution [78].

Stereolithography consists in an additive fabrication process which allows the fabrication of parts starting from a computer-aided design (CAD) file; the latter describes the geometry and size of the parts to be printed. Therefore, the STL file format was developed, and it will be the one used in this work, since a stereolithographic printer will be used. An STL file lists the coordinates of triangles that together form the surface of the entire 3D structure. The structure is virtually divided in layers with the same thickness used in the layer-by-layer fabrication process (often in the range 25-100  $\mu\text{m}$ ). At the end, all the data are uploaded into the stereolithography apparatus (SLA) and the structure is printed, as shown in Fig.2.18.

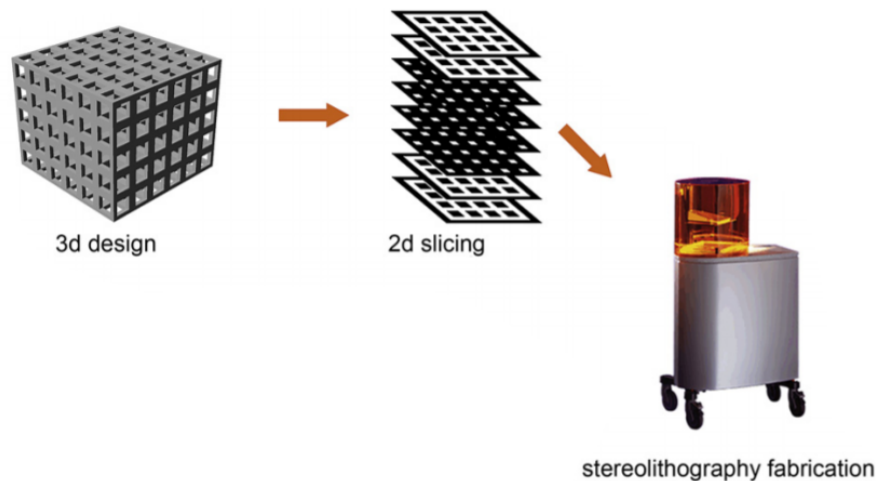


Figure 2.18: Stereolithography main steps: 3D design realization, 2D-slicing, printing; [77]

The manufacturing of 3D objects employing stereolithography is based on the controlled solidification of a liquid resin through a mechanism of photo-polymerization. Exploiting a laser beam and a building stage both controlled by a computer, a pattern is illuminated on the surface of a resin. As a consequence, the resin in the pattern is solidified to a defined depth, which is made to adhere to a support platform. After photo-polymerization of the first layer is performed, the platform is moved away from the surface and the built layer is recoated with new liquid resin. A pattern (often the same as the pre-

vious one) is then cured in this new second layer. If the curing depth is slightly larger than the platform step height, good adherence to the first layer can be obtained due to the fact that unreacted functional groups on the solidified structure in the first layer polymerize with the cured resin in the second layer. These steps are repeated to construct a solid, three-dimensional object, until the computer has finished to read the inserted design. After washing the excess unpolymerized resin, a post-curing step with ultraviolet light is often performed in order to improve the rigidity and the mechanical properties of the structures through the conversion of reactive groups (since before this step it is incomplete). A scheme of this system is showed in Fig.2.19.

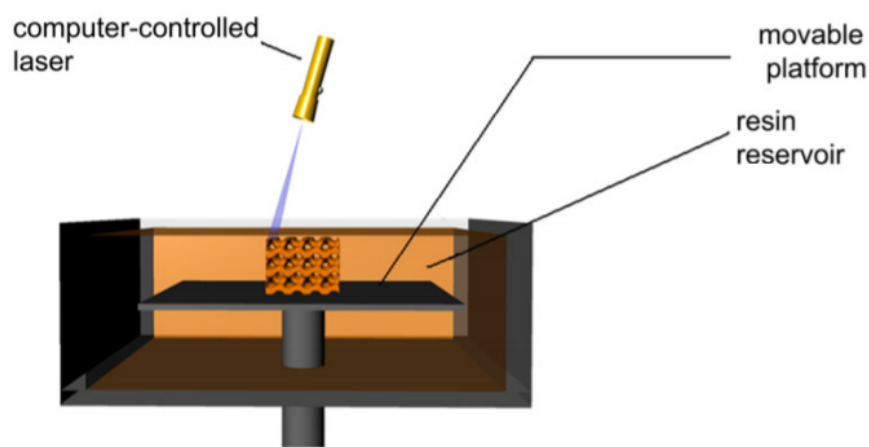


Figure 2.19: Scheme of the internal structure of a bottom-to-top stereolithography apparatus, with laser, moveable plate and resin reservoir; [77]

Structures are manufactured with a bottom-to-top approach starting from a support platform which moves below the resin surface. A very thin layer of resin is illuminated from above, and cured on top of the structure as it is built in a layer-by-layer manner.

A top-to-bottom approach (shown in Fig.2.20) is becoming increasingly more popular.

With this setting, the light is projected on a transparent, non-adhering plate from underneath (the transparent plate forms the bottom of the vessel that contains the resin), and the support or the platform is dipped into the resin from above. Even if the mechanical stresses enforced on the structures are stronger, since the objects must be separated from the bottom plate after each layer has been illuminated,



Where  $D_p$  and  $E_c$  denote the penetration depth and the critical energy, respectively, of a specific resin for a specific setup. If the cure depth is plotted as a function of the applied irradiation dose, a working curve is obtained, which helps to determine and set the correct settings for stereolithography fabrication. The previous expression derives from the Lambert-Beer equation, which describes the exponential decay of light intensity when it is absorbed by a medium. In photo-polymerizations, the time at which the gel point is reached linearly depends on the light intensity at that specific location; consequently, the cure depth increases logarithmically with time, and therefore also with the applied irradiation energy. When the energy amount exceeds the critical energy required to reach the gel point, a solidified layer forms at the resin surface. The critical energy depends on the concentrations of photo-initiator, of dissolved oxygen and of other inhibiting species. The penetration depth of light into the resin is strictly linked to the extinction coefficient of Lambert-Beer equation. A high value of this parameter corresponds to a low light penetration depth, leading to a very accurate control of the polymerization process and a strongly reduced over-cure rate. The penetration depth can be decreased by increasing the photo-initiator concentration, or by including a dye in the resin (since it competes with the photo-initiator in light absorption phenomena). Reducing the penetration of the light into the resin will lead to longer building times.

## MATERIALS

---

The materials, chemicals, and solvents employed in this work are:

- Acetone, purchased from Sigma-Aldrich
- 2-propanol (isopropyl alcohol), purchased from Sigma-Aldrich
- Ethanol (ethyl alcohol), purchased from Merck Group/Carlo Erba
- Sulphuric acid, purchased from Sigma-Aldrich
- De-ionized water
- Poly(ethylene glycol) diacrylate (PEGDA-575), purchased from Sigma-Aldrich
- Phenyl(2,4,6-trimethylbenzoyl)phosphine oxide (Irgacure 819), purchased from BASF
- Poly(3,4-ethylenedioxythiophene)-polystyrene sulfonate (PEDOT:PSS, Clevios PH 1000), purchased from Heraeus
- Dimethyl-sulphoxide (DMSO), purchased from Technic
- Silver conductive paint, purchased from RS
- Spot HT, purchased from Spot-A Materials

## 3.1 PEGDA-575

The poly(ethylene-glycol)-diacrylate (acronym: PEGDA) is a polymer whose structure can be easily understood looking at his name: its basic structure is formed by a long chain of poly(ethylene-glycol), shown in Fig.3.1.

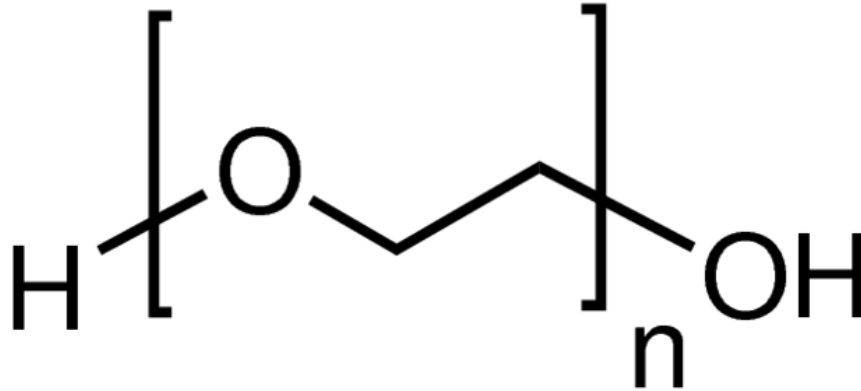


Figure 3.1: Chemical structure of poly(ethylene glycol), [84]

Each chain is characterised by a certain length, denoted by the subscript  $n$ . The fundamental molecule of PEGDA differs, from the one of simple PEG, in the termination groups, since it presents two acrylate groups on the two sides of the chain, as shown in Fig.3.2.

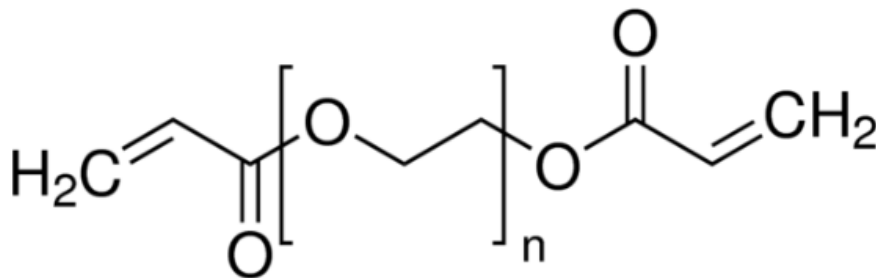


Figure 3.2: Chemical structure of poly(ethylene glycol)diacrylate, [84]

The length of the chain, or equivalently the number of monomers which constitutes the entire molecular chain, is denoted by the subscript  $n$ ; inside the polymeric resin, each chain is characterised by a different length, and therefore by a different molecular weight, and all together they determine the average molecular weight, defined as the statistical average molecular weight of all the polymer chains inside the system. Mathematically, it is expressed as:

$$M_n = \frac{\sum N_i M_i}{\sum N_i} \quad (3.1)$$

where  $M_i$  denotes the molecular weight of a single chain and  $N_i$  is the number of chains with that specific molecular weight. Average molecular weight can be predicted considering the polymerization mechanism exploited and can be determined using methods which calculates the number of molecules in a sample of a given weight. This parameter affects the mechanical properties of the resin, in fact a higher average molecular weight means having a resin characterised by a higher viscosity (since it will have longer chains). Moreover it will lead also to a lower reticulation rate since the number of acrylate termination groups (which ensures the reticulation of the polymer from resin form to solid state) is reduced in the entire volume with respect to a resin with a lower average molecular weight. Furthermore, longer chains bestow better elastic properties to PEGDA, since they withstand better to mechanical stresses, while resins with low molecular weight exhibit shorter and more branched chains which reduces mechanical resistance [85]. In this work, a PEGDA with an average molecular weight equal to 575 g/mol has been employed.

Regarding optical properties, PEGDA is transparent to visible light. Therefore, when mixed with PEDOT (which by contrast is black) they can be easily distinguished using an optical microscope [86].

This polymer is commercially available in the form of hydrogel, and recently it has gained a lot of popularity in biomedical field mainly due to two advantageous properties: low cytotoxicity, and high biocompatibility [87]. In this work, PEGDA-525 was purchased from Sigma-Aldrich.

## 3.2 PHOTO-INITIATORS AND IRGACURE 819

A photo-initiator, a molecule or a compound which can create reactive species when exposed to UV or visible radiation, is required in order to start the reticulation. Many resins exist whose polymerization is triggered by the absorption of UV or visible light, and in this case this mechanism of reticulation is called photo-polymerization. The radiation which impinges on the polymeric system provides only the energy required to start the reaction (and this step is called initiation) but it doesn't affect the following steps of propagation and termination, which are only temperature-dependent reactions. Photo-initiators can be exploited in both main classes of polymerization: radical, which consists in the formation of the long chain through the addition of free radicals which successively add up to the end of the main chain, and ionic, where the reactive species which lead to the formation of the chains are the ions inside the solution. Photo-initiators can be organic or inorganic compounds. When they absorb a sufficient amount of energy from the light, they split and transform in intermediate reagents, in most cases radicals. The photo-initiator must be characterised by a very high absorbance relative to the wavelength of the impinging radiation in order to undergo a fast splitting and generation of radicals.

Radical polymerization starts after the emergence inside the system of a free radical which is able to interact with the monomers or with the previously formed chains. The free-radicals bond themselves to a monomer (or to another chain) leading to the formation of a macro-radical (a big molecule with a radical at one of its ends), which in turn will bond to another monomer or chain. All these successive steps lead to a rapid increase of the molecular weight. After the first radicals have been formed and the polymerization has been initiated, the propagation step occurs. This phase of the polymerization consists in the addition of the various monomers to the long polymeric chains through the mechanism of radical addition, leading to a general lengthening of the molecular chains (if the monomers add up to the end of the chain) and to the ramification of the system (if the monomers are linked to a point inside the chain). Propagation will proceed until any chain long enough to establish additional ramifications (due to the interaction between different chains) or elongations can be found inside the system. The last phase of polymerization is called termination, and it can occur through three different mechanisms: recombination, disproportion and inhibition. Recombination takes place when two polymeric chains are linked to one another in order to form a single bigger and longer chain, exploiting two radicals at the end of each chain. Disproportion instead is the prevailing mechanism when two chains do not bond together but instead react

with the transfer of a hydrogen atom from one chain to the other, terminating with two different chains. Inhibition occurs when a free radical is used to terminate the chain and occluding a further radical propagation.

Photo-initiators can undergo a very fast splitting of their bond upon the absorption of a photon of the incoming radiation, or alternatively they can form excited states (called triplets) which decay after a long time yielding the possibility of creating a second reaction (such as the transfer of a hydrogen atom which leads to the creation of another radical). Typically the photo-initiators which belongs to the first class contain aromatic carbonyl groups, which absorb the energy of the impinging radiation breaking the C-C bond near this group, and leading to the formation of the radical; in this case, the formation of the radical is energetically favoured with respect to the formation of an excited state such as a singlet or a triplet. By contrast the photo-initiators of the second kind need a co-initiator in order to jump to an excited state, which in this case is an energetically predominant phenomenon. In fact, after the absorption of a photon, the triplet excited state is favoured with respect to the breaking of the C-C bond adjacent to the aromatic carbonyl group, due to the fact that the energy required for the triplet state is lower than the energy required to break the bond. Then the triplet state reacts with a co-initiator (usually an alcohol or an amine) ejecting a hydrogen atom in order to reach a state with a lower energy, leading to the generation of a radical on the co-initiator.

In this work, was employed a photo-initiator called phenyl(2,4,6-trimethylbenzoyl)phosphine oxide (commercial name: Irgacure 819), which is a photo-initiator belonging to the class denominated BAPO (bis(acyl)phosphanoxides), and it has gained a consistent popularity for stereolithographic processes. This kind of photo-initiators can be synthesized in two ways: in a more traditional one starting from phosphane and two acyl chlorides which, in the presence of a base, they lead to the formation of a bis(acyl)phosphane (called BAP) and then to a bis(acyl)phosphanoxide after oxidation using hydrogen peroxide; a second way to synthesize it consists in exploiting the reaction between a phosphorus anion (bound to two metallic atoms) and an acyl chloride. In particular Irgacure 819 is synthesized starting from dichloro-phenylphosphine ( $\text{PhPCl}_2$ ), lithium ion, and 2,4,6-trimethylbenzoyl chloride. The structure of Irgacure 819 is shown in Fig.3.3.

This molecule is able, upon absorption of UV light, to create radicals, which are very reactive and can lead very easily to the reticulation of polymers that contain acrylate groups. The formation of



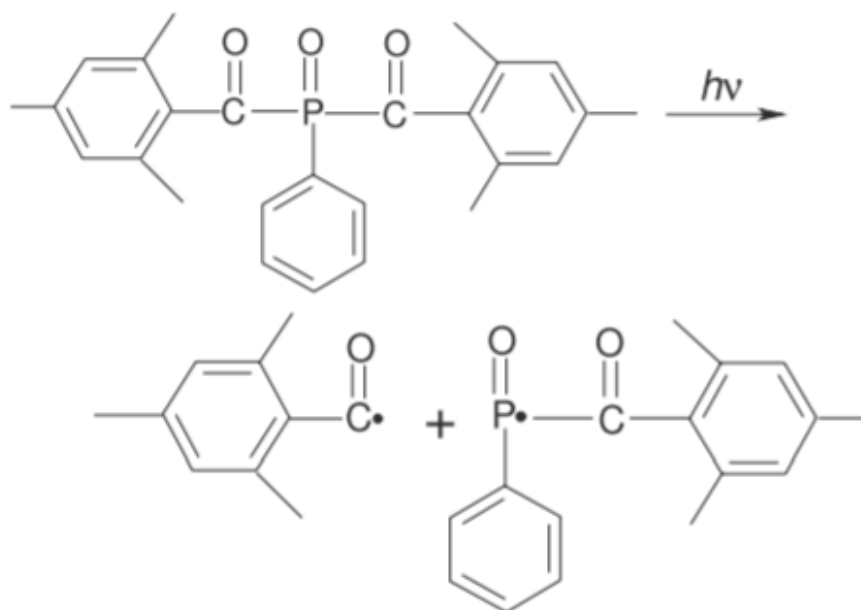


Figure 3.4: Radical formation starting from Irgacure, [84]

polymer; this mechanism is denominated cross-linking of the polymer.

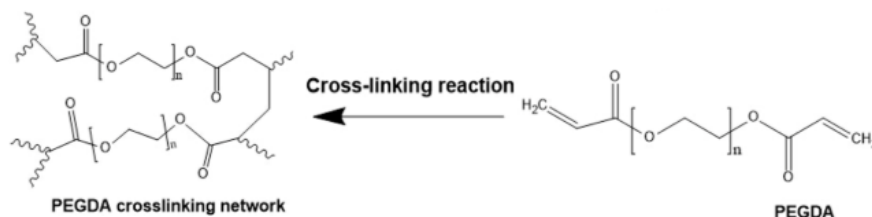


Figure 3.5: Cross-linking mechanism, [84]

After the reaction is complete, the remaining monomers and radicals are eliminated. After the photo-polymerization, PEGDA becomes a thermosetting polymer, which means that after this process it can not be shaped or plastically deformed.

Photo-initiators belonging to the class of BAPO are consistently exploited since, the presence of a phosphorus atom in the center of the molecule leads to a faster rate of phosphoric radical formation and consequently to a higher reactivity with acrylate groups, as demonstrated in the works of Sumiyoshi. Moreover, the presence of the two 2,4,6-trimethyl-benzoyl groups linked to the phosphorus atom make this photo-initiator bifunctional, since from a single photo-initiator molecule two radicals will be formed.

Photo-initiators of the class of BAPO undergo radical activation and formation at a wavelength in the range between UV and visible, therefore around 350 – 430nm. In particular, for Irgacure 819, absorption peak arises just before 400nm for short exposure times and slightly above 400nm for longer times of exposure (Fig.3.6).

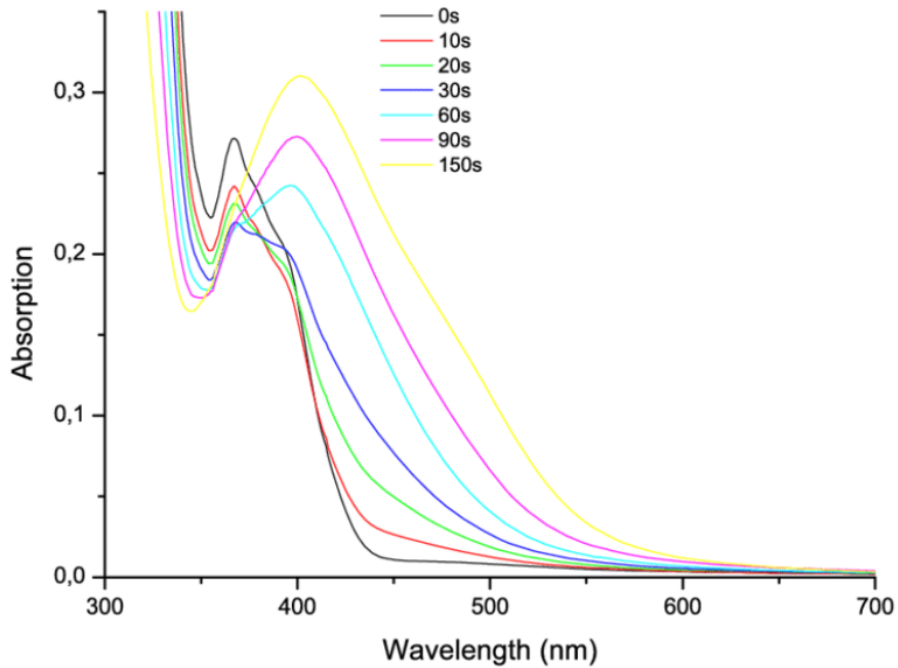


Figure 3.6: Absorption spectrum of Irgacure 819, [84]

Radiation with a wavelength in this range can penetrate more efficiently inside the resin, while light characterised by a shorter wavelength, even if it will be more energetic, will have a lower absorption length, polymerizing only the surface of the resin.

In this work, Irgacure 819 was purchased from the company BASF.

### 3.3 CONDUCTIVE POLYMERS AND PEDOT:PSS

In order to fabricate a functional and operative device a conductive polymer must be exploited. Conductive polymers constitute a class of plastic materials which mix the good mechanical and physical properties of polymers, such as good chemical versatility and biocompatibility, good processability, high flexibility, low cost of production, with the efficient electrical properties typical of semiconductor materials. For this reason, they find various applications in different fields: in electronics as diodes, electrodes, supercapacitors, batteries, OLED, solar cells; in biomedical engineering as biosensors and bioactuators, drug delivery systems, and in tissue engineering [88]. Despite all these attractive properties, conductive polymers show some drawbacks such as low thermal stability and low environmental stability since moisture and air humidity worsen their physical and electrical properties [88].

Two different kinds of conductive polymers exist: the extrinsic conductive polymers (ECP) constituted by an insulating or dielectric polymer matrix which is made conductive using a conductive filler (which can be inorganic such as metallic powders or organic), and the intrinsic conductive polymers (ICP) which are intrinsically conductive due to their atomic and molecular structure.

Therefore, in extrinsic conductive polymers a composite material is formed, and according to the amount of filler inside the polymeric matrix and to the dispersion efficiency of the filler itself, a general sigmoidal behaviour of the electrical conductivity with respect to the amount of filler is obtained (Fig.3.7).

For low volume portions of the filler the effect of the latter is not significant and the conductivity is very low close to the one of the insulating matrix. At certain volume portion of the filler a sharp increase in conductivity can be noticed due to the fact that the amount of filler is high enough to make the polymeric matrix conductive (the conductivity sharply increases in a very narrow range of filler concentration). Finally, for high volume portions of the filler a saturation of the conductivity occurs. Percolation is explained with the fact that a conductive path is achieved inside the material thanks to the conductive charges inside the matrix [89],[90],[91].

The nature of the filler used can be metallic, such as particles made of iron, copper, aluminium, nickel, silver, gold. Also other inorganic fibres or particles can be used, provided that they are covered and functionalized with some metallic material. Another choice can be

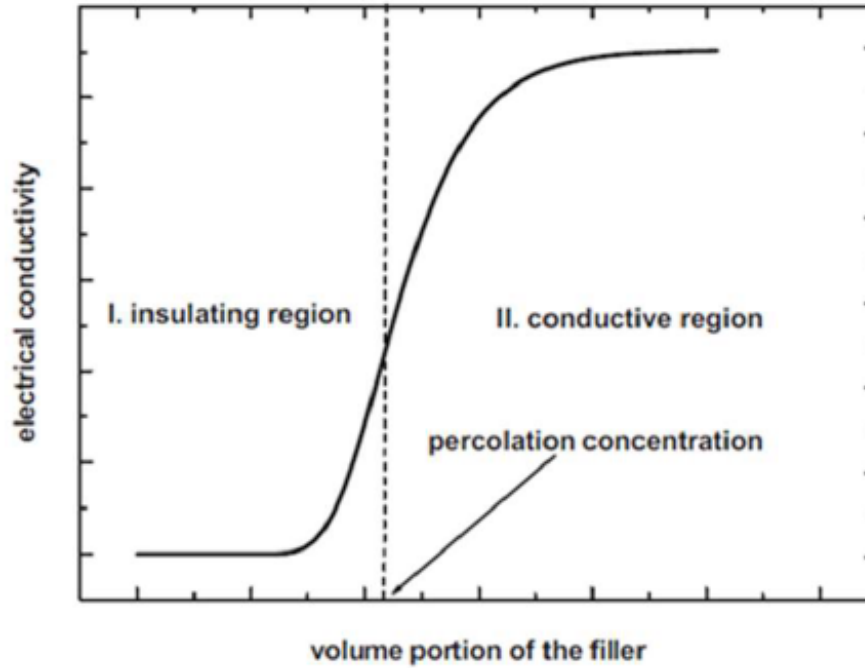


Figure 3.7: Sigmoidal model of the percolation curve, [84]

employing a filler of carbon nature, in the form of carbon black, graphite, graphene, or carbon nanotube [92]. The improvement of the conductive properties of the resin can be achieved also exploiting an ICP: the final product will be constituted by two different polymeric phases.

A polymer, in order to be electrically conductive without the addition of a filler, must present a conjugate structure, which means showing an alternation of single and double bonds among the carbon atoms along the polymeric chain. A carbon atom is characterised by four valence orbitals which can lead to some hybridizations, in particular if a double bond is present this atom show an hybridization denominated  $sp^2$ ; with this hybridization, three of the orbitals can form very strong  $\sigma$ -bonds, while the remaining orbital forms a weaker bond with the adjacent atom, and this bis denominated  $\pi$ -bond. Since all the  $\pi$ -orbitals of the carbon atoms are located over the plane of the molecule, all of these orbitals coming from all the double bonds along the chain overlap with one another leading to a delocalization of the electrons on the macromolecule. This phenomenon has also a quantum physics reason, since the alternance of single and double bonds decreases the extent of the forbidden energy gap between valence and conduction bands to a value around 1.5eV, which is very similar to the energy gaps of semiconductors. Despite this fact, and although the conductivity is increased with respect to polymers with saturate bonds, the conductivity of these conjugate molecules is

still lower than the conductivity of semiconductors [93].

Therefore, a doping must be performed, and this can be accomplished with a redox reaction (leading to a p-type or n-type doping): with an oxidative process (exploiting Br<sub>2</sub>, I<sub>2</sub>, or AsF<sub>5</sub>) which leads to the oxidation of the polymeric chain and to the reduction a free radical with a positive charge (radical cation) [93]. Consequently, this leads to a decrease of the number of the electrons present on the chain. Alternatively, with a reductive process, where the chain is reduced and the doping agent is oxidized, leading to an increase of negative charge along the chain. In both cases, the charge is delocalized along the chain which leads to a decrease of the ionization energy and to an increase of the electronic affinity, allowing the generation of new charges. Doping allows the charge to flow along the polymeric chain due to the formation of intermediate sub-bands between the valence and conduction bands. In fact, in this way the electrons are weakly bound to the chain and can jump from one chain to the other when a voltage is applied, leading to the generation of a current. This process increases the conductivity of the polymer by orders of magnitude [93].

In an oxidative process, a spatial distortion is generated around the charge, due to the higher energy left on that portion of the chain, and this distortion leads to an enclosing of the charge by the polymeric reticule, which localizes the charge and, with the generated radical cation, forms a structure denominated polaron (Fig.3.8). This polaron constitutes a localized state inside the forbidden gap of the polymer and permits the electrical conductivity since it moves along the chain when a voltage is applied.

If another oxidation is performed, the radical cation of the polaron is removed, leading to the creation of another structure called bipolaron; thanks to this mechanism is possible to create a double polaron which is energetically favoured with respect to two single polarons added together. Another structure that can be formed is the so-called soliton, which consists in an electronic wave which moves along the molecular chain at constant velocity; this entity is translated in the band structure with the arising of localized levels inside the forbidden gap, increasing the conductivity. If the polymer is heavily doped, a continuous band is formed merging the levels of polarons, bi-polarons and solitons.

Applying a voltage between the ends of the polymer chain the charge can be moved leading to the generation of a current [94]. There

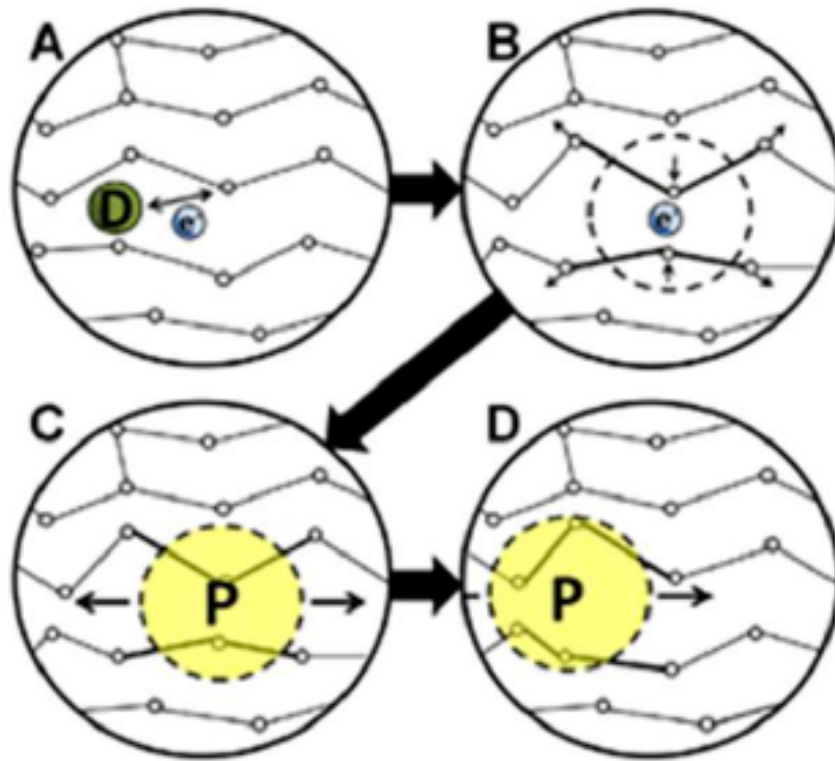


Figure 3.8: Polaron generation mechanism, [84]

are two mechanisms through which the charge is transported along the chains: the first one consists in the transport of charge through localized spots or through energetic levels of polarons, bi-polarons and solitons; with the second mechanism the charge is moved exploiting tunnel effect.

Intrinsically conductive polymers show some drawbacks: the most important one is the fact that they are often insoluble in many solvents, due to the alternance of single and double bonds which stiffen the chains. The solubility of these polymers in organic solvents can be achieved through the functionalization with appropriate substituents along the chain. But this mechanism does not constitute a valid solution for doped polymers: even if the solubility is improved, the electrical properties are worsened due to the fact that introducing certain substituents along the chain limits the effect of polarons generation, leading to a less efficient doping and decreasing the conductivity [95]. An alternative can be realized placing counter-anions in correspondence of the substituents, using a protonic acid. In this way, the electrical properties can be tuned controlling the size and the mobility of the counter-ion of the dopant [96]. Another drawback of conductive polymers is that the conductivity falls off with time. This decrease of conductivity is due to an increase of oxygen atoms number inside the polymeric chain. This process is irreversible, in fact covalent bonds

are formed between oxygen atoms from the air and carbon atoms in the chain, which break the alternance of conjugated single and double bonds, interrupting the path for the transport of charge [97].

The polymer called poly(3,4-ethylenedioxythiophene), PEDOT, belongs to the ICP class, and it is one of the most intensively studied conductive polymers due to its high conductivity, low cost, biocompatibility and good mechanical properties. In fact, PEDOT is employed for a large variety of applications.

Physical properties of PEDOT are determined by the morphology, by the crystallinity and by the molecular weight of the chains which form the polymer. Furthermore, another important fact which affect the properties of PEDOT is the doping level which will determine its conductivity.

PEDOT is produced exploiting a process of chemical or electrochemical polymerization of the EDOT monomer. A typical reaction involves the molecule of EDOT and the iron(III) p-toluenesulfonate [98]. The reaction consists in two successive steps (Fig.3.9): the oxidative polymerization of the monomer in order to obtain poly-thiophene (which is a neutral molecule); then, oxidative doping of the poly-thiophene in order to obtain a conductive poly-cation occurs.

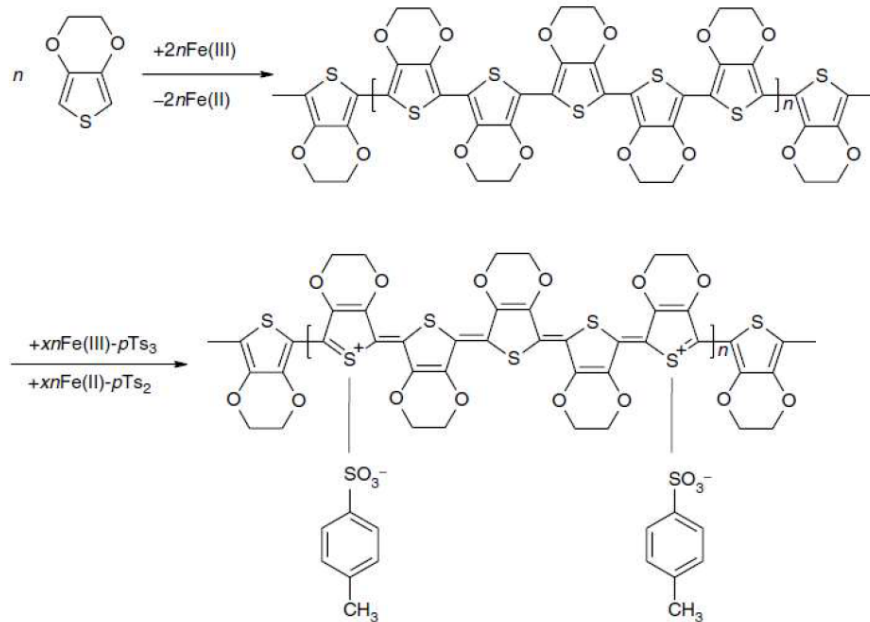


Figure 3.9: EDOT polymerization reaction, [84]

Reaction speed is determined by the slowest step (this is the so-called principle of the rate-determining step), and each one is characterized by a specific reaction rate constant. In this reaction oxidation of EDOT monomer into a polycation occurs. Then there is formation of dimers starting from the free radicals and followed by the oxidation of these dimers. Once a sufficient number of dimers has been generated, the process goes on with the propagation of the chain. At the end the termination groups of each chain are oxidized and successively they react between one another in order to form the final chains of PEDOT. At the end of the polymerization process, the oligomers are further doped through successive oxidations (Fig.3.10).

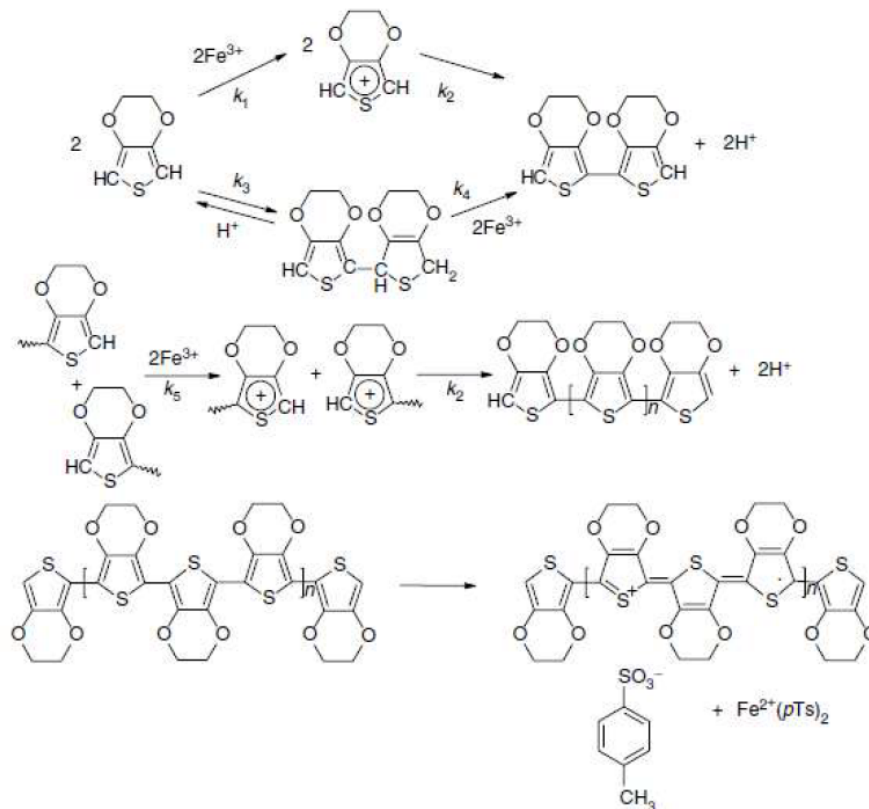


Figure 3.10: PEDOT doping mechanism, [84]

Since PEDOT is insoluble in the most commonly used solvents, poly-styrene sulfonate (PSS) is exploited in order to increase its solubility: PSS is a water-soluble polymer, and enhances the dispersion of PEDOT in aqueous solutions, through the formation of a complex denominated PEDOT:PSS. The structure of PEDOT:PSS is showed in Fig.3.11.

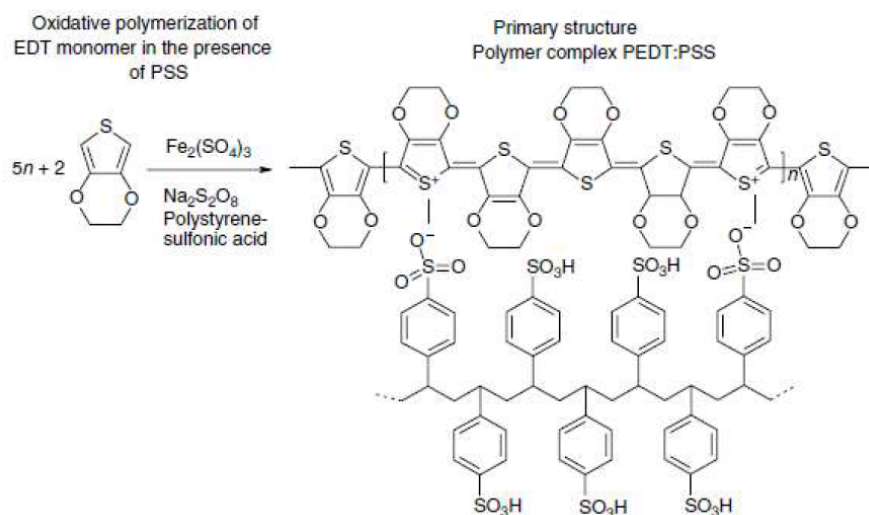


Figure 3.11: PEDOT:PSS formation, [84]

PSS has two main functions: the first one consists in balancing the charge of the counter-ion of PEDOT, while the second purpose is to disperse the long polymeric chains of PEDOT in water thanks to the fact that it leads to the creation of micro-dispersions made of particles of PEDOT surrounded by PSS. In the doped and conductive state, PEDOT:PSS shows a conductivity in the range between  $1$  and  $10\text{S} \cdot \text{cm}^{-1}$ ; reduction to the neutral state leads to a decrease of charge carriers inside the chains of PEDOT, lowering the conductivity [99].

For this work, Clevios PH 1000 was purchased from Heraeus. In order to obtain a printable resin with good mechanical properties, PEDOT underwent a treatment in sulphuric acid and then mixed with PEGDA, as will be explained in the experimental section

### 3.4 SPOTHT

Another resin has been exploited in this work in order to realize some parts of the OECT, especially some structural part like the substrate of the transistor (in order to physically insulate it from the substrate) and the vat which will contain the electrolyte for the various measurements. This is the commercial resin called Spot-HT, purchased from Spot-A Materials. This resin, once processed with stereolithography, it's hard, tough, impact and abrasion resistant, and cannot be contaminated with chemicals and water, that is way it constitutes a perfect solution in order to confer a tough and resistant structure to the OECTs. Moreover this resin is able to withstand to temperatures above 120 °C, allowing thermal processes. It is also characterized by low viscosity and high curing speed, factor which minimizes health risks.

This version of the resin has been acquired pre-mixed with a yellow opaque pigment. The chemical structure, the number and the natures of the components of the resin and their concentrations are unknown.

For this work, Spot HT was purchased from the company Spot-A Materials.

### 3.5 SURFACTANTS AND DMSO

When two polymers are mixed, the chains can interact leading to the creation of a homogeneous mixture made of a single phase, or by contrast to a heterogeneous mixture made of two separate phases [100]. The level of compatibility between the two polymers affects the properties of the polymer mixture, and the interaction between the two components are ruled by the laws of surface tension: when this tension between the two phases is proximate to zero there is complete mixability, while for high surface tensions there will be a more pronounced phase separation and, in some cases, the precipitation of one of the two phases can occur. Surface tension can be reduced employing the so-called surfactant, which are formed by molecules characterized by complementary hydrophobic and hydrophilic regions which can be bound to the polymeric chains through secondary bonds or that can interact with the functional groups of the polymer.

The system PEGDA-PEDOT is not characterized by a high mixability between the two components, and in order to enhance the dispersion and the stability and to reduce the precipitation of the phases, dipolar aprotic surfactants can be exploited [101],[102]; moreover surfactants can enhance electrical properties, in fact Kim et al. [103] demonstrated that PEDOT:PSS conductivity can be increased through the addition of a surfactant called DMSO.

Regarding the system PEGDA-PEDOT, this surfactant it is able to enhance the dispersion of PEDOT inside the matrix and to increase the conductivity of the system [2009] [119], even if the mechanism is not still clear: Kim et al. [103] hypothesized that this increase in conductivity is due to the fact that DMSO has a screening behaviour against PSS, while Petterson et al. [111] supposed that DMSO could induce a rearrangement of the chains leading to a better conduction among them.

Dimethyl sulfoxide (acronym DMSO) is one of the most commonly used surfactants, since it increases conductivity and in general enhances electrical properties of many polymer mixtures, among which it can be found the mixture PEGDA-PEDOT. DMSO is a colourless liquid at room temperature. It is a polar, aprotic solvent with high hygroscopic properties (ability of absorbing water molecules from the environment). The molecular structure of DMSO is showed in Fig.3.12.

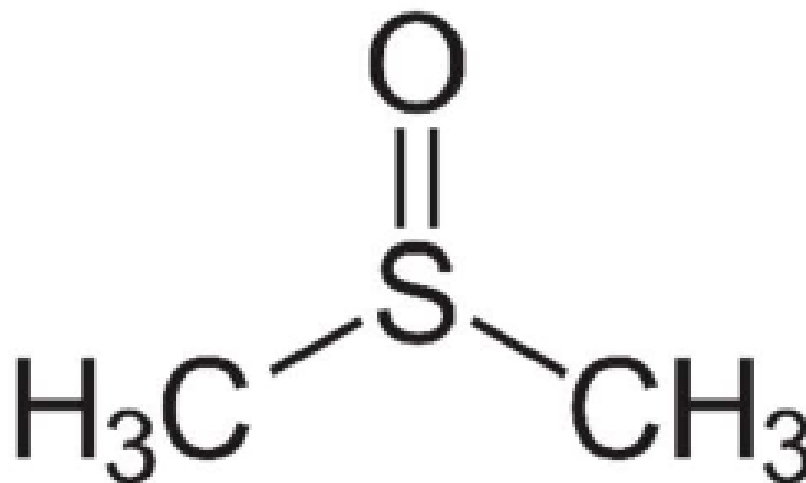


Figure 3.12: Chemical structure of DMSO, [84]

The polar and nucleophilic properties of DMSO are due to the presence of the electron pair available between the oxygen and sulphur atoms of the molecule [106],[107],[108]. It is also characterized by a low level of toxicity [109].

For this work, the surfactant DMSO was purchased from the company Technic.

## METHODS AND EXPERIMENTAL SECTION

---

A list of all the instrumentation employed in this work is presented here:

- Oven, granted by Binder
- Vacuum pump, granted by Edwards (model XDS10)
- Optical microscope, granted by Leica Microsystems (model MDC56)
- Sonicator, granted by Branson (model 250)
- Electronic balance, granted by Kern (model 520)
- Heating-magnetic stirrer, granted by Arec.X
- Stereolithographic printer, granted by Microla Optoelectronics s.r.l.
- Centrifuge, granted by Ohaus (model Frontier 5706)
- UV lamp, granted by Hamamatsu (model LC8)
- Sourcemeter (1 channel), granted by Keithley (model 6430)
- Spurcementer (2 channels), granted by Keysight (model B2912A)
- Ultraturrax, granted by IKA (model T10 Standard)

## 4.1 OBTAINING PEDOT FROM CLEVIOS PH 1000 (PEDOT:PSS)

The process consists in separating PSS from PEDOT, since the former leads to a decrease of the conductivity.

With this process, conductivity is increased due to the fact that the process of PSS removal from PEDOT leads to a new conformation of the chains which from a spiral structure acquire a linear structure [104]. From Raman spectroscopy analysis [103] it has been supposed that the conformational change of the chain implies a change in the resonance structure of PEDOT, which passes from a benzoid to a quinoid structure, as shown in Fig.4.1.

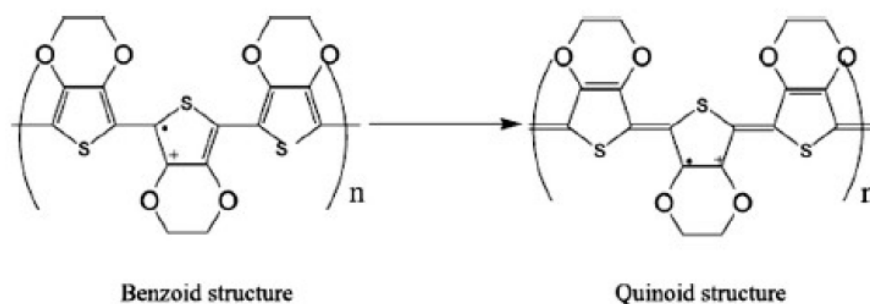


Figure 4.1: Benzoid and quinoid structures of PEDOT, [84]

Spiral conformation is favoured in the presence benzoid structure, while a linear or an extended spiral conformation is favoured in the quinoid structure [105].

From literature review, it has been found that a method useful to remove PSS from Clevios PH 1000 consists in exploiting sulphuric acid [112]. The first preliminary step consists in diluting sulphuric acid in water: therefore, 13.95mL of sulfuric acid are diluted in 486.05mL of deionized water in order to obtain a solution of  $H_2SO_4$  0.5M; after this step, 50mL of Clevios pH 1000 are added to the solution and then the mixture is stirred at room temperature for few minutes. The solution shows itself as in Fig.4.2.

Then the solution is left overnight in order to let the PEDOT precipitate and separate from the sulfuric acid and PSS. After one night, most of PEDOT is precipitated at the bottom of the beaker. From this point two different procedures can be followed, which exploit two different solvents where the grinding of PEDOT grains can be performed: sulphuric acid and ethanol. The two different solvents and procedures led to different results for conductivity. The precipitations



Figure 4.2: Clevios precipitation in sulphuric acid 0.5 M

in sulphuric acid and ethanol will be denominated first and second method respectively. Here follows the protocol for the first method:

- Centrifuge for 4min at 4000rpm; in this way the PEDOT will be pushed towards the bottom of the falcon, while the sulfuric acid will float on the top of the falcon (Fig.4.3)
- Remove the supernatant liquid (which is a mixture of sulfuric acid, deionized water and PSS) (Fig.4.4)

- Repeat these steps until all the liquid part is removed from the falcon
- Add sulphuric acid in order to bring the volume to 50mL and use the Ultraturrax (level 4) to grind the PEDOT for 20min
- Remove the sulfuric acid and fill the falcon with ethanol, and use the centrifuge again for 10min at 4000rpm
- After the centrifuge, remove the supernatant and put the precipitated PEDOT in the fridge at 4°C to avoid degradation (Fig.4.5)



Figure 4.3: Centrifuge employed to separate precipitate and supernatant

Instead the second precipitation procedure consists in:

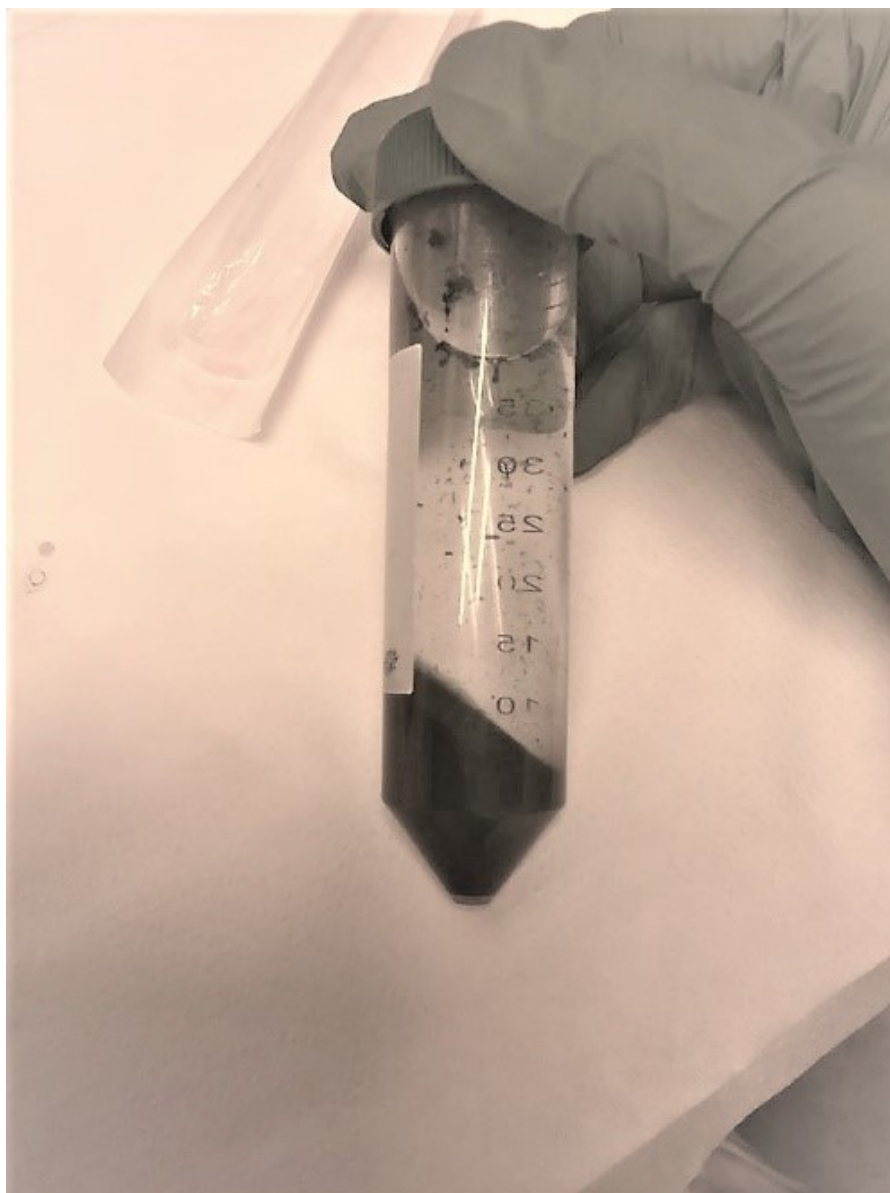


Figure 4.4: Phase separation at the end of the centrifugation

- Centrifuge the components for 4min at 4000rpm; in this way the PEDOT will be pushed towards the bottom of the falcon, while the sulfuric acid will float on the top of the falcon
- Then, remove the supernatant liquid (which is a mixture of sulfuric acid, deionized water and PSS)
- Repeat these steps until all the liquid part is removed from the falcon
- In a new falcon, put 15g of PEDOT and 15mL of ethanol, and use the Ultraturrax (level 4) to grind the PEDOT for 20min
- Perform the centrifugation again at 4000rpm for 10min

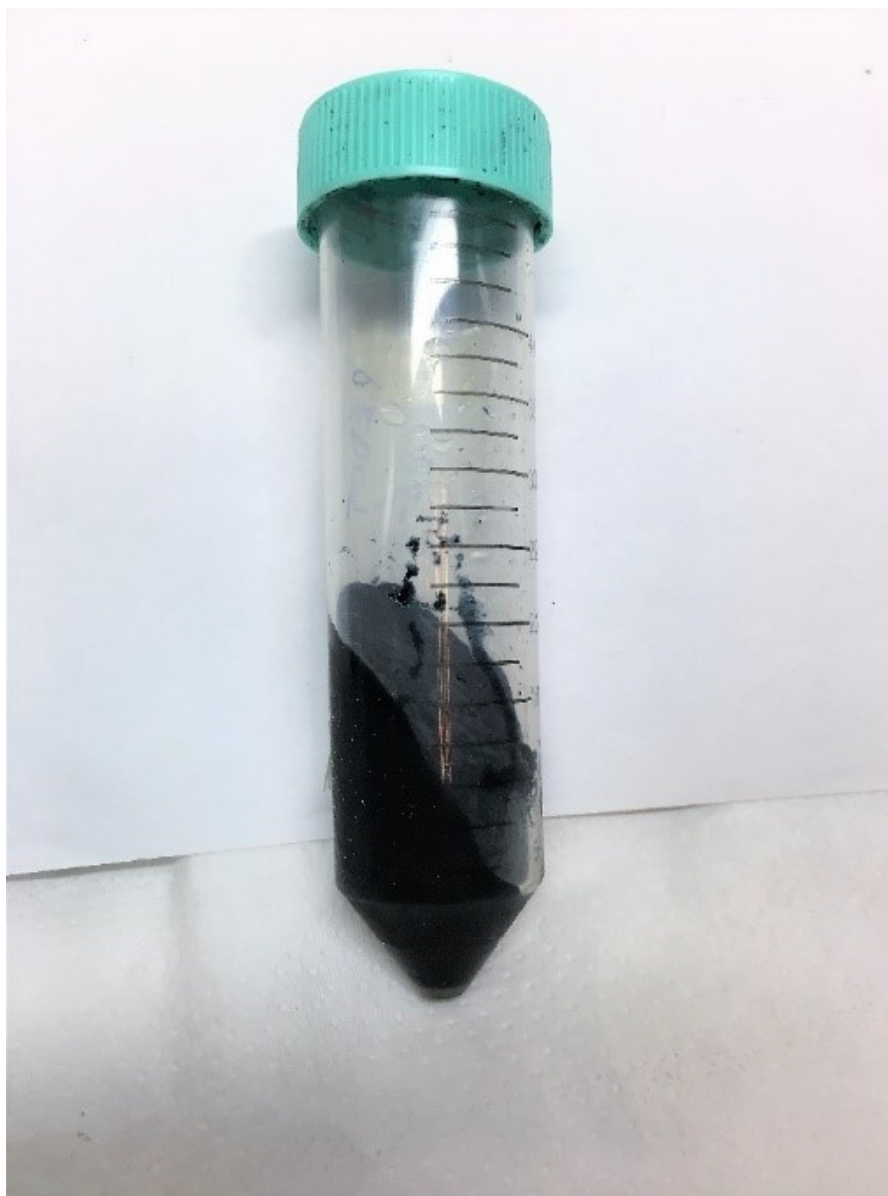


Figure 4.5: Precipitated PEDOT at the end of the process

- Remove the supernatant and put the precipitated PEDOT in the fridge at 4°C

The centrifuge step is critical in order to eliminate any liquid residues inside the PEDOT. Ultraturax step instead is fundamental in order to reduce the dimensions of the grains of PEDOT, so that a uniform and homogeneous precipitate is obtained. It has been demonstrated that the time of Ultraturax does not influence the final conductivity of the polymeric mixture [84].

#### 4.2 RESIN COMPOSITION

In order to obtain a printable and stable resin, the correct proportions and quantities of the different components must be mixed. Following a previous research [84], which studied the correct quantities of PEGDA, photo-initiator, PEDOT, and DMSO, the following composition has been made:

- In a falcon, 40g of PEGDA 575 are mixed with 0.40g of Irgacure 819, in order to have 1%wt of photo-initiator with respect to the resin mass
- Sonification of the mixture for 15min with cold jacket (sonication cycle: pulse 10s ON, 5s OFF, 40% of maximum power); the cold jacket avoids the sharp increase of temperature due to the rapid movement of the sonicator; this temperature rising can lead to an undesired preliminary polymerization of PEGDA
- After sonication, and then mix PEGDA with the correct amount of PEDOT: for the OECT used in this work the proportion 55 : 45 for PEGDA-PEDOT has been used
- Then, the solution is mixed with the DMSO, inserting 2.5%wt of the surfactant with respect to the matrix

### 4.3 STEREOLITHOGRAPHIC PROCESS

The printing system exploited in this work is a stereolithographic apparatus (produced and purchased by Microla Optoelectronics s.r.l.), denominated SLA, which can be customized according to particular needs, changing the process parameters. This stereolithographic printer is equipped with a 405nm wavelength laser, mounted on a scanner able to cover a surface of 170x200mm<sup>2</sup>. Two different boards control the mechanics of the apparatus and the laser source. These two systems can be controlled through the dedicated software Microla3D and through the software BeamConstruct. The latter generates the instructions to print the three-dimensional object. The printer employed in this work is showed in Fig.4.6.

The main fundamental parameters for the printing process are: writing speed (the velocity of the laser source along the reticulation path), laser power, the hatch spacing (defined as the distance between two close and consecutive line paths of the laser). These parameters, if set up correctly, lead to an accurate photo-polymerization of the employed resin. In particular, writing speed defines the time for the absorption of the radiation by the resin: each resin is characterised by a different absorption threshold leading to different curing degrees. A very low laser speed can lead to an “over-polymerization” since the laser radiates a point for a very long time, while high speeds can lead to “under-polymerization” since the laser passes rapidly on that spot without triggering the process of polymerization. Also the laser power is a very important parameter, since if a low laser power under the absorption threshold of the resin is applied, no polymerization will occur, while an extremely high power above absorption threshold will lead to the over-polymerization of the resin creating strong mechanical strains which can involve damage and deformation of the sample. Even the hatch spacing should be chosen very carefully to have mechanical stability: again, a wide hatch spacing leads to regions of the final product which are not polymerized, softening the structure and leading to fracture, while a narrow hatch spacing leads to over-polymerization of border regions between two line-paths; usually, in stereolithographic printing systems, hatch spacing is maintained at a value equal to 50µm.

Another important parameter is the layer thickness, defined along the vertical axis (z axis). In this system the layer thickness is set equal to 100µm.

Once the object is printed, it is possible to analyse the final product at the optical microscope and check the deviations from the nominal



Figure 4.6: Stereolithographic apparatus employed in this work

dimensional values defined by the design.

The stereolithographic printer is mainly composed by: the laser, the metal plate, the resin vat, and the re-coater (also called doctor blade). On the metal plate the liquid resin is spread and made uniform by the re-coater; the resin vat works as a reservoir of resin and must be put below the metal plate: the plate lowers inside it and the resin accumulates on it; after that it rises and the re-coater passes levelling the resin on the metal plate. Before printing, the re-coater must be set up at a height equal to the layer thickness with respect to the metal

plate (equal to the layer thickness).

A low-energy light (such as the yellow light) was used during every process of printing, in order to avoid preliminary polymerization of the resin which could have compromised the optimal outcoming of the final product.

Two kinds of samples were printed in this work: firstly, a parallelepiped of dimensions 3mm(height) x 5mm(width) x 100mm(length), which was printed with the purpose of studying the best proportions of the mix PEGDA-PEDOT in order to have a conductive, printable and stable sample at the same time. For this sample, the best parameter combination was laser power equal to 15mW and laser speed equal to 2000mm/s.

Samples with different PEGDA-PEDOT proportions (Fig.4.7) can be easily distinguished looking at their colour since a sample with a very low amount of PEDOT will be characterised by a colour similar to the one of PEGDA, while a sample with a heavy amount of conductive filler will be characterised by a bluish or black colour.



Figure 4.7: Samples with different PEGDA-PEDOT proportions

The central part of this work was the so-called organic electrochemical transistor (OECT), which was characterised by a more complex design, and by different materials among its parts. Two different channel widths (one of  $700\mu\text{m}$  and the other of  $300\mu\text{m}$ ) were integrated in the same substrate. The compact and exploded models, and the geometry of the OECT are depicted in Fig.4.8, Fig.4.9, and Fig.4.10 respectively.

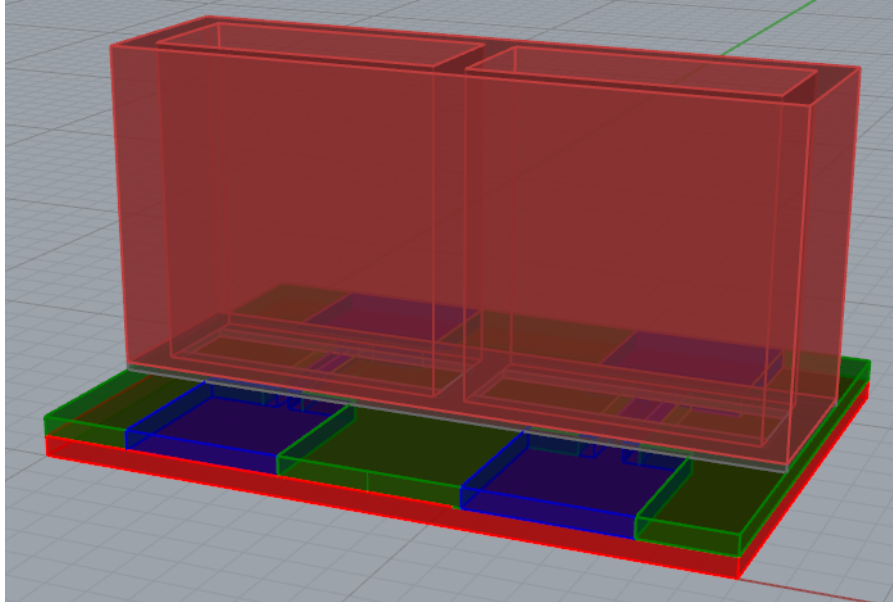


Figure 4.8: Compact model of the OECT design, developed with the software Rhinoceros

This device is composed of the following parts:

- A substrate made of Spot HT; parameters used: laser power 30mW, laser speed 1800mm/s for internal lines and 2000mm/s for border lines; this layer is useful in order to insulate the functional part from possible metal surfaces, and to have an easily detachable surface from the moveable plate after the printing process
- The functional part, comprising of source and drain contacts and the conductive channel, made of PEGDA-PEDOT; parameters used: laser power 35mW, laser speed 2000mm/s for both internal and border lines; this is the functional part which is involved in the conduction and in the interaction with the electrolyte
- A level with a complementary geometry with respect to the previous one, made of Spot HT; parameters used: laser power

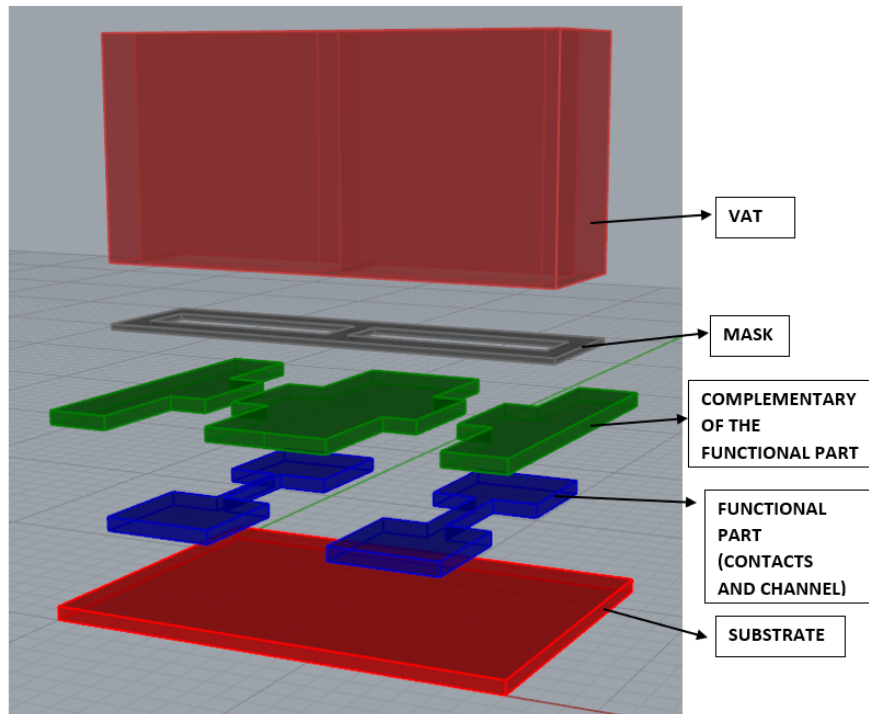


Figure 4.9: Exploded model of the OEET design, developed with the software Rhinoceros

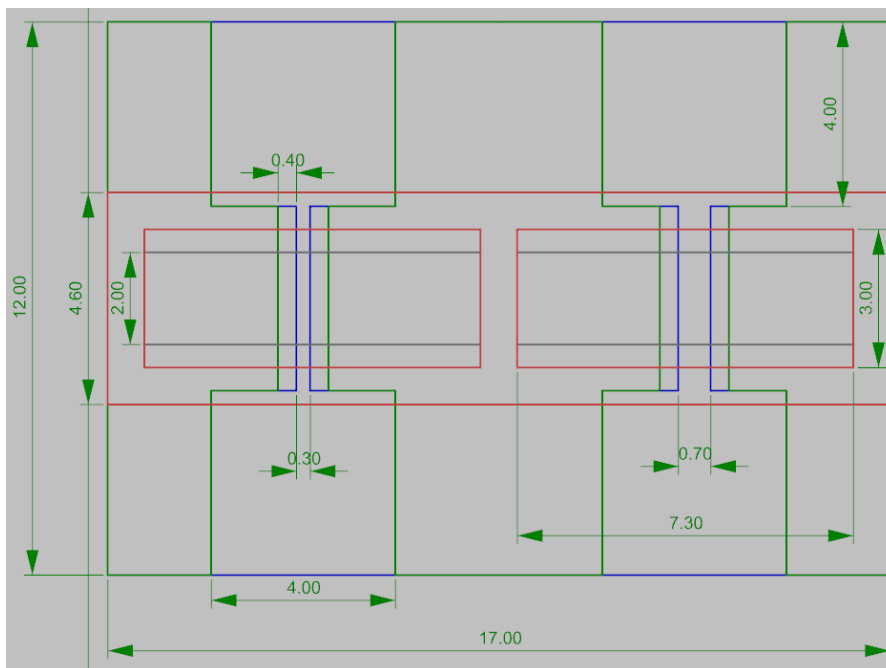


Figure 4.10: Technical view of the OEET, useful to observe the main geometrical parameters of the section

55mW, laser speed 1800mm/s for internal lines and 2000mm/s for border lines; this is the part of the device which is realized and levelled with the functional part of PEGDA-PEDOT, and

this is a fundamental structural part since a vat for the electrolyte must be realized above the contacts; this step must be taken under control very carefully since a heavy amount of resin is polymerized (a layer of thickness equal to  $500\mu\text{m}$ ) therefore a wrong laser power could lead to over-polymerization; a spacing between the channels and the “negative” was inserted in order to avoid over-polymerization of the insulating Spot HT above the conductive channel, which could result in covering and masking parts of the functional part and to a decrease of the section of the channel and consequently to a higher resistance

- A mask, in order to shorten the channel with the goal to obtain a better performance, made of Spot HT; parameters used: laser power  $35\text{mW}$ , laser speed  $1800\text{mm/s}$  for internal lines and  $2000\text{mm/s}$  for border lines
- The vat, made of Spot HT; parameters used: laser power  $35\text{mW}$ , laser speed  $1800\text{mm/s}$  for internal lines and  $2000\text{mm/s}$  for border lines; this container will hold the electrolyte during the measurements, and due to the presence of the complementary of the contacts, it will avoid the pouring out of the solution which can compromise the measurement

The nominal value of the final vat at the end of the printing process was  $172.3\text{mm}^3$ .

After the printing process, the samples and the devices were carefully cleaned in 2-propanol in order to eliminate any contamination coming from the outer environment and from the printing apparatus, and to eliminate any layer or resin residual which was not polymerized.

#### 4.4 THERMAL TREATMENT

After printing the OECTs, a thermal treatment is needed in order to remove any residual of the solvents used during the entire process. This treatment increases also the conductivity of the PEGDA-PEDOT, due to polymerization of residual unpolymerized chains. In fact, after the stereolithography process only the 40 – 50% of the total amount of PEDOT chains are polymerized, therefore this thermal treatment is needed in order to complete the polymerization of the remaining chains. The thermal treatment consists in the following steps:

- The OECT is placed in the oven with temperature rising from room temperature (25°C) to 120°C under vacuum
- The device is maintained at 120°C for 1h
- The temperature is let to drop down towards 25°C

The oven employed in this work is shown in Fig.4.11.

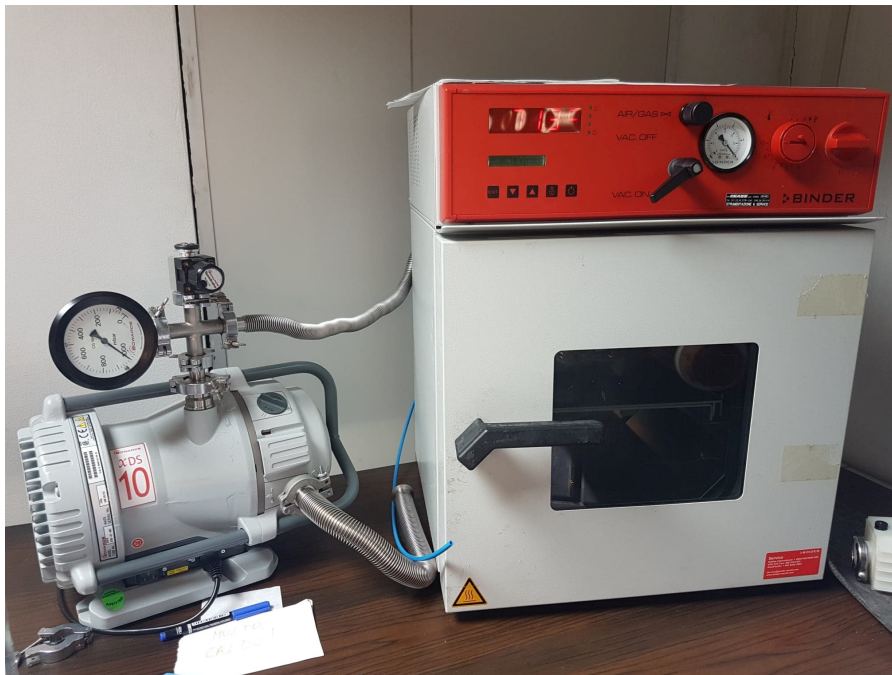


Figure 4.11: Oven and vacuum pump employed to perform the thermal treatment

#### 4.5 METALLIZATION OF THE CONTACTS

In order to perform the electrical characterizations source and drain contacts must undergo a process of metallization in order to have an efficient charge carrier injection in the conductive channel. Being PEDOT a p-type conductor, an efficient hole injection from the source to the polymer is required. Therefore it should be used a noble metal with high work function. In this work a silver paste has been used, which allowed for good adhesion on the polymeric material and efficient charge carrier injection [113].

#### 4.6 ELECTRICAL CHARACTERIZATIONS

Regarding the chemresistors samples at different PEDOT concentrations, a simple resistance measurement has been performed, exploiting a single channel sourcemeter (Keithley 6430). From the resistance measurements, the corresponding values of conductivity have been extrapolated, and the percolation curve (conductivity vs concentration) has been obtained.

OECT devices instead have been characterized in a cleanroom environment with a Keysight B2912A. Four different set of measurements have been performed:

- Channel resistance measurements in dry condition (no gate applied) with a drain-source sweep between  $-1V$  and  $+1V$ , and a scan rate of  $50mV/s$
- The output characteristic of the transistor at different gate voltages; six values of gate voltage were considered ( $-1V$ ,  $-0.6V$ ,  $-0.2V$  and the corresponding positive values), while the sweep on the drain-source voltage was in the range  $-1.5V$  to  $+1V$ , and the scan rate used was equal to  $10mV/s$
- The trans-characteristic of the transistor: seven different values for the drain-source voltage were considered (from  $-100mV$  to  $-700mV$  with steps of  $100mV$ ), while the sweep on the gate-source voltage was performed between  $-750mV$  and  $+1000mV$ , and the scan rate used was equal to  $5mV/s$
- A rise-time and fall-time analysis, with a square-wave signal able to turn on and off the device; the signal period was  $40s$  with duty cycle  $50\%$ ; in this way the transient behaviour of the device was analysed; in particular it was measured the time required by the transistor to pass from the ON state to the OFF and from the OFF state to the ON state; five cycles were performed, and the average value of these times was calculated; in

order to compute the rise-time and the fall-time, the 90% and 10% threshold have been used

For the last three measurements, the electrolyte employed was NaCl 100mM. A volume of 150 $\mu$ L was inserted into the vat of the device, where successively the gate electrode was connected. These measurements were performed on both the channel widths.

The scan rate is a very important since it influences the response of the device (especially at the beginning of the measurement) and the stability of the curves; the higher is the scan rate, higher is the amount of leakage current which flows through the gate electrode (therefore the corresponding current limit on the channel). The set-up used for this set of analysis is showed in Fig.4.12 and Fig.4.13.

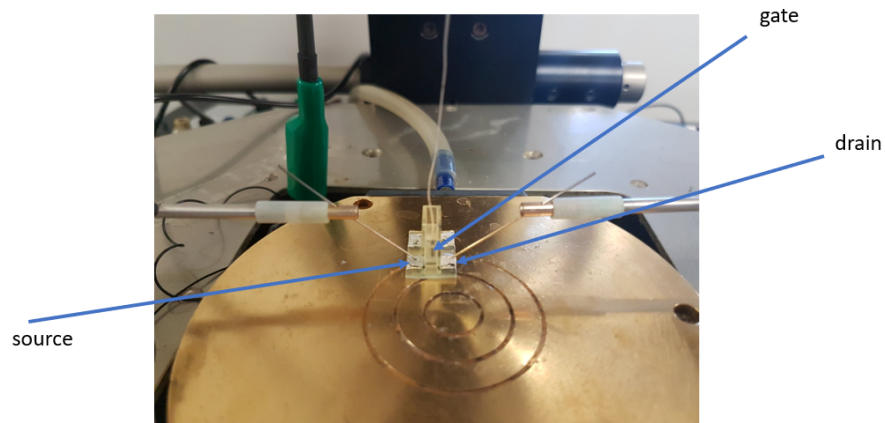


Figure 4.12: OECT under analysis and setup



Figure 4.13: Sourcemeter and instrumentation employed for the analysis

## RESULTS AND DISCUSSION

## 5.1 MORPHOLOGICAL CHARACTERIZATION

Both Clevios PH 1000 (aqueous solution of PEDOT:PSS) and PEDOT precipitated with the procedure described in the experimental section have been analysed and characterised using a Field Emission Scanning Electron Microscope (FESEM) and a Transmission Electron Microscope (TEM). Clevios PH 1000 has been characterised with a FESEM instrument (Fig.5.1).

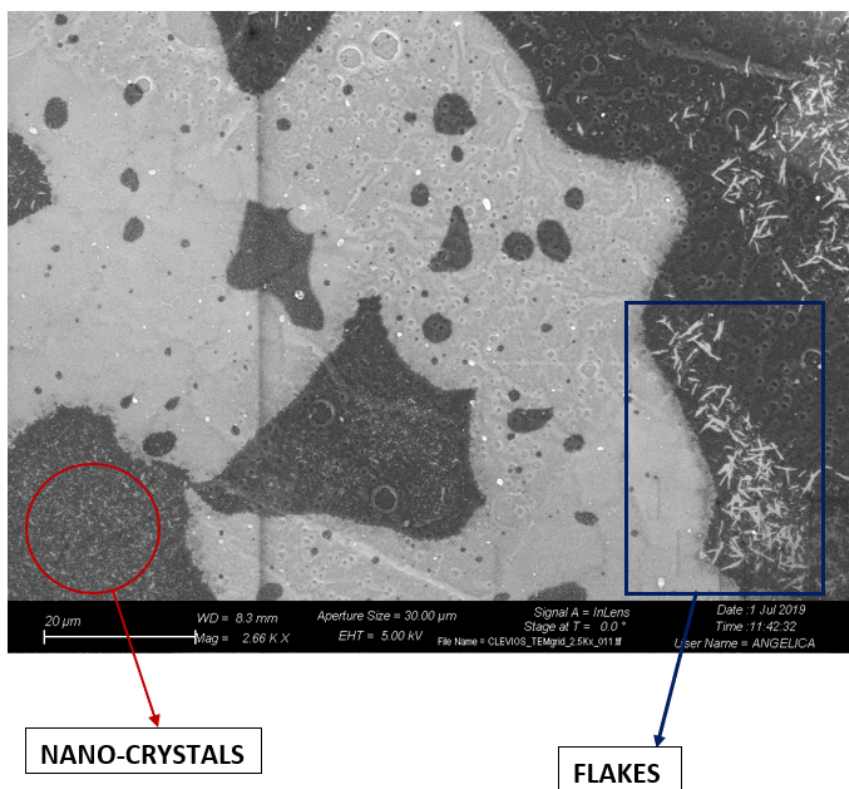


Figure 5.1: A FESEM image of Clevios PH 1000, where the presence of crystals and flakes can be noticed

PEDOT:PSS appears as an inhomogeneous solution. It can be noticed the presence of two distinct phases. Inside the darker one the occurrence of some nanocrystals and some flakes can be observed. These flakes and nanocrystals are quite homogeneous from a geometrical point of view, since Clevios PH 1000 is a commercial solution with an established and well-known production process. A detail of

the flakes in the solution is showed in Fig.5.2, in order to highlight the homogeneous dispersion and the homogeneous size distribution.



Figure 5.2: Homogeneous dispersion of flakes in Clevios PH 1000

The nanoflakes have an average size equal to 50nm.

The precipitated PEDOT was characterised using TEM (5.3).

Precipitated PEDOT appears as an inhomogeneous mixture of different structures. Some small crystals inside an amorphous framework can be observed. The average size of these small crystals is around 1 – 2nm (Fig.5.4).

Some big flakes can be observed, which derive from the packing of smaller flakes during centrifugation step. The PEDOT crystals and flakes are the structures which allow, when inserted in an insulating resin such as PEGDA, the creation of a conductive path along which the charge can be transported, leading to the generation of a current. Also aggregation of flakes can be observed (Fig.5.5).

Comparing precipitated PEDOT with the previous figures about PEDOT:PSS, it can be stated that after precipitation, PEDOT results less homogeneous, but the compact crystals allows to have good

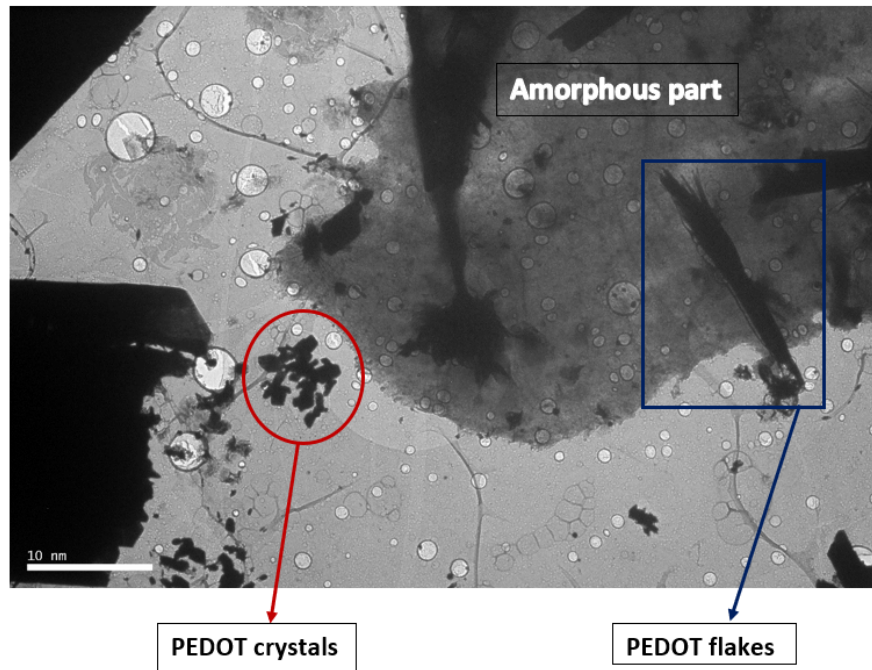


Figure 5.3: A TEM image of precipitated PEDOT

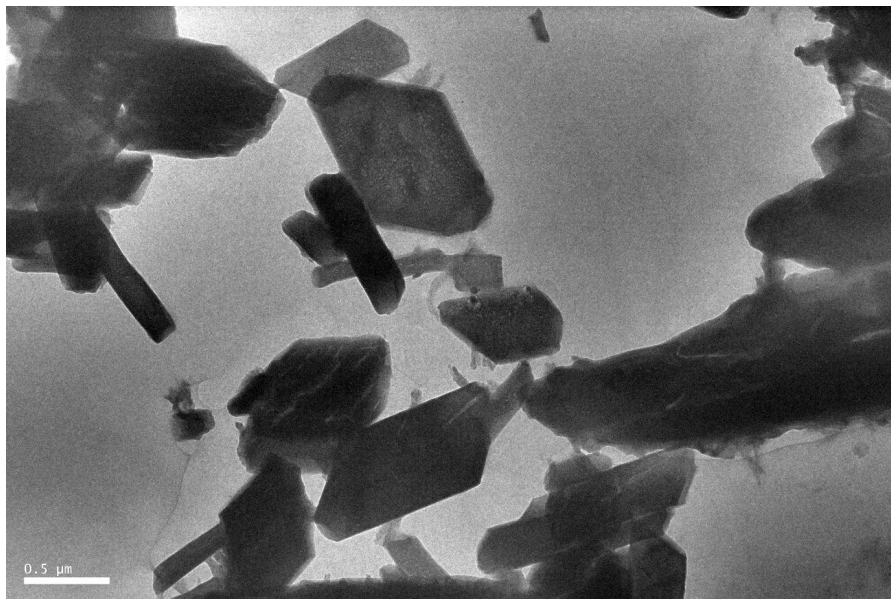


Figure 5.4: PEDOT crystals

conductive performances in the devices containing PEGDA-PEDOT blend.

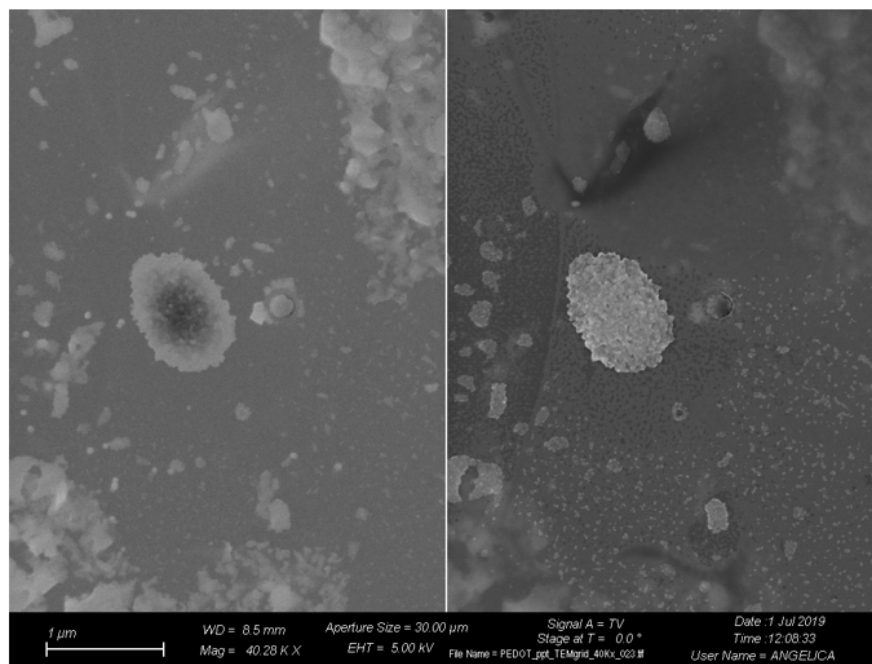


Figure 5.5: Aggregation of PEDOT flakes

## 5.2 COMPARISON BETWEEN THE TWO PRECIPITATION METHODS

Regarding the first precipitation method, the one performed in sulphuric acid, samples with PEDOT concentrations from 0% to 75% were printed, and for each one the resistance was extrapolated from IV curve; knowing the physical dimensions of the samples, the resistivity (or equivalently the conductivity) could be calculated. Plotting the conductivity value for each sample against the PEDOT percentage in the formulation, the percolation curve has been obtained (Fig.5.6). The data are plotted in semi-logarithmic scale (on the y axis).

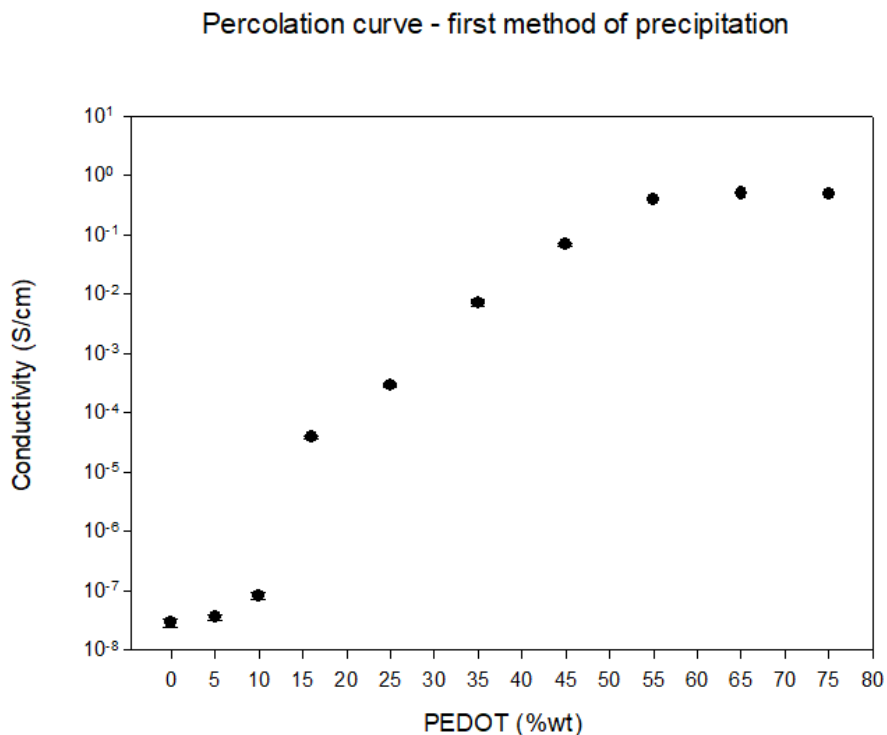


Figure 5.6: Percolation curve obtained using the old precipitation method (in sulphuric acid); data are in semi-logarithmic scale (on the y-axis)

It can be noticed that this data fit quite well the sigmoidal model for the percolation curve described in chapter 3. With low concentrations of PEDOT there is not an appreciable difference in the conductivity values between 0% and 35%, and these values are characterised by a low order of magnitude. This is due to the fact that there is not enough conductive PEDOT to create a conductive path for the electron charge to be transferred. After a “threshold” value, around 40% of PEDOT concentration, a sharp increase in conductivity occurs, until it reaches a saturation value (denominated “plateau”) around  $5 \cdot 10^{-1} \text{ S} \cdot \text{cm}^{-1}$ , with 65% of PEDOT. The 40% of PEDOT concen-

tration constitutes a threshold after which the conductivity increases every time a small amount of PEDOT is added to the resin mix that must be printed; the higher is the amount of PEDOT, the more conductive chains will be present inside the resin which allows charge transport. After the saturation value, for each addition of PEDOT, the conductivity doesn't increase but remains constant.

It must be underlined the fact that for high quantities of PEDOT (above 50%), the samples are difficult to print and moreover they are not very stable from a structural and mechanical point of view; in fact, if an excessive amount of conductive filler is present, there is not enough PEGDA to confer structural properties to the final product.

The same study was performed regarding the second method of precipitation and fractionation of PEDOT (in ethanol). The data are plotted again exploiting the semi-logarithmic scale.

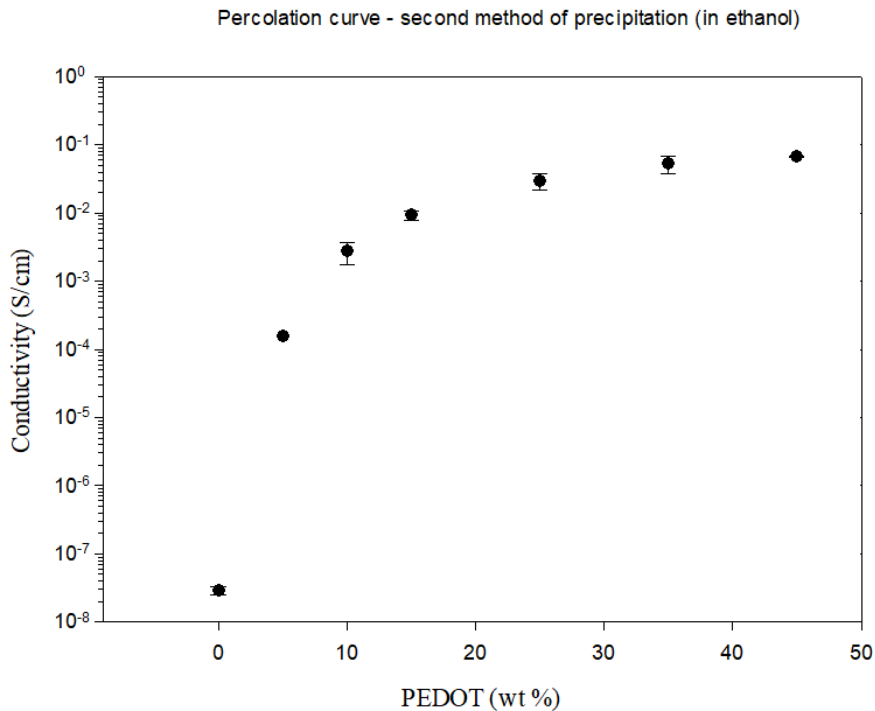


Figure 5.7: Percolation curve obtained using the new precipitation method (in ethanol); data are in semi-logarithmic scale (on the y-axis)

In this case it can be noticed that the saturation value for conductivity is already achieved for a PEDOT concentration between 25% and 35%. Moreover this value of conductivity (around  $10^{-1} \text{ S} \cdot \text{cm}^{-1}$ ) at this PEDOT concentration is orders of magnitude higher with respect to the previous case (which was in the range  $10^{-4}$ - $10^{-2} \text{ S} \cdot \text{cm}^{-1}$ ). By

Table 5.1: Densities and boiling point of ethanol and sulphuric acid, the two solvents used in the precipitation procedures

	Density ( $\text{kg} \cdot \text{m}^{-3}$ )	Boiling point ( $^{\circ}\text{C}$ )
Ethanol	789	78.37
Sulphuric acid	1840	337

contrast, in the previous case the saturation value of conductivity (always around  $10^{-1} \text{S} \cdot \text{cm}^{-1}$ ) was reached for a PEDOT concentration in the range 55 – 60%.

Therefore the second precipitation method (in ethanol) leads to better results with respect the first process (in sulphuric acid); in fact, samples with a lower concentration of PEDOT (which are also stable from a mechanical point of view) and with higher electrical conductivity can be printed. In this way a certain amount of conductive material can be saved, reducing the costs to produce these samples.

The physical-chemical reason for these higher values of conductivity is that ethanol is a lighter and more volatile solvent with respect to sulphuric acid: in fact its density is lower than the one of  $\text{H}_2\text{SO}_4$  ( $789 \text{kg} \cdot \text{m}^{-3}$  against  $1840 \text{kg} \cdot \text{m}^{-3}$  respectively), and even its boiling point is much lower with respect to the sulphuric acid ( $78.37^{\circ}\text{C}$  against  $337^{\circ}\text{C}$  respectively). All these values are summarized in Tab.5.1.

Therefore, density of ethanol is less than half of the density of sulphuric acid, and for this reason it can be better separated from the precipitated PEDOT during centrifugation step; by contrast, sulphuric acid is heavier and therefore it is not efficiently separated from PEDOT, resulting in contamination in the final formulation of the resin. Moreover ethanol shows a lower boiling point with respect to  $\text{H}_2\text{SO}_4$ , therefore it evaporates faster and more easily than sulphuric acid, leaving low or null contamination in the final precipitate. If some contaminations are left inside PEDOT at the end of the entire process, these contaminations will lead to a lower conductivity since these solvents are insulating; moreover, if a precise quantity of PEDOT is required in order to have a certain formulation if there are solvents contaminations not the entire mass of the filler inserted in the polymeric matrix will be constituted by PEDOT; therefore, a lower quantity of PEDOT than the one desired will be present inside the mixture. That is the reason for which it is better to have a lighter and more volatile solvent during the PEDOT treatment.

With the first precipitation method, the best PEDOT concentration that constituted a good trade-off between conductivity and printing efficiency was 45%; with lower PEDOT concentrations, not enough

high performances are achieved, while with higher PEDOT concentrations a very difficult-to-print resin mix is obtained. Therefore the first samples were printed with 45% of PEDOT, while with the new formulation, the best choice for PEDOT concentration is constituted by 35%. These considerations are convincing and valid for bulk samples, such as the chemresistors, while for smaller and thinner devices such as the channel of the OEECT studied in this work, always the 45% PEDOT concentration has been used in order to have a well conductive device. Despite in the new formulation the best PEDOT concentration in order to have good printing efficiency and conductivity is 35%, the functional part of the OEECT (source, drain and channel) is constituted by a very thin layer of PEGDA-PEDOT, and this concentration is not enough to have good performances of the transistors.

Therefore, with OEECTs, even with the new formulation it has been chosen to use the 45% concentration, otherwise with lower concentration, the quantity of PEDOT required to create the conductive path inside the mix would not be enough.

The results can be summarized in order to appreciate the differences in conductivity between precipitation in ethanol and sulphuric acid (Fig.5.8).

It can be stated that the second precipitation method (in ethanol) leads to higher conductivity values, since with both PEDOT percentages (15% and 35%) conductivity is higher with respect to the first method (in sulphuric acid). From the graph it can also be highlighted the fact that, as described in the experimental section, the time spent to fractionate the PEDOT with Ultra Turrax, thus the dimensions of the particles, doesn't affect the conductivity of the final product. Despite this, it is still a fundamental step in the precipitation process, since it allows to have smaller grains of PEDOT and to make the resin uniform. Therefore, after these considerations, an UltraTurrax time equal to 20min was chosen for this process.

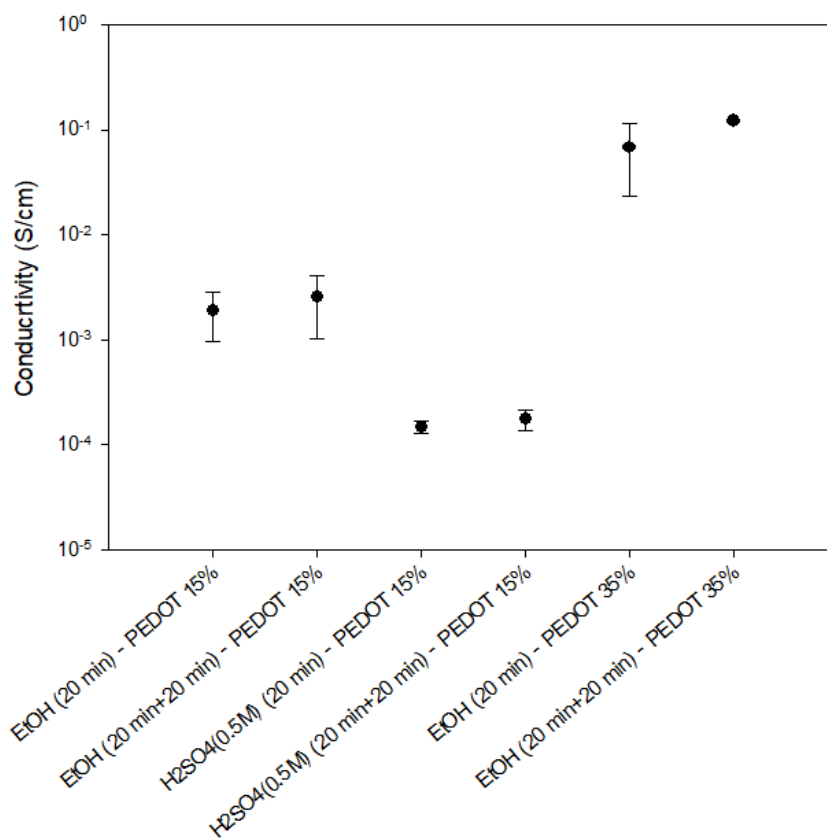


Figure 5.8: Summary of the best conductivity values of both precipitation method; in the label of the x-axis, at first the solvent used is declared, then the time of UltraTurrax between parentheses, and then the percentage of PEDOT in the polymeric mixture

The OECT after the printing process appears as in Fig.5.9.

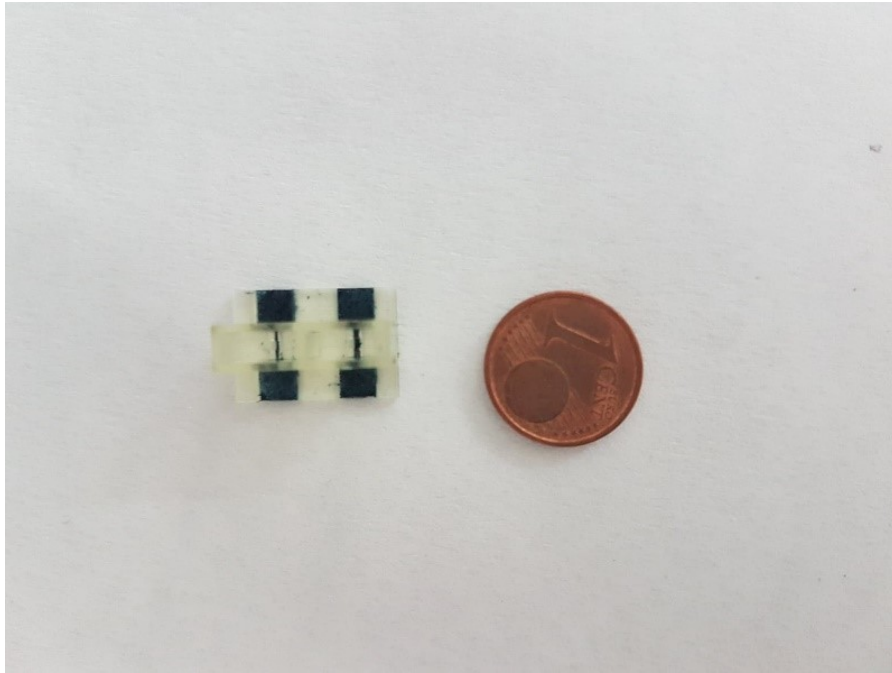


Figure 5.9: An example of printed OECT

Observing the OECT at the optical microscope, the tolerance with respect to the nominal measures and sizes can be noticed (Fig.5.10 and Fig.5.11).

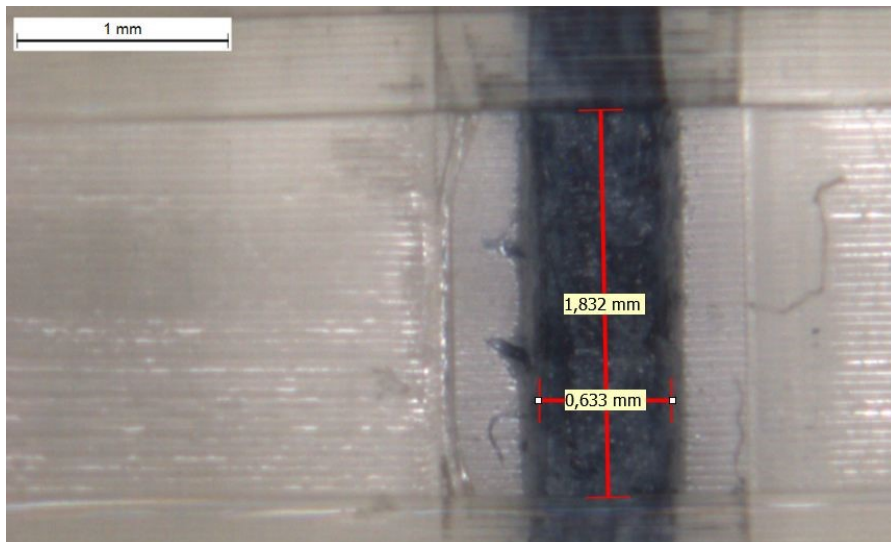


Figure 5.10: Optical microscope view of the 700 $\mu$ m wide channel

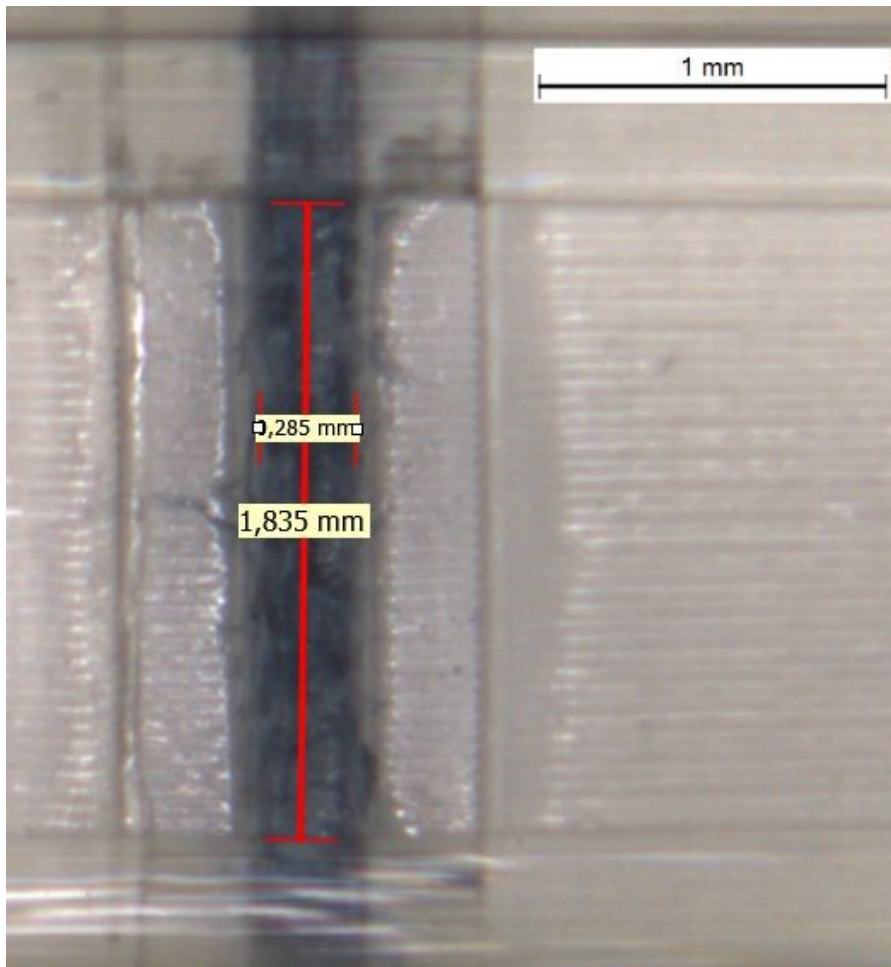


Figure 5.11: Optical microscope view of the 300 $\mu$ m wide channel

### 5.3 THERMAL TREATMENT EFFECTIVENESS

As explained in the experimental section, after the stereolithographic process, a thermal treatment is required.

Employing a sourcemeter (Keithley 6430) the current flowing in the channel due to the application of a voltage between source and drain, was measured. From the results, the resistance was computed and plotted along. This measure was performed on samples which underwent the thermal treatment and samples which did not (Fig.5.12).

It can be clearly noticed that the resistance, for the samples which have undergone the thermal treatment, is two orders of magnitude lower than the resistance of the samples which were not treated ( $\sim 10^2 \Omega$  against  $\sim 10^4 \Omega$  respectively); this is due to the fact that with the thermal treatment, all the solvents residuals are evaporated and leave the system, while if some contaminations remain inside the functional

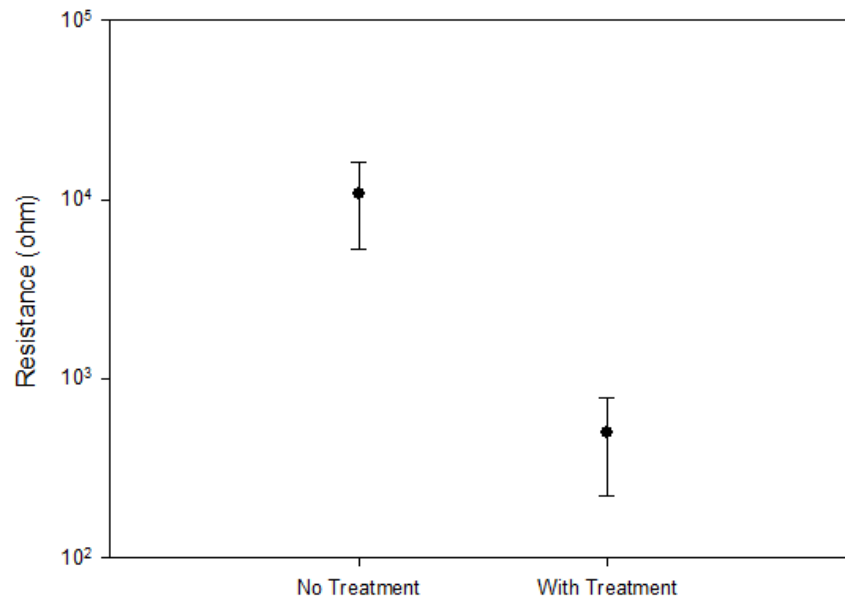


Figure 5.12: Resistance values of samples with and without thermal treatment

part of the device, the performances will be affected; moreover, the thermal treatment allows the completion of the polymerization of the resin mix chains, since after the stereolithography, only a certain percentage of the chains are reticulated.

## 5.4 ELECTRICAL CHARACTERIZATION OF ORGANIC ELECTROCHEMICAL TRANSISTORS

### 5.4.1 Resistance measurement

Before performing the output characteristic and the trans-characteristic characterization, a resistance measurements of the device channel must be performed in order to check if the device under analysis is conductive and behaves like a usual resistor. No electrolyte was loaded into the container of the transistor, thus leaving the gate voltage floating. The drain voltage was swept between  $-1\text{V}$  and  $+1\text{V}$  while measuring the drain current. The resistance was extrapolated from the slope of the IV curve measured (Fig.5.13).

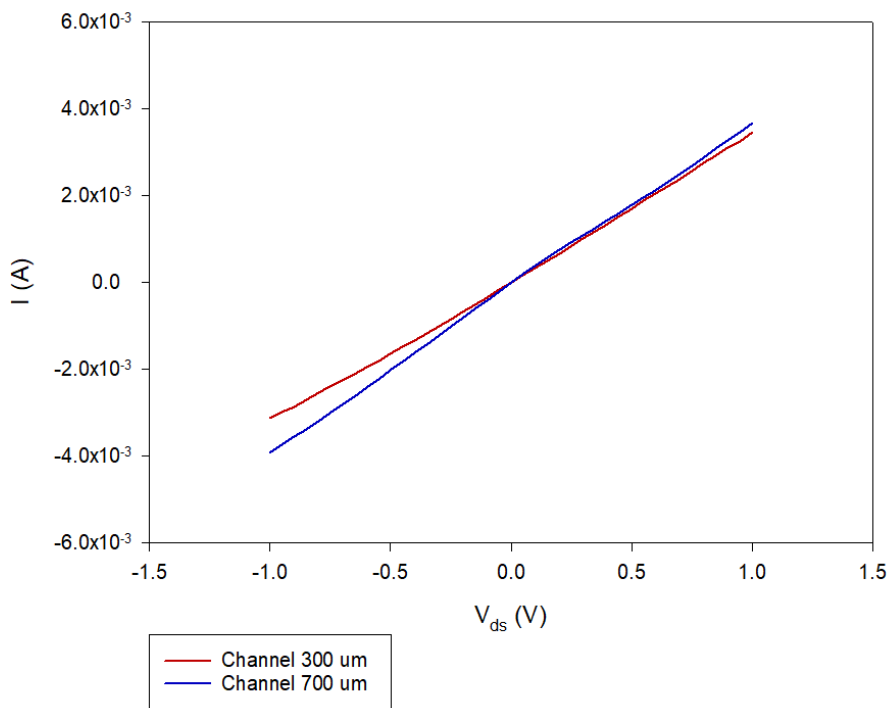


Figure 5.13: IV curves of the OEET; sweep along drain voltage, gate voltage floating

As can be noticed from the curve, both devices (with two different channel widths) show a linear current-voltage characteristic, typical of resistor elements. Taking the inverse of the slope of the characteristic, the resistance of the channel can be calculated (on the order of  $10^3 \Omega$  for the  $700 \mu\text{m}$  wide channel and on the order of  $10^4 \Omega$  for the  $300 \mu\text{m}$  wide channel). By contrast, the slope of the straight line represents the conductance of the system (on the order of  $10^{-3} \text{S}$  for the  $700 \mu\text{m}$  wide channel and on the order of  $10^{-4} \text{S}$  for the  $300 \mu\text{m}$  wide channel).

### 5.4.2 Trans-characteristic measurement

OECTs transduce gate voltage variations in drain current variations proportional to the transconductance of the device. This can be extrapolated from the trans-characteristic curve as the derivative of the drain current with respect to the gate voltage, using eq.(2.1). The transconductance gives indications on the transduction efficiency and switching speed of the device; the higher is the slope (the steeper the transfer curve), the larger the change in drain current for a given gate voltage variation. This means that if the curve slope is very high, two very narrow gate voltage values can be distinguished (since their corresponding current values will be different) and that the device will be switched very fast with respect to an OECT characterised by a lower slope. Using a sourceter, the trans-characteristic was measured in a gate voltage window from  $-750\text{mV}$  to  $+1\text{V}$ , and for different drain voltages between  $-100\text{mV}$  and  $-500\text{mV}$ , with steps of  $100\text{mV}$ . As an example, are shown (Fig.5.14 and Fig.5.15) the trans-characteristics for both channels dimensions, for the OECTS printed with the two different precipitation methods (in sulphuric acid and in ethanol), at a fixed drain voltage of  $-500\text{mV}$ .

Transcharacteristic at  $V_{ds} = -500\text{ mV}$  - First method of precipitation (in sulphuric acid)

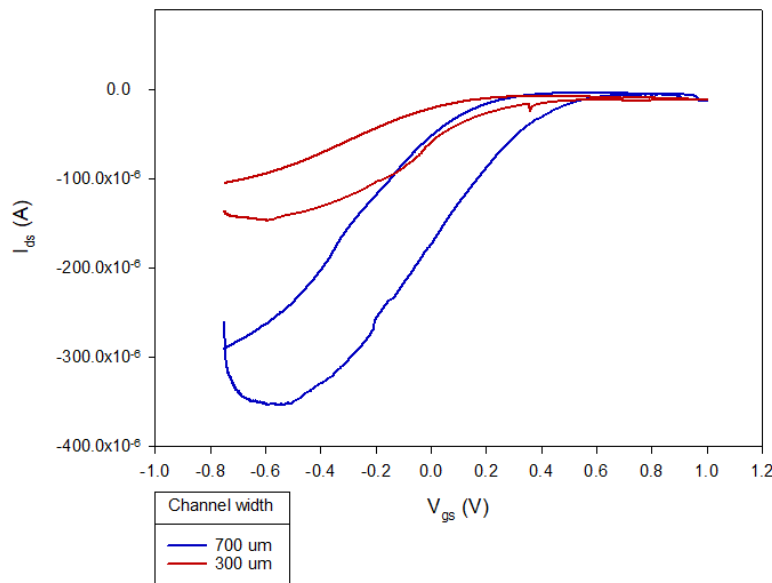


Figure 5.14: Trans-characteristic of OECT printed with the first precipitation method (in sulphuric acid)

The first thing that can be noticed is that the OECTs operate as a traditional normally-ON (or depletion mode) p-MOSFET, as ex-

Transcharacteristic at  $V_{ds} = -500$  - Second precipitation method (in ethanol)

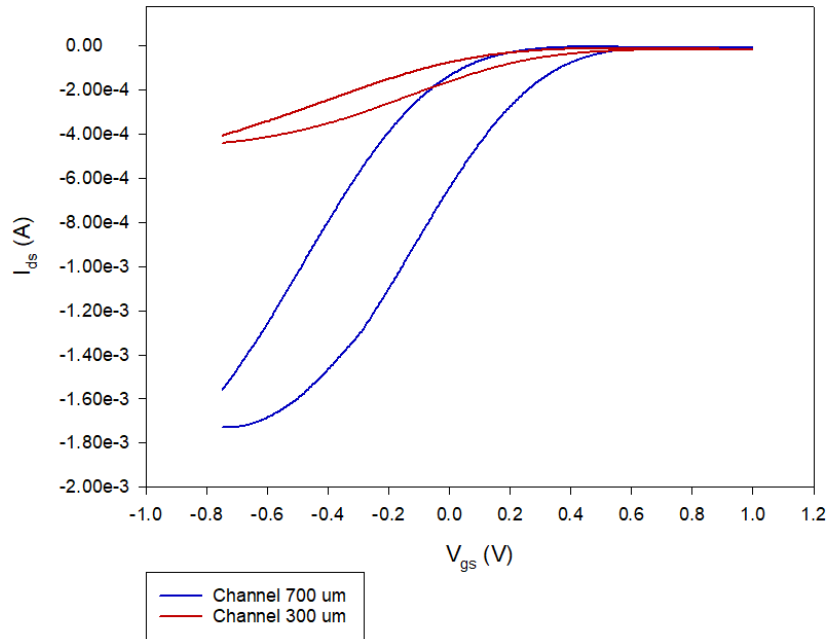


Figure 5.15: Trans-characteristic of OEECT printed with the second precipitation method (in ethanol)

pected from the doping/de-doping mechanism described in chapter 2. As can be noticed from the graphs, there is an enhancement in the current between the devices printed with PEDOT precipitated in sulphuric acid with respect to the devices printed with PEDOT precipitated in ethanol. In the latter, the current in the ON state at a gate voltage of  $-750\text{mV}$  is higher compared to the former for both channel dimensions. The enhancement can be appreciated more evidently with the channel width of  $700\mu\text{m}$ , since the current in the ON state is increased of one order of magnitude ( $10^{-3}\text{A}$  against  $10^{-4}\text{A}$ ). For the channel width of  $300\mu\text{m}$ , the increase in the ON current is of 3 orders of magnitude, while for the  $700\mu\text{m}$  wide channel this increase is of 4 orders of magnitude. Moreover, it can be noticed that there is a difference in the current flowing through the two different channel widths: as expected, the narrower channel shows lower current values due to the fact that its section is smaller, which leads to a higher resistance.

Again, differences between the two precipitation methods can be appreciated, especially for  $700\mu\text{m}$  wide channel also in this case. In fact, the peak transconductance in the new device is one order of magnitude better than the transistor printed with the old method ( $10^{-3}\text{S}$  against  $10^{-4}\text{S}$ ): therefore, this device is characterised by a better switching efficiency than the first one. Unfortunately, this ad-

vantage could not be appreciated for the 300 $\mu\text{m}$  wide channel, since for both kinds of device the order of magnitude of the transconductance was  $10^{-4}\text{S}$ , even if for the new devices this value was slightly higher in absolute value. And, also regarding transconductance, it is straightforward to notice that there is a difference between the two different channel widths. In fact, a higher amount of current flows in the 700 $\mu\text{m}$  wide channel, and consequently its transconductance (and also switching efficiency) will be higher with respect to the 300 $\mu\text{m}$  wide channel.

Another important parameter is threshold voltage, which can be easily computed taking the intersection of the straight line which approximates the trans-characteristic in the ON state, with the horizontal axis of voltages. The OECTs present a strong hysteresis in the trans-characteristic due to the inherently slow doping/de-doping process. All the values of threshold reported in the following are referred to the IV measured sweeping the gate voltage from negative to positive values. A set of tables with all the values of  $I_{\text{on}}$ ,  $I_{\text{off}}$ ,  $I_{\text{on}}/I_{\text{off}}$ ,  $g_m$  and  $V_{\text{th}}$ , computed at  $V_{\text{ds}} = -100\text{mV}$ ,  $-500\text{mV}$  for both channels and both precipitation methods, is presented in Fig.5.16, Fig.5.17, Fig.5.18, Fig.5.19.

$V_{\text{drain}} = -100\text{mV}$	Channel 700 $\mu\text{m}$				Channel 300 $\mu\text{m}$			
	$I_{\text{on}}$ [A]	$I_{\text{off}}$ [A]	$g_m$ [S]	$V_{\text{th}}$ [V]	$I_{\text{on}}$ [A]	$I_{\text{off}}$ [A]	$g_m$ [S]	$V_{\text{th}}$ [V]
Sample 1	$-8.403 \cdot 10^{-5}$	$-1.041 \cdot 10^{-7}$	$1.51 \cdot 10^{-4}$	0.234	$-9.805 \cdot 10^{-5}$	$-1.282 \cdot 10^{-7}$	$1.798 \cdot 10^{-4}$	0.288
Sample 2	$-3.136 \cdot 10^{-5}$	$-7.400 \cdot 10^{-7}$	$6.400 \cdot 10^{-5}$	0.276	$-3.225 \cdot 10^{-5}$	$-1.04 \cdot 10^{-7}$	$4.310 \cdot 10^{-5}$	0.2662

Figure 5.16: First precipitation (in sulphuric acid),  $V_{\text{ds}} = -100\text{mV}$

$V_{\text{drain}} = -100\text{mV}$	Channel 700 $\mu\text{m}$				Channel 300 $\mu\text{m}$			
	$I_{\text{on}}$ [A]	$I_{\text{off}}$ [A]	$g_m$ [S]	$V_{\text{th}}$ [V]	$I_{\text{on}}$ [A]	$I_{\text{off}}$ [A]	$g_m$ [S]	$V_{\text{th}}$ [V]
Sample 10	$-3.377 \cdot 10^{-4}$	$-3.76 \cdot 10^{-7}$	$6.296 \cdot 10^{-4}$	0.636	$-9.065 \cdot 10^{-5}$	$-1.336 \cdot 10^{-7}$	$1.32 \cdot 10^{-4}$	0.243
Sample 11	$-4.031 \cdot 10^{-4}$	$-4.8 \cdot 10^{-7}$	$6.484 \cdot 10^{-4}$	0.122	$-4.497 \cdot 10^{-5}$	$-8.7 \cdot 10^{-7}$	$7.21 \cdot 10^{-5}$	0.328
Sample 17	$-1.576 \cdot 10^{-4}$	$-1.08 \cdot 10^{-7}$	$2.612 \cdot 10^{-4}$	0.189	$-3.694 \cdot 10^{-4}$	$-4.01 \cdot 10^{-7}$	$5.24 \cdot 10^{-4}$	0.218
Sample 18	$-2.61 \cdot 10^{-4}$	$-1.59 \cdot 10^{-7}$	$4.36 \cdot 10^{-4}$	0.133	$-6.074 \cdot 10^{-5}$	$-1.776 \cdot 10^{-7}$	$9.72 \cdot 10^{-5}$	0.389

Figure 5.17: Second precipitation (in ethanol),  $V_{\text{ds}} = -100\text{mV}$

$V_{drain} = -500 \text{ mV}$	Channel 700 $\mu\text{m}$				Channel 300 $\mu\text{m}$			
	$I_{on} [\text{A}]$	$I_{off} [\text{A}]$	$g_m [\text{S}]$	$V_{th} [\text{V}]$	$I_{on} [\text{A}]$	$I_{off} [\text{A}]$	$g_m [\text{S}]$	$V_{th} [\text{V}]$
Sample 1	$-3.960 \cdot 10^{-4}$	$-1.743 \cdot 10^{-7}$	$6.382 \cdot 10^{-4}$	0.063	$-4.358 \cdot 10^{-4}$	$-2.13 \cdot 10^{-7}$	$6.698 \cdot 10^{-4}$	0.066
Sample 2	$-1.417 \cdot 10^{-4}$	$-1.710 \cdot 10^{-7}$	$2.240 \cdot 10^{-4}$	0.094	$-1.441 \cdot 10^{-4}$	$-2 \cdot 10^{-7}$	$1.851 \cdot 10^{-4}$	0.085
Sample 3	$-2.902 \cdot 10^{-4}$	$-1.285 \cdot 10^{-7}$	$6.06 \cdot 10^{-4}$	0.123	$-1.047 \cdot 10^{-4}$	$-1.202 \cdot 10^{-7}$	$1.351 \cdot 10^{-4}$	0.123

Figure 5.18: First precipitation (in sulphuric acid),  $V_{ds} = -500\text{mV}$ 

$V_{drain} = -500 \text{ mV}$	Channel 700 $\mu\text{m}$				Channel 300 $\mu\text{m}$			
	$I_{on} [\text{A}]$	$I_{off} [\text{A}]$	$g_m [\text{S}]$	$V_{th} [\text{V}]$	$I_{on} [\text{A}]$	$I_{off} [\text{A}]$	$g_m [\text{S}]$	$V_{th} [\text{V}]$
Sample 10	-0.0015	$-5.9 \cdot 10^{-7}$	0.0021	0.0832	$-4.062 \cdot 10^{-4}$	$-1.663 \cdot 10^{-7}$	$5.052 \cdot 10^{-4}$	0.135
Sample 11	-0.0016	$-8.93 \cdot 10^{-7}$	0.0024	0.023	$-1.873 \cdot 10^{-4}$	$-6.9 \cdot 10^{-7}$	$2.58 \cdot 10^{-4}$	0.105
Sample 17	$-8.867 \cdot 10^{-4}$	$-5.3 \cdot 10^{-7}$	0.0012	0.025	$-1.7 \cdot 10^{-3}$	$-4.981 \cdot 10^{-7}$	0.0022	0.103
Sample 18	-0.0011	$-2.14 \cdot 10^{-7}$	0.0016	0.0795	$-3.403 \cdot 10^{-4}$	$-1.945 \cdot 10^{-7}$	$4.08 \cdot 10^{-4}$	0.176

Figure 5.19: Second precipitation (in ethanol),  $V_{ds} = -500\text{mV}$ 

The differences in transconductance, threshold voltage, and ON/OFF current ratio can be summarized and better appreciated in Fig.5.20, Fig.5.21, and Fig.5.22.

According to these graphs, the better choice for transconductance and  $I_{on}/I_{off}$  is the device with a 700  $\mu\text{m}$  wide channel, and printed exploiting the PEDOT precipitated in ethanol. In fact, these devices, with respect to the others, are characterised by a better transconductance (one order of magnitude higher,  $10^{-3}\text{S}$  against  $10^{-4}\text{S}$ ), and a better ON/OFF ratio (one order of magnitude higher,  $10^4$  against  $10^3$ ) which means that is easier to switch on and off the transistor. Despite the fact it is characterised by a higher threshold voltage (on the order of  $10^{-1} - 10^{-2}\text{V}$  against  $10^{-3}\text{V}$ ). Even if a low threshold is better since it would be easier to switch off the device, for this kind of device a slightly higher threshold voltage is desired, since it will be exploited as a biosensor (and therefore as an amplifier): thus, with a higher threshold, a good transconductance (at negative gate voltages near 0) is achieved.

Considering the new devices, printed with PEDOT precipitated in ethanol, the trans-characteristic at seven different drain voltages, from  $-100\text{mV}$  to  $-700\text{mV}$  with steps of  $100\text{mV}$ , has been plotted for both channels. The curves for the  $700\mu\text{m}$  wide channel are showed in

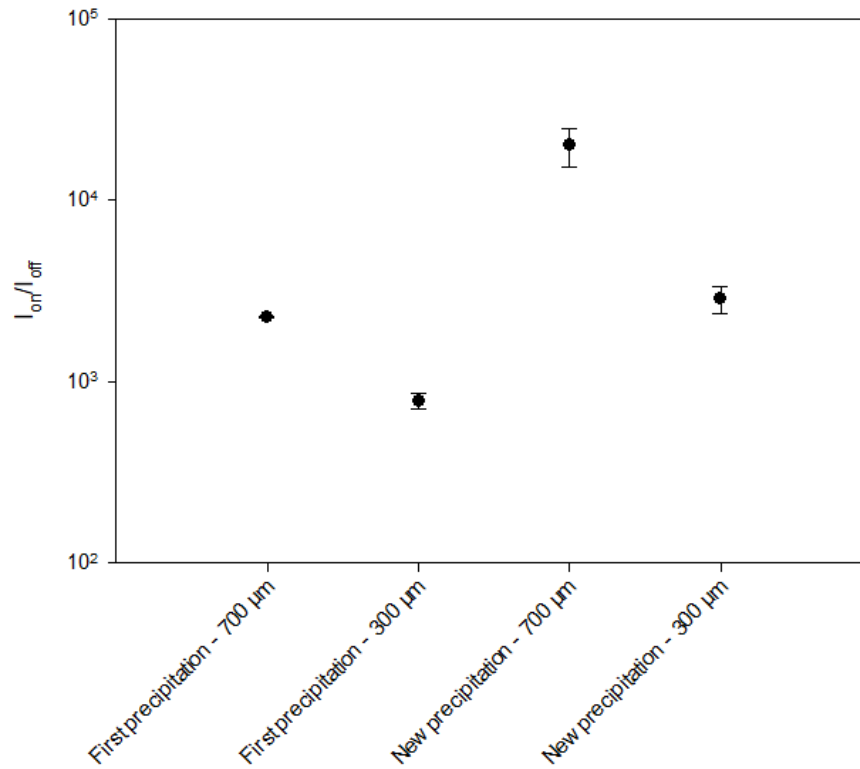


Figure 5.20: Comparison of  $I_{on}/I_{off}$  ratios between first and second precipitation methods, and between the two channel widths

Fig.5.23.

As can be noticed from the curves, there is an increase of the ON current and of the transconductance for more negative drain voltages, until a saturation value for both physical quantities is reached due to channel pinch-off. The threshold voltage decreases for higher drain voltages (in absolute value), as occurs in traditional MOSFETs, until it reaches a saturation value. The behaviours of transconductance and threshold voltage as a function of drain voltages are shown in Fig.5.24 and Fig.5.25

Analysing the plots, it can be stated that the best drain voltages at which the OECT can be operated as sensors are  $-500\text{mV}$  and  $-600\text{mV}$ , where both transconductance and threshold voltage reach a saturation value. Moreover, these drain voltage values are the best trade-off between a too high drain voltage (which could to breakdown, ruining the device) and a too low drain voltage which means having a low switching efficiency and worse performances in terms of current and transconductance.

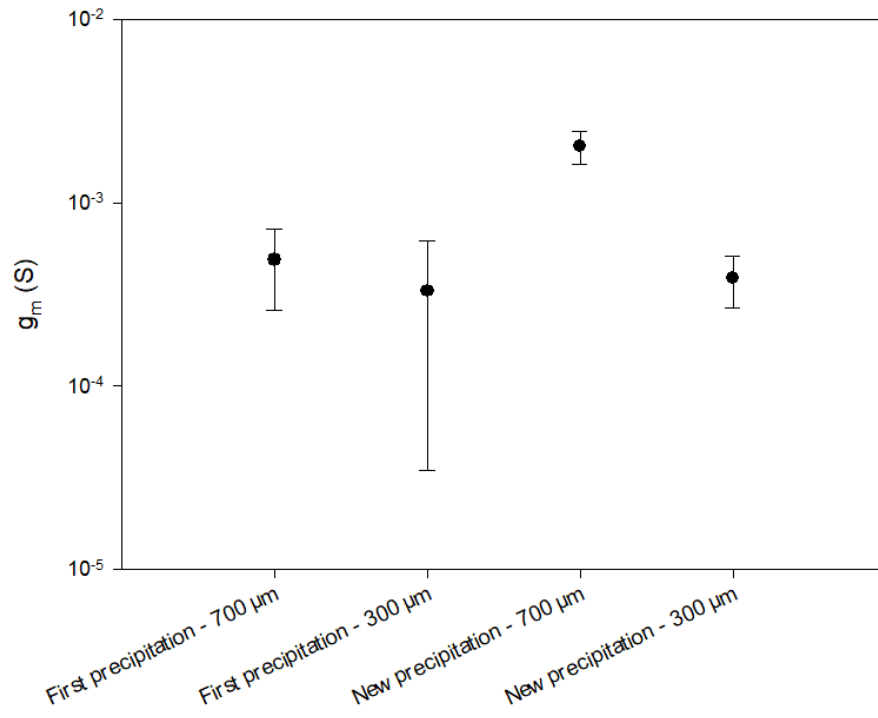


Figure 5.21: Comparison of transconductance values between first and second precipitation methods, and between the two channel widths

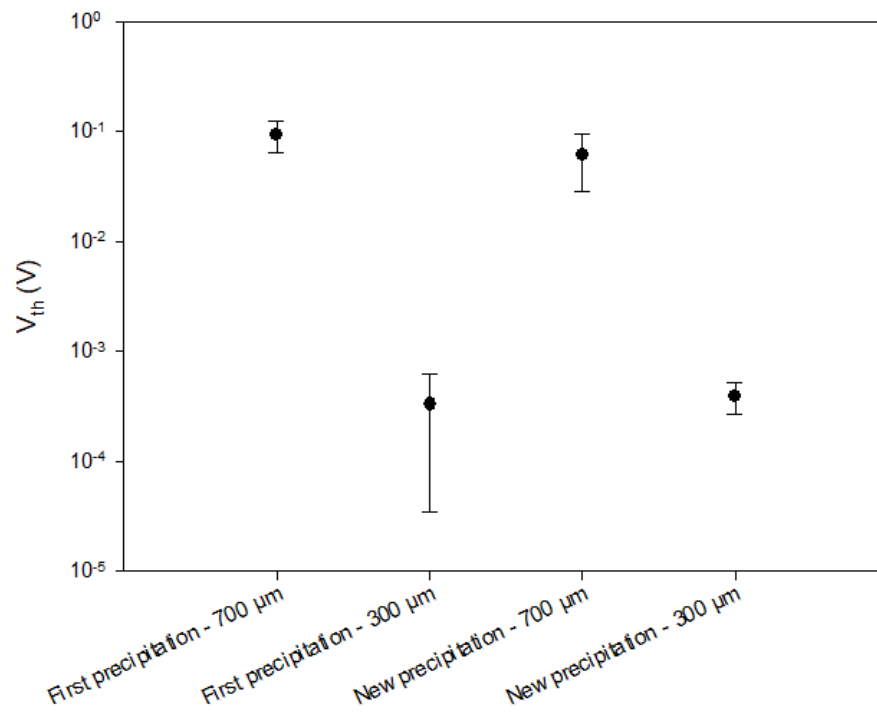


Figure 5.22: Comparison of threshold voltages between first and second precipitation methods, and between the two channel widths

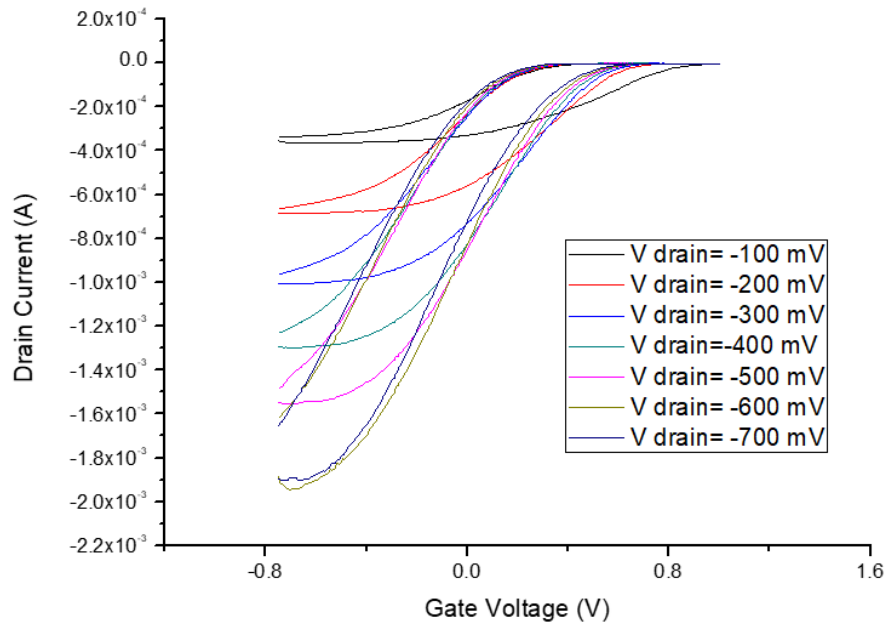


Figure 5.23: Trans-characteristic curves at different drain voltages, for 700  $\mu\text{m}$  wide channel

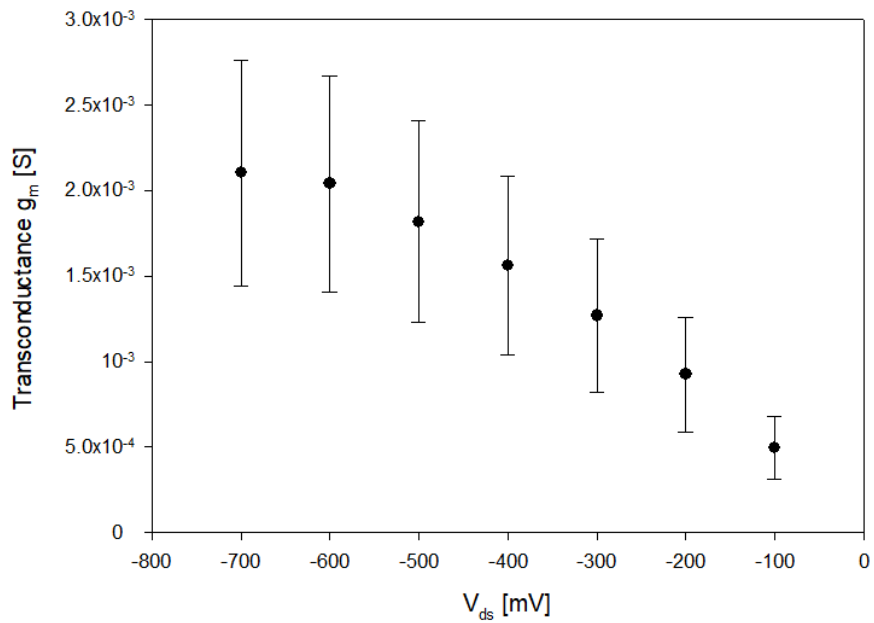


Figure 5.24: Transconductance values at different drain voltages, for 700  $\mu\text{m}$  wide channel

The same considerations can be made for the 300  $\mu\text{m}$  wide channel, whose trans-characteristic is shown in Fig.5.26.

Transconductance and threshold voltage behaviours as a function of drain voltage, for the 300  $\mu\text{m}$  wide channel, are shown in Fig.5.27

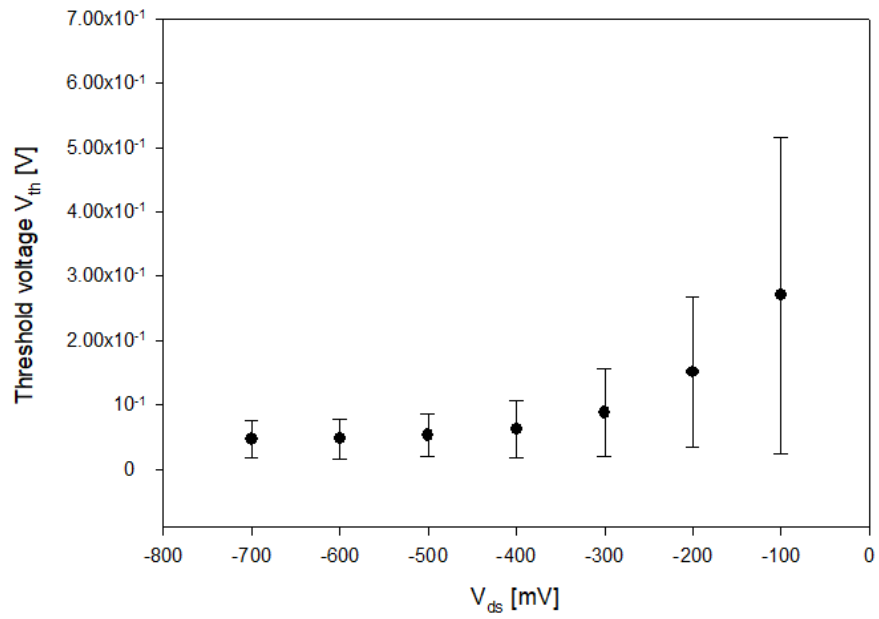


Figure 5.25: Threshold voltages at different drain voltages, for 700 $\mu\text{m}$  wide channel

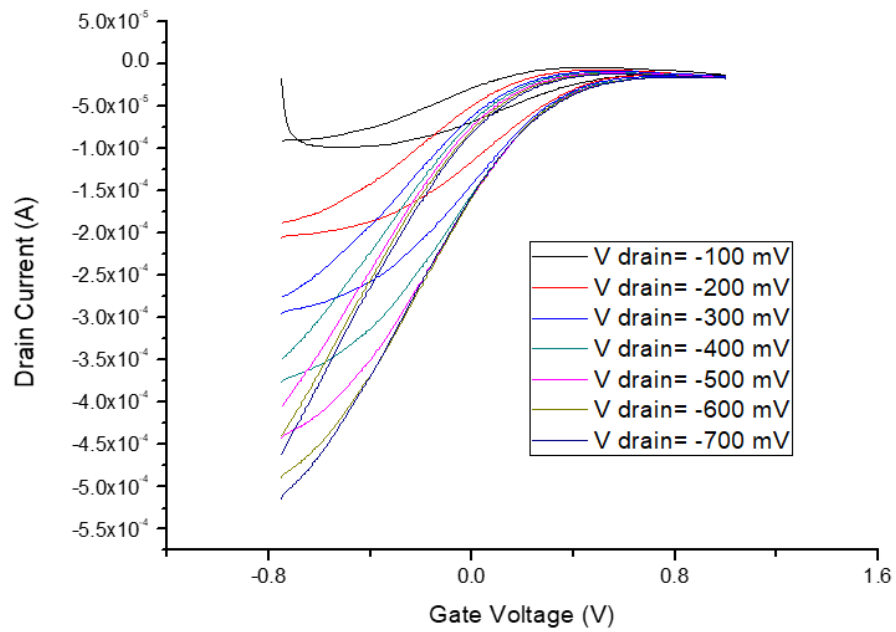


Figure 5.26: Trans-characteristic curves at different drain voltages, for 300 $\mu\text{m}$  wide channel

and Fig.5.28.

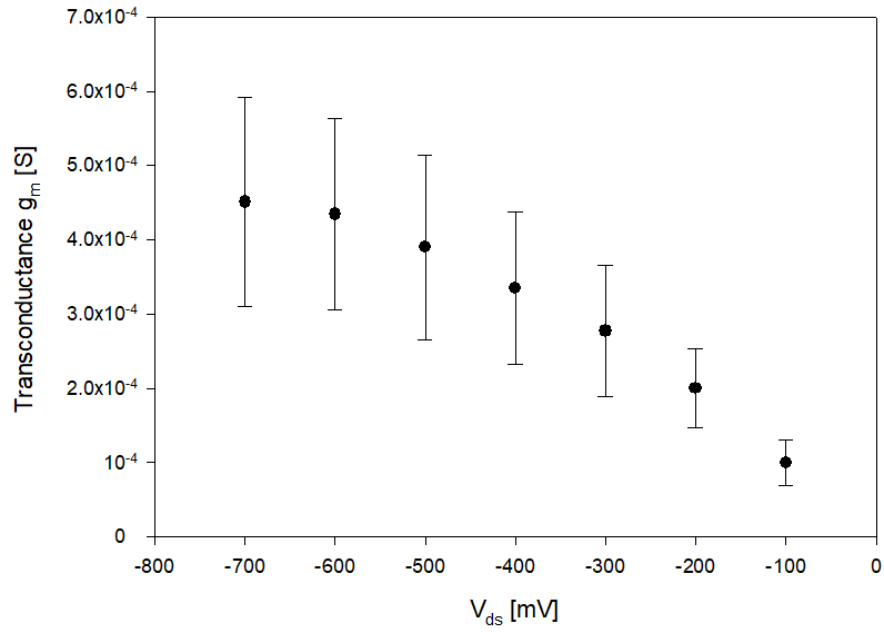


Figure 5.27: Transconductance values at different drain voltages, for 300 $\mu$ m wide channel

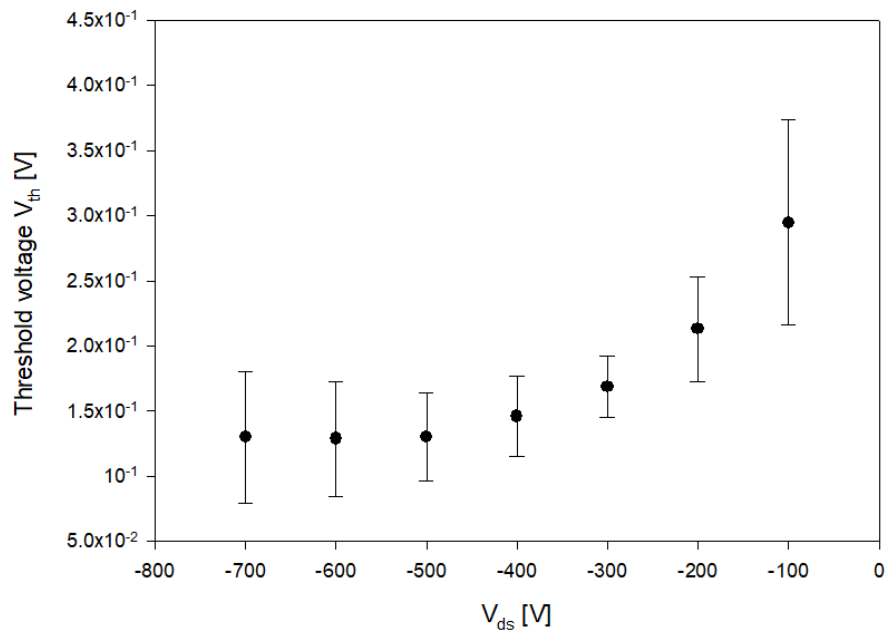


Figure 5.28: Threshold voltages at different drain voltages, for 300 $\mu$ m wide channel

Also for this channel width, the best operating condition relies in a drain voltage around  $-500\text{mV}$ ,  $-600\text{mV}$ .

### 5.4.3 Output characteristic measurements

Then the output characteristic was measured for both channels. The output characteristic represents current flowing between the drain and the source as a function of the corresponding voltage between the two contacts. In this case the drain voltage window chosen for the measurement was from  $-1.5\text{V}$  to  $+1\text{V}$ , and the characteristic was plotted for six different gate voltages. Output characteristics of  $700\mu\text{m}$  wide channel, at different gate voltages, are shown in Fig.5.29.

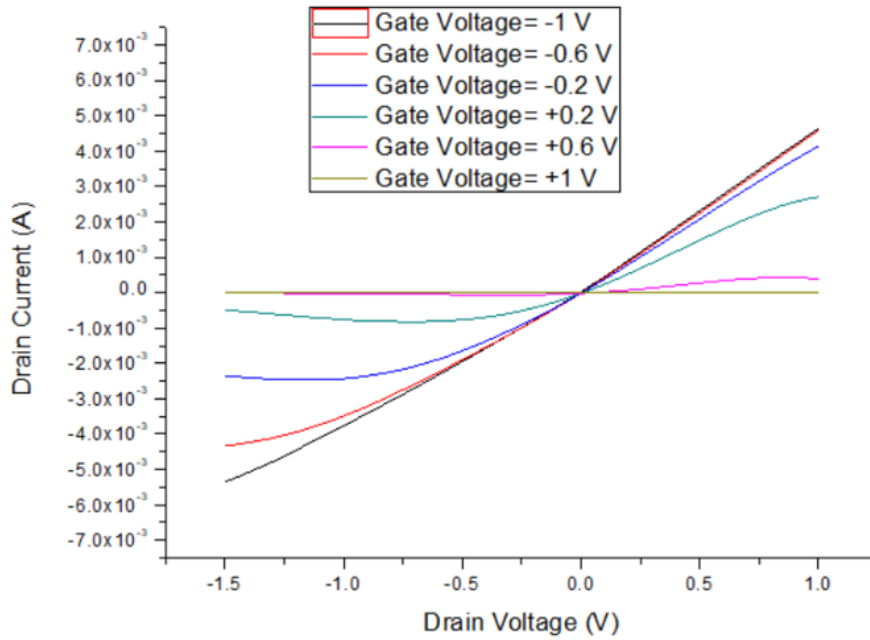


Figure 5.29: Output characteristics at different gate voltages, for  $700\mu\text{m}$  wide channel

It can be noticed that, at a gate voltage equal to  $-1\text{V}$  behaves like a linear resistor, since the corresponding curve is practically a straight line, with a constant slope and therefore a constant conductance (or equivalently a constant resistance). This is due to the fact that, according to the trans-characteristic curve, the OECT is deeply in the ON state at this gate voltage, independently from the drain voltage applied. For lower (in absolute value) gate voltages, the output characteristic reaches a saturation due to channel pinch-off.

The slope of the curves (which represent the conductance) at different gate voltages, in the linear regime, has been plotted (Fig.5.30).

The same considerations can be made for the  $300\mu\text{m}$  wide channel, whose output characteristics at different gate voltages and conduc-

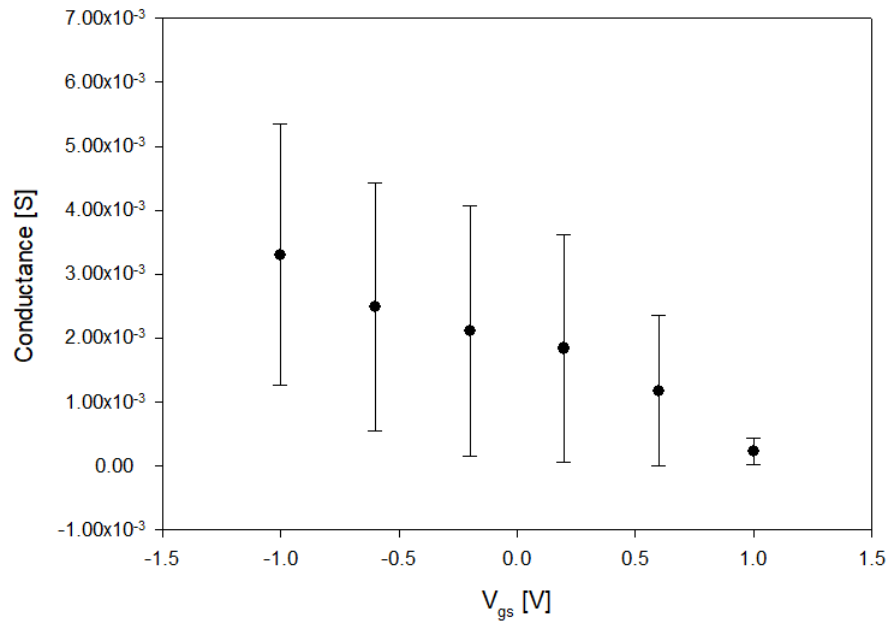


Figure 5.30: Conductance values at different gate voltages, for 700 $\mu\text{m}$  wide channel

tance behaviour as a function of gate voltage are shown in Fig.5.31 and Fig.5.32 respectively.

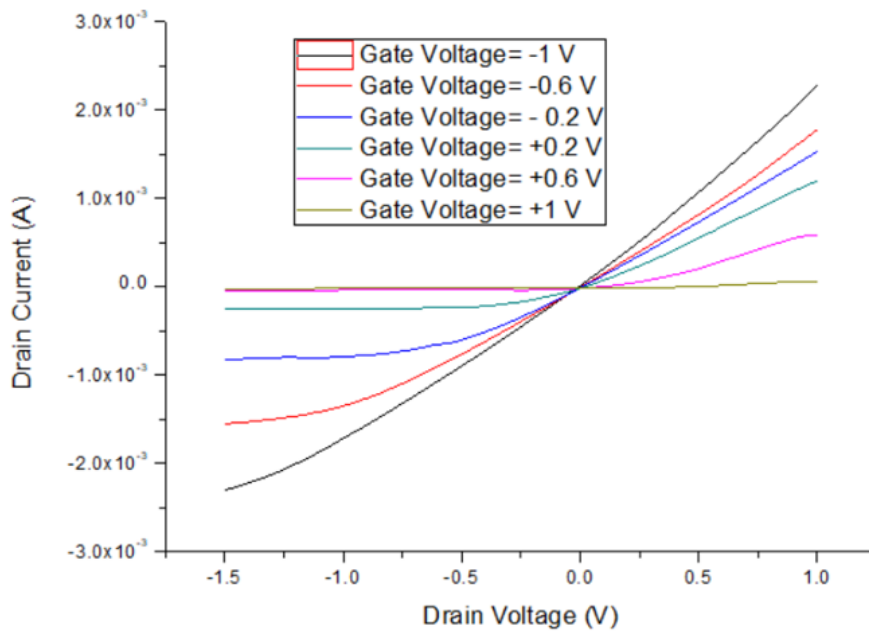


Figure 5.31: Output characteristics at different gate voltages, for 300 $\mu\text{m}$  wide channel

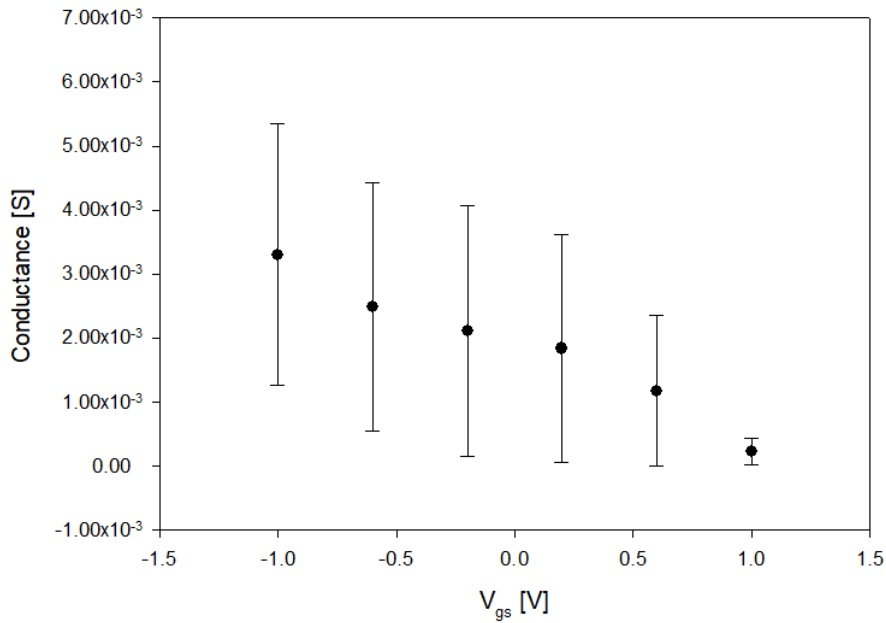


Figure 5.32: Conductance values at different gate voltages, for 300 $\mu\text{m}$  wide channel

#### 5.4.4 Rise-time and fall-time analysis

The transient behaviour of the devices was analysed. In order to do this, a voltage at which the OEET is in the ON state was kept constant for a period of time, and then switched to another voltage at which the OEET is in the OFF state and kept constant for the same period of time. In each step the current was measured. This voltage switching was repeated for five times. In Fig.5.33, Fig.5.34, and Fig.5.35 follow the results for the 700 $\mu\text{m}$  wide channel, which show the voltage and current values during each cycle, the current behaviour and the values considered for the rise-time, the current behaviour and the values considered for the fall-time, respectively.

For the rise-time and fall-time, the 90% and the 10% of the current flowing in the system have been considered. The average rise-time (which corresponds to the time required to switch off the transistor) turned out to be equal to be 2.62s while the average fall-time (or equivalently, the time required to switch on the device) is equal to 4.88s. the switching-off time is lower than the switching-on time due to the fact that the de-doping process in order to shut down the channel and decrease the current is faster than the process required to trigger and generate the current.

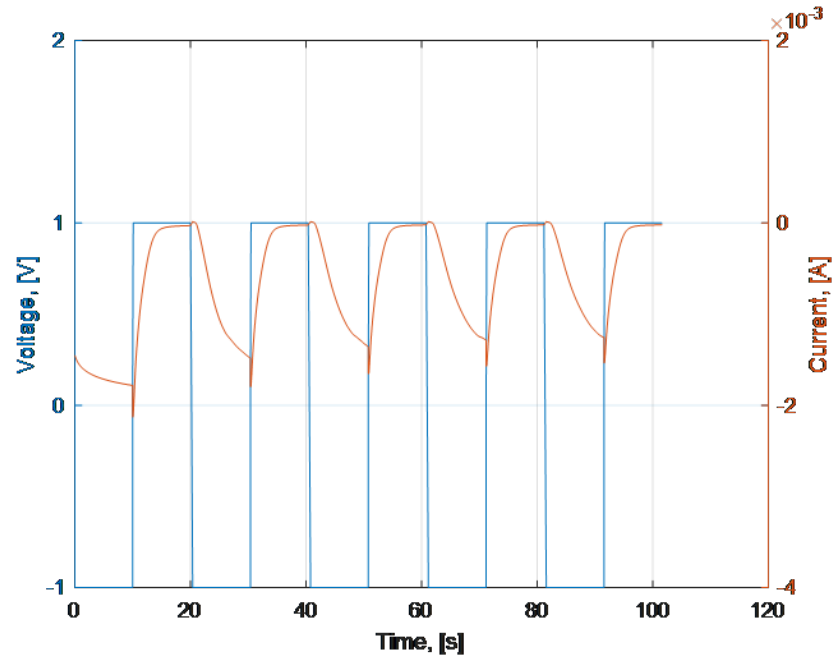


Figure 5.33: Input square wave and corresponding current measured, for  $700\mu\text{m}$  wide channel

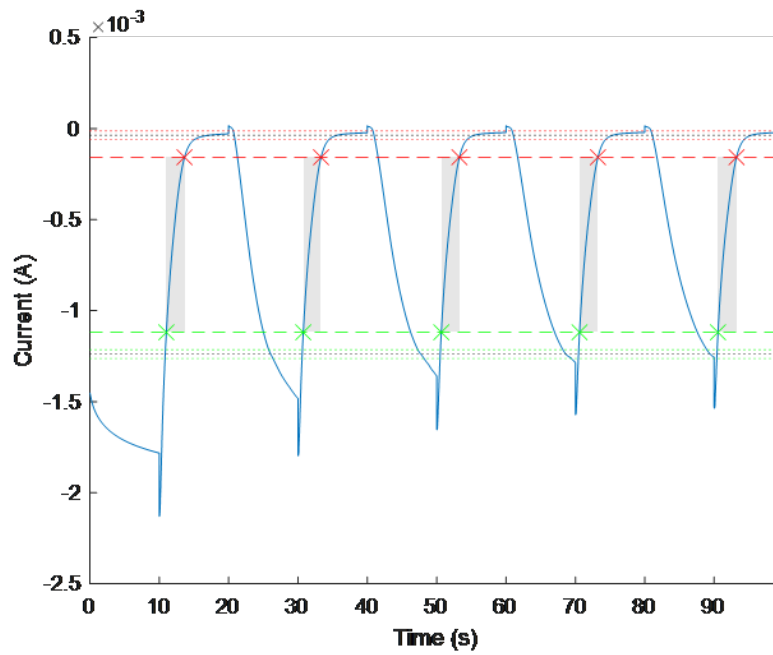


Figure 5.34: Rise-time analysis, for  $700\mu\text{m}$  wide channel, considering the 90% and 10% of the current flowing in the channel

Regarding the  $300\mu\text{m}$  wide channel, the behaviour is the same, and also the time values obtained were very similar, since they turned out to be equal to 2.19s and 4.37s for rise and fall time respectively.

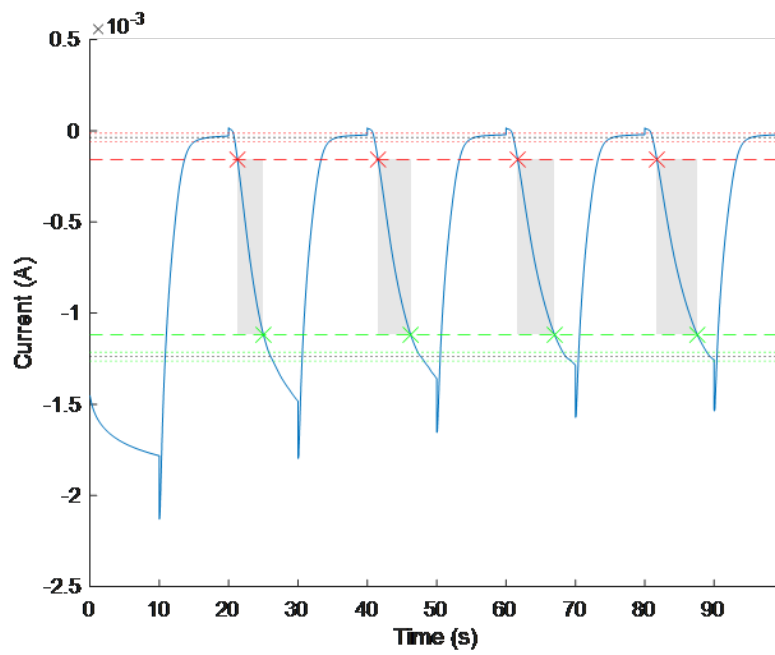


Figure 5.35: Fall-time analysis, for 700 µm wide channel, considering the 90% and 10% of the current flowing in the channel

## CONCLUSION

---

The effectiveness of the stereolithographic process for printing organic electrochemical transistor was proven and verified. The process proved to be very efficient and very suitable for this kind of devices, with also a satisfying repeatability. Moreover, the accuracy of the process was assessed, since the final product did not show excessive geometrical variances with respect to the nominal dimensions. Stereolithography also proved to be safe, both for the final product, since no contaminations occurred after the printing process, and for operators, since no toxic compounds are used. At last, stereolithography proved to be a very customizable process, according to the different needs, since every part of the device and every polymeric resin had its own laser and mechanical parameters. Therefore, in the future this process could be used to print a large variety of transistors and devices, with different geometries, with different materials and for different purposes. Future studies should focus on finding a method to speed up the entire process, making it even more efficient. A very efficient way to obtain a semiconducting organic material was found, which allowed to obtain very good performances of the OECTs in terms of conductivity. The printed devices were tested and characterised in order to find the best operating conditions, proving to be efficient devices with good performances in terms of switching times, amplification, and transconductance: they showed to have a slower response than traditional MOSFET, but their great advantage is the fact that they can operate at very low voltages with respect to traditional devices, avoiding breakdown phenomena which could ruin the transistors. The larger channel ( $700\mu\text{m}$  in width) proved to be the best solution between the two tested, in terms of transconductance, and on/off current ratio. Future studies and works should focus on finding physical and technological solutions to have better performances with scaled (both in length and width) devices. Moreover, many kinds of biological analytes should be tested, with different concentrations, in order to find the best operating conditions for each analyte and to develop the organic electrochemical transistors in the field of biosensors.

## BIBLIOGRAPHY

---

- [1] L. Kergoat, B. Piro, M. Berggren, et al. "Advances in organic transistor-based biosensors: from organic electrochemical transistors to electrolyte-gated organic field-effect transistors." In: *Analytical and BioAnalytical Chemistry* (2011).
- [2] L. C. Clark and C. Lyons. "Electrode systems for continuous monitoring in cardiovascular surgery." In: *Annals of the New York Academy of Sciences* (1962).
- [3] S. Forrest. "The path to ubiquitous and low-cost organic electronic appliances on plastic." In: *Nature* (2004).
- [4] M. Berggren, D. Nilsson, and N. Robinson. "Organic materials for printed electronics." In: *Nature Materials* (2007).
- [5] K. Vaeth. "OLED-display technology." In: *Journal of Information Display* (2003).
- [6] H. Hoppe and N. Sariciftci. "Organic solar cells: an overview." In: *Journal of Materials Research and Technology* (2004).
- [7] C. Bartic and G. Borghs. "Organic thin-film transistors as transducers for (bio) analytical applications." In: *Analytical and BioAnalytical Chemistry* (2006).
- [8] J. Mabeck and G. Malliaras. "Chemical and biological sensors based on organic thin-film transistors." In: *Analytical and BioAnalytical Chemistry* (2006).
- [9] L. Wang, D. Fine, D. Sharma, et al. "Nanoscale organic and polymeric field-effect transistors as chemical sensors." In: *Analytical and BioAnalytical Chemistry* (2006).
- [10] J. Locklin and Z. Bao. "Effect of morphology on organic thin film transistor sensors." In: *Analytical and BioAnalytical Chemistry* (2006).
- [11] C. Dimitrakopoulos and P. Malenfant. "Organic thin film transistors for large area electronics." In: *Advanced Materials* (2002).
- [12] D. Venkateshvaran et al. "Approaching disorder-free transport in high-mobility conjugated polymers." In: *Nature* (2014).
- [13] M. Nikolka et al. "High operational and environmental stability of high-mobility conjugated polymer field-effect transistors through the use of molecular additives." In: *Nature Materials* (2017).
- [14] P. Bergvel. "Development of an ion-sensitive solid-state device for neurophysiological measurements." In: *IEEE Transaction on Biomedical Engineering* (1970).

- [15] H. White, G. Kittlesen, and M. Wrighton. "Chemical derivatization of an array of three gold microelectrodes with polypyrrole: fabrication of a molecule-based transistor." In: *Journal of the American Chemical Society* (1984).
- [16] E. Paul, A. Ricco, and M. Wrighton. "Resistance of polyaniline films as a function of electrochemical potential and the fabrication of polyaniline-based microelectronic devices." In: *Journal of Physical Chemistry* (1985).
- [17] S. Chao and M. Wrighton. "Characterization of a solid-state polyaniline-based transistor: water vapor dependent characteristics of a device employing a poly(vinyl alcohol)/phosphoric acid solid-state electrolyte." In: *Journal of the American Chemical Society* (1987).
- [18] J. Thackeray, H. White, and M. Wrighton. "Poly(3-methylthiophene)-coated electrodes: optical and electrical properties as a function of redox potential and amplification of electrical and chemical signals using poly(3-methylthiophene)-based microelectrochemical transistors." In: *Journal of Physical Chemistry* (1985).
- [19] J. Thackeray and M. Wrighton. "Chemically responsive microelectrochemical devices based on platinized poly(3-methylthiophene): variation in conductivity with variation in hydrogen, oxygen, or pH in aqueous solution." In: *Journal of Physical Chemistry* (1986).
- [20] S. Kirchmeyer and K. Reuter. "Scientific importance, properties and growing applications of poly(3,4-ethylenedioxythiophene)." In: *Journal of Materials Chemistry* (2005).
- [21] P. Bartlett and Y. Astier. "Microelectrochemical enzyme transistors." In: *Chemical Communications* (2000).
- [22] J. Rivnay, I. Sahika, A. Salleo, et al. "Organic electrochemical transistors." In: *Nature Reviews, Materials* (2018).
- [23] D. Bernards and G. Malliaras. "Steady-state and transient behavior of organic electrochemical transistors." In: *Advanced Functional Materials* (2007).
- [24] D. Khodagholy et al. "High transconductance organic electrochemical transistors." In: *Nature Communications* (2013).
- [25] A. Elschner, S. Kirchmeyer, W. Lovenich, et al. "PEDOT, Principles and Applications of an Intrinsically Conductive Polymer." In: *CRC Press* (2010).
- [26] C. Nielsen et al. "Molecular design of semiconducting polymers for high-performance organic electrochemical transistors." In: *Journal of the American Chemical Society* (2016).

- [27] J. Rivnay et al. "Organic electrochemical transistors with maximum transconductance at zero gate bias." In: *Advanced Materials* (2013).
- [28] D. Khodagholy et al. "In vivo recordings of brain activity using organic transistors." In: *Nature Communications* (2013).
- [29] J. Rivnay et al. "High-performance transistors for bioelectronics through tuning of channel thickness." In: *Science Advances* (2015).
- [30] X. Strakosas, M. Bongo, and R. Owens. "The organic electrochemical transistor for biological applications." In: *Journal of Applied Polymer Science* (2015).
- [31] P. Lin and F. Yan. "Organic thin-film transistors for chemical and biological sensing." In: *Advanced Materials* (2012).
- [32] D. Nilson, N. Robinson, M. Berggren, et al. "Electrochemical logic circuits." In: *Advanced Materials* (2005).
- [33] P. Hutter, T. Rothlander, G. Scheipl, et al. "All screen-printed logic gates based on organic electrochemical transistors." In: *IEEE Transactions on Electronic Devices* (2015).
- [34] P. Gkoupidenis, N. Schaefer, B. Garlan, et al. "Neuromorphic functions in PEDOT: PSS organic electrochemical transistors." In: *Advanced Materials* (2015).
- [35] Y. van de Burgt et al. "A non-volatile organic electrochemical device as a low-voltage artificial synapse for neuromorphic computing." In: *Nature Materials* (2017).
- [36] V. Prigodin, F. Hsu, Y. Kim, et al. "Electric Field Control of Charge Transport in Doped Polymers." In: *Synthetic Metals* (2005).
- [37] N. Robinson, P. Svensson, D. Nilsson, et al. "On the Current Saturation Observed in Electrochemical Polymer Transistors." In: *Journal of Electrochemical Society* (2006).
- [38] A. Giovannitti et al. "N-type organic electrochemical transistors with stability in water." In: *Nature Communications* (2016).
- [39] A. Laiho, F. R. Herlogsson L., et al. "Controlling the dimensionality of charge transport in organic thin-film transistors." In: *Proceedings of the National Academy of Sciences of the United States of America* (2011).
- [40] A. Giovannitti et al. "Controlling the mode of operation of organic transistors through side-chain engineering." In: *Proceedings of the National Academy of Sciences of the United States of America* (2016).
- [41] F. Cicoira et al. "Influence of device geometry on sensor characteristics of planar organic electrochemical transistors." In: *Advanced Materials* (2010).

- [42] P. Hutter, T. Rothlander, A. Haase, et al. "Influence of geometry variations on the response of organic electrochemical transistors." In: *Applied Physics Letters* (2013).
- [43] A. Bard and L. Faulkner. *Electrochemical Methods: Fundamentals and Applications*. 2011.
- [44] D. Koutsouras et al. "Impedance spectroscopy of spun cast and electrochemically deposited PEDOT:PSS films on micro-fabricated electrodes with various areas." In: *ChemElectroChem* (2017).
- [45] C. Proctor, J. Rivnay, and G. Malliaras. "Understanding volumetric capacitance in conducting polymers." In: *Journal of Polymer Science Part B: Polymer Physics* (2016).
- [46] P. Andersson, D. Nilsson, P. Svensson, et al. "Active Matrix Displays Based on All-Organic Electrochemical Smart Pixels Printed on Papers." In: *Advanced Materials* (2002).
- [47] D. Nilsson, M. Chen, T. Kugler, et al. "Bi-stable and Dynamic Current Modulation in Electrochemical Organic Transistors." In: *Advanced Materials* (2002).
- [48] D. Nilsson, T. Kugler, P. Svensson, et al. "An all-organic sensor-transistor based on a novel electrochemical transducer concept printed electrochemical sensors on paper." In: *Sensors and Actuators* (2002).
- [49] Z. Zhu, J. Mabeck, C. Zhu, et al. "A simple poly(3,4-ethylene dioxythiophene)/poly(styrene sulfonic acid) transistor for glucose sensing at neutral pH." In: *Chemical Communications* (2004).
- [50] M. Alam, J. Wang, Y. Guo, et al. "Electrolyte-Gated Transistors Based on Conducting Polymer Nanowire Junction Arrays." In: *Journal of Physical Chemistry B* (2005).
- [51] J. Lu, J. Pinto, and A. MacDiarmid. "Apparent dependence of conductivity of a conducting polymer on an electric field in a field effect transistor configuration." In: *Journal of Applied Physics* (2002).
- [52] P. Blom, M. de Jong, and M. van Munster. "Electric-field and temperature dependence of the hole mobility in poly(p-phenylene vinylene)." In: *Physical review B* (1997).
- [53] G. Buzsaki. *Rhythms of the brain*. 2006.
- [54] J. Friedlein, S. Shaheen, G. Malliaras, et al. "Optical measurements revealing nonuniform hole mobility in organic electrochemical transistors." In: *Advanced Electronic Materials* (2015).
- [55] D. Martin et al. "The morphology of poly(3,4-ethylenedioxythiophene)." In: *Polymer Reviews* (2010).

- [56] A. Nardes et al. "Microscopic understanding of the anisotropic conductivity of PEDOT: PSS thin films." In: *Advanced Materials* (2007).
- [57] Y. Wang et al. "A highly stretchable, transparent, and conductive polymer." In: *Science Advances* (2017).
- [58] E. Stavrinidou et al. "Direct measurement of ion mobility in a conducting polymer." In: *Advanced Materials* (2013).
- [59] J. Rivnay et al. "Structural control of mixed ionic and electronic transport in conducting polymers." In: *Nature Communications* (2016).
- [60] S. Inal, G. Malliaras, and J. Rivnay. "Optical study of electrochromic moving fronts for the investigation of ion transport in conducting polymers." In: *Journal of Materials Chemistry* (2016).
- [61] M. Asplund, T. Nyberg, and O. Inganas. "Electroactive polymers for neural interfaces." In: *Polymers Chemistry* (2010).
- [62] M. ElMahmoudy et al. "Tailoring the electrochemical and mechanical properties of PEDOT:PSS films for bioelectronics." In: *Macromolecular Materials and Engineering* (2017).
- [63] A. Hakansson et al. "Effect of (3-glycidylxypropyl) trimethoxysilane (GOPS) on the electrical properties of PEDOT:PSS films." In: *Journal of Polymers Science Part B: Polymers Physics* (2017).
- [64] D. Mantione et al. "Low-temperature cross-linking of PEDOT:PSS films using divinylsulfone." In: *ACS Applied Materials and Interfaces* (2017).
- [65] J. Izdebska and S. Thomas. *Printing on Polymers: Fundamentals and Applications*. 2015.
- [66] K. Suganama. *Introduction to Printed Electronics*. 2014.
- [67] H. Kipphan. *Handbook of Print Media*. 2001.
- [68] H. Klauk. *Organic Electronics: Materials, Manufacturing, and Applications*. 2006.
- [69] M. Singh, H. Haverinen, P. Dhagat, et al. "Inkjet printing-process and its applications." In: *Advanced Materials* (2010).
- [70] A. Teichler, J. Perelaer, and U. Schubert. "Inkjet printing of organic electronics – comparison of deposition techniques and state-of-the-art developments." In: *Journal of Materials Chemistry* (2013).
- [71] B. de Gans, P. Duineveld, and U. Schubert. "Inkjet Printing of Polymers: State of the Art and Future Developments." In: *Advanced Materials* (2004).

- [72] G. Martin, S. Hoath, and I. Hutchings. "Inkjet printing - the physics of manipulating liquid jets and drops." In: *Journal of Physics: Conference Series* (2008).
- [73] G. Mattana, A. Loi, M. Woytasik, et al. "Inkjet-Printing: A New Fabrication Technology for Organic Transistors." In: *Advanced Materials Technology* (2017).
- [74] S. Logothetidis. *Handbook of Flexible Organic Electronics: Materials, Manufacturing and Applications*. 2014.
- [75] M. Chabinyč, W. Wong, A. Arias, et al. "Printing Methods and Materials for Large-Area Electronic Devices." In: *IEEE Proceedings* (2005).
- [76] M. Ling and Z. Bao. "Thin Film Deposition, Patterning, and Printing in Organic Thin Film Transistors." In: *Chemistry of Materials* (2004).
- [77] P. Melchels, J. Feijen, and W. Grijpma. "A review on stereolithography and its applications in biomedical engineering." In: *Biomaterials* (2010).
- [78] S. Maruo and K. Ikuta. "Submicron stereolithography for the production of freely movable mechanisms by using single-photon polymerization." In: *Sensors and Actuators A: Physical* (2002).
- [79] Y. Lu, G. Mapili, G. Suhali, et al. "A digital micro-mirror device-based system for the microfabrication of complex, spatially patterned tissue engineering scaffolds." In: *Journal of Biomedical Materials Research* (2006).
- [80] P. Melchels, J. Feijen, and W. Grijpma. "A poly(D,L-lactide) resin for the preparation of tissue engineering scaffolds by stereolithography." In: *Biomaterials* (2009).
- [81] J. Choi, R. Wicker, S. Lee, et al. "Fabrication of 3D biocompatible/biodegradable micro-scaffolds using dynamic mask projection microstereolithography." In: *Journal of Materials Processing Technology* (2009).
- [82] L. Han, G. Mapili, S. Chen, et al. "Projection microfabrication of three-dimensional scaffolds for tissue engineering." In: *Journal of Manufacturing Science and Engineering* (2008).
- [83] R. Liska, M. Schuster, R. Infhur, et al. "Photo-polymers for rapid prototyping." In: *Journal of Coatings Technology and Research* (2007).
- [84] S. Romano et al. *Tesi Magistrale: sviluppo di nuovi materiali polimerici elettricamente conduttivi per stampanti 3D stereolitografiche*. 2018.
- [85] J. Mazzoccoli, D. Feke, H. Baskaran, et al. "Mechanical and cell viability properties of crosslinked low- and high-molecular weight poly(ethylene glycol) diacrylate blends." In: *Journal of Biomedical Materials Research* (2009).

- [86] H. Zhang, L. Wang, L. Song, et al. "Controllable Properties and Microstructure of Hydrogels Based on Crosslinked Poly(ethylene glycol) Diacrylates with Different Molecular Weights." In: *Journal of Applied Polymer Science* (2010).
- [87] A. Sabnis, M. Rahimi, C. Chapman, et al. "Cytocompatibility studies of an in situ photopolymerized thermoresponsive hydrogel nanoparticle system using human aortic smooth muscle cells." In: *Journal of Biomedical Materials Research* (2009).
- [88] H. Bai and G. Shi. "Gas Sensors Based on Conducting Polymers." In: *Sensors* (2007).
- [89] P. Bujard, K. Munk, and G. Kuehnlein. "Thermal conductivity of a chain of particles in close contact in a matrix of epoxy resin." In: *Thermal Conductivity* (1994).
- [90] G. Wu, J. Lin, Q. Zheng, et al. "Correlation between percolation behavior of electricity and viscoelasticity for graphite filled high density polyethylene." In: *Polymers* (2006).
- [91] W. Thongruang, R. Spontak, and C. Balik. "Correlated electrical conductivity and mechanical property analysis of high-density polyethylene filled with graphite and carbon fiber." In: *Polymers* (2002).
- [92] J. Yang, Y. Liu, S. Liu, et al. "Conducting polymer composites: material synthesis and applications in electrochemical capacitive energy storage." In: *Materials Chemistry Frontiers* (2017).
- [93] A. MacDiarmid and A. Heeger. "Organic metals and semiconductors: The chemistry of polyacetylene,  $(\text{CH})_x$ , and its derivatives." In: *Synthetic Metals* (1980).
- [94] R. Balint, N. Cassidy, and S. Cartmell. "Conducting polymers: Toward a smart biomaterial for tissue engineering." In: *Acta Biomaterialia* (2014).
- [95] Y. Li. "Conducting Polymers." In: *Organic Optoelectronics Materials, Chemistry* (2015).
- [96] Y. Cao, P. Smith, and A. Heeger. "Counter-ion induced processibility of conducting polyaniline." In: *Synthetic Metals* (1993).
- [97] H. Munsted. "Ageing of electrically conducting materials." In: *Polymers* (1988).
- [98] T. Skotheim and J. Reynolds. *Conjugated Polymers: Theory, Synthesis, Properties, and Characterization*. 2006.
- [99] T. Johansson, L. Petterson, and O. Inganas. "Conductivity of de-doped poly(3,4-ethylenedioxythiophene)." In: *Synthetic Metals* (2002).

- [100] J. Parameswaranpillai, S. Thomas, and Y. Grohens. *Polymer Blends: State of the Art, New Challenges, and Opportunities, in Characterization of Polymer Blends: Miscibility, Morphology, and Interfaces*. 2015.
- [101] J. Lee, K. Rana, B. Seo, et al. "Influence of nonionic surfactant-modified PEDOT:PSS on graphene." In: *Carbon* (2015).
- [102] W. Obeidat and A. Sallam. "Evaluation of Tadalafil Nanosuspensions and Their PEG Solid Dispersion Matrices for Enhancing Its Dissolution Properties." In: *AAPS PharmSciTech* (2014).
- [103] J. Kim, J. Jung, L. D.E., et al. "Enhancement of electrical conductivity of poly(3,4-ethylenedioxythiophene)/poly(4-styrenesulfonate) by a change of solvents." In: *Synthetic Metals* (2002).
- [104] X. Crispin, S. Marciniak, W. Osikowicz, et al. "Conductivity, morphology, interfacial chemistry, and stability of poly(3,4-ethylene dioxythiophene)-poly(styrene sulfonate): A photoelectron spectroscopy study." In: *Journal of Polymer Science art B: Polymer Physics* (2003).
- [105] Y. Xia and J. Ouyang. "PEDOT:PSS films with significantly enhanced conductivities induced by preferential solvation with cosolvents and their application in polymer photovoltaic cells." In: *Journal of Materials Chemistry* (2011).
- [106] N. David. "The pharmacology of dimethylsulfoxide." In: *Annual review of Pharmacology and Toxicology* (1972).
- [107] N. Kharasch and B. Thyagarajan. "Structural Basis for biological activities of dimethyl sulfoxide." In: *Annals of the New York Academy of Sciences* (1983).
- [108] W. MacGregor. "The chemical and physical properties of DMSO." In: *Annals of the New York Academy of Sciences* (1967).
- [109] L. Rubin. "Toxicity of dimethyl sulfoxide, alone and in combination." In: *Annals of the New York Academy of Sciences* (1975).
- [110] O. Dimitriev, D. Grinko, Y. Noskov, et al. "PEDOT:PSS films: Effect of organic solvent additives and annealing on the film conductivity." In: *Synthetic Metals* (2009).
- [111] L. Petterson, S. Ghosh, and O. Inganas. "Optical anisotropy in thin films of poly(3,4-ethylenedioxythiophene)-poly(4-styrenesulfonate)." In: *Organic Electronics* (2002).
- [112] H. Meen, K. Chen, Y. Chen, et al. "The Effects of Dilute Sulfuric Acid on Sheet Resistance and Transmittance in Poly(3,4-ethylenedioxythiophene):Poly(styrenesulfonate) Films." In: *International Journal of Photoenergy* (2013).
- [113] A. Kumatani, Y. Li, P. Darmawan, et al. "On Practical Charge Injection at the Metal/Organic Semiconductor Interface." In: *Scientific Reports* (2013).